MARMARA UNIVERSITY

INSTITUTE FOR GRADUATE STUDIES IN PURE AND APPLIED SCIENCES

METABOLIC NETWORK-BASED ANALYSIS OF CHEESE STARTER CULTURES AS A MICROBIAL COMMUNITY

EMRAH ÖZCAN

Ph.D. THESIS

Department of Bioengineering

Thesis Supervisor

Prof. Dr. Ebru TOKSOY ÖNER

Thesis CO- Supervisor

Assoc. Prof. Dr. Tunahan ÇAKIR

ISTANBUL, 2019

MARMARA UNIVERSITY

INSTITUTE FOR GRADUATE STUDIES IN PURE AND APPLIED SCIENCES

METABOLIC NETWORK-BASED ANALYSIS OF CHEESE STARTER CULTURES AS A MICROBIAL COMMUNITY

EMRAH ÖZCAN
(724213002)

Ph.D. THESIS

Department of Bioengineering

Thesis Supervisor

Prof. Dr. Ebru TOKSOY ÖNER

Thesis CO- Supervisor

Assoc. Prof. Dr. Tunahan ÇAKIR

ISTANBUL, 2019

MARMARA UNIVERSITY
INSTITUTE FOR GRADUATES STUDIES
IN PURE AND APPLIED SCIENCES

Emrah Özcan, a Doctor of Philosophy student of Marmara University Institute for Graduate Studies in Pure and Applied Sciences, defended his thesis entitled "**Metabolic network-based analysis of cheese starter cultures as a microbial community**", on 25.11.2019 and has been found to be satisfactory by the jury members.

Jury Members

Prof. Dr. Ebru TOKSOY ÖNER (Advisor)
Marmara University .....

Assist. Prof. Pınar PİR (Jury Member)
Gebze Technical University .....

Assoc. Prof. Kazım Yalçın ARĞA (Jury Member)
Marmara University.....

Prof. Dr. Süleyman YILDIRIM (Jury Member)
Medipol University.....

Assist. Prof. Emrah NİKEREL (Jury Member)
Yeditepe University.....

APPROVAL

Marmara University Institute for Graduate Studies in Pure and Applied Sciences Executive Committee approves that Emrah Özcan be granted the degree of Doctor of Philosophy in Department of Bioengineering on 11.12.19 (Resolution no: 2019/25-92

Director of the Institute
Prof. DE. Bülent İkiel

ACKNOWLEDGMENT

First and foremost, I want to express my sincere gratitude to my thesis advisor Ebru Toksoy Öner for her continuous guidance, generous support, and valuable advice. She is also the mother of this thesis in a way, as she directed me towards cheese starter cultures after I decided to work on microbial community modelling.

I also wish to thank my co-advisor Tunahan Çakır, who introduced me to the systems biology perspective, many years ago, which has changed my outlook on bioscience. This introduction has shaped the course my academic career. Although Emrah Nikerel was not formally a supervisor, he has also supported me greatly. His feedback, the discussions we had and his guidance have been greatly appreciated.

Bas Teusink, head of Systems Biology Lab -formerly Systems Bioinformatics Lab- at Vrije Universiteit Amsterdam, also needs a special thank you. Part of this study was carried out and completed at VU Amsterdam, where Bas Teusink supervised me. I have learned a lot about how to ask the right questions and to look at science from a different perspective, and I have also taken advantage of his experience in modelling. The time I have spent at his lab has made me more critical, analytical and multidisciplinary.

This work received financial support from The Scientific and Technological Research Council of Turkey through TUBITAK 2211-C and 2214-A programs and the Marmara University Scientific Research Project Fund through Project No: FEN-C-DRP-091116-0498. I appreciate being able to carry out this research because of this support.

I would like to thank some of my friends and colleagues who contributed to this study during my thesis journey: Merve Seven from Yeditepe University for her all help and sharing her experience on the experimental studies and for performing the qPCR experiments. Burcu Şirin from Yeditepe University for her help on HPLC analyses. S. Selvin Selvi from IBSB Lab, Marmara University for her help on the glucose analysis and amino acid omission experiments. Merve Enginer Hasköylü from the same lab for all help when I was away from Marmara University. During the literature survey in the very early phase of my thesis, I ran into the PhD thesis of Oylum Erkuş from Wageningen University. I met her later on in Izmir and she shared her experience on dairy origin lactic

acid bacteria communities with me. I appreciate her for not only sharing her extensive knowledge on lactic acid bacteria, but also for supplying me with *L. lactis* MG1363 strain.

I also want to thank Frank Bruggeman, Herwig Bachmann, Douwe Molenaar, Brett Olivier, Eunice van Pelt-Kleinjan, Sebastian Mendoza, Sieze Douwenga, Daan de Groot, Chrats Melkonian, Rinke van Tatenhove-Pel and Paul Iturbe Espinoza from the Systems Biology Lab at VU Amsterdam for providing a supportive and inspiring working environment and for their support through discussions and advice.

And not just for this thesis, but also for their support and love during my whole my life: thank you to my family. Anne, baba, Esin, Esra Abla ve Bülend Abi doktoranın uzun ve meşakkatli sürecinde sizlerden uzaktaydım, belki dosdoğru bu doktora çalışmasına değil ama dosdoğru tüm hayatımda emeğiniz var, bu da bir yerde bu tezin varlığının sizin sayenizde olduğunu gösterir. Eksik olmayın, var olun, sizi çok seviyorum ve çok teşekkür ediyorum.

Suki and Willy, the best cats in the world, they have motivated me with their philosophical attitude and have calmed me by purring while writing this thesis.

Karen, je bent de geheime held van deze thesis. Het afgelopen jaar was het meest intense jaar van deze promotie, en je hebt dit met me meegedragen. Bedankt voor je geduld en begrip. Je hebt het plezier maar ook de stress meegemaakt, zoals we alles zullen delen. Ik ben dankvoor voor het leven dat we samen creëeren.

October 2019 **Emrah Özcan**

TABLE OF CONTENTS

ACKNOWLEDGMENT i

ÖZET vi

ABSTRACT vii

CLAIM OF ORIGINALITY viii

SYMBOLS ix

ABBREVIATION x

LIST OF FIGURES xiii

LIST OF TABLES xvii

1. INTRODUCTION 1

1.1. An Overview of Lactic Acid Bacteria and Cheese Starter Cultures 1

1.2. Metabolic Network-Based Analysis of LAB 5

1.2.1. Metabolic network reconstruction and constraint-based analysis of metabolic networks 6

1.2.2. Dynamic flux balance analysis (dFBA) 9

1.2.3. Microbial community metabolic modelling 11

1.2.3.1. Supra-organism metabolic modelling 12

1.2.3.2. Multi-species metabolic modelling 13

1.3. Aim and Overall Design of This Study 16

2. MATERIALS AND METHODS 20

2.1. Organisms and Growth Medium 20

2.2. Fermentation Conditions 21

2.2.1. Fermentation conditions for the study of the genome-scale metabolic network reconstruction of *Leu. mesenteroides* 22

2.2.2. Fermentation conditions for the pure and co-cultures 22

2.3. Experimental Analyses 23

2.3.1. Analysis of biomass and extracellular compounds 23
2.3.2. Carbon balance 24
2.3.3. Estimation of the relative microbial abundance in co-cultures 24
2.3.4. Analyses of essential amino acid requirements for *Leu. mesenteroides* .. 25
2.4. Computational Analyses 26
2.4.1. Genome Annotation 26
2.4.2. Reconstruction of *Leu. mesenteroides* genome-scale metabolic network model 26
2.4.3. GSMMs used in this study 27
2.4.4. Flux balance analysis for GSMM of *Leu. mesenteroides* 28
2.4.5. The dynamic flux balance analysis (dFBA) for pure cultures 29
2.4.6. Parameter estimation 31
2.4.7. Dynamic co-culture metabolic modelling 32
3. RESULTS AND DISCUSSION 35
3.1. Genome-Scale Metabolic Network Model of *Leu. mesenteroides* 35
3.1.1. Model reconstruction and validation 35
3.1.2. Model-based investigation of heterolactic fermentation and flavour metabolism in *Leu. mesenteroides* in anaerobic conditions 39
3.1.3. Metabolic shift and stimulation of growth in *Leu. mesenteroides* under aerobic conditions 45
3.1.4. Effect of different carbon sources on growth profiles in *Leu. mesenteroides* 47
3.1.5. Comparison of the GSMMs *of Leu. mesenteroides* subsp. *cremoris* and *Leu. mesenteroides* subsp. *mesenteroides* 50
3.2. Overview of The Pure and Co-Culture Batch Results 52
3.2.1. Pure Culture Batch Profiles 52
3.2.2. Co-Culture Batch Profiles 56

3.2.3. Individual biomass profiles in the co-cultures 62
3.2.4. Amino acid profiles of pure and co-cultures 63
3.3. The Dynamic Metabolic Network Modelling of Pure and Co-Cultures 65
3.3.1. Parameter estimation 65
3.3.2. Dynamic flux balance analysis (dFBA) for pure cultures 68
3.3.3. Dynamic co-culture metabolic modelling 74
3.3.4. Individual flux rate profiles of co-culture members 81
4. CONCLUSION AND RECOMMENDATIONS 88
5. REFERENCES 94
APPENDIX A 108
APPENDIX B 115
APPENDIX C 117
APPENDIX D 118
APPENDIX E 119
APPENDIX F 120
APPENDIX G 122
APPENDIX H 123
AUTOBIOGRAPHY 126

ÖZET

BİR MİKROBİYAL TOPLULUK OLARAK PEYNİR STARTER KÜLTÜRLERİNİN METABOLİK AĞ-BAZLI ANALİZİ

Doğada neredeyse hiç saf mikrobiyal kültür yoktur, aksine mikroorganizmalar diğer organizmalarla etkileşim halindedir ve farklı türler aynı habitatı paylaşır. Dolayısıyla, mikrobiyal topluluk çalışmaları, doğayı daha iyi anlayabilmemize yardımcı olur. Bu tez kapsamında bir mikrobiyal topluluk olan peynir starter kültürleri çalışılmıştır. Bu amaçla süt ürünleri kökenli ve peynir starter kültürlerinde sıklıkla kullanılan laktik asit bakterilerinden olan *Lactococcus lactis* subsp. *cremoris*, *Lactococcus lactis* subsp. *lactis*, *Streptococcus thermophilus* ve *Leuconostoc mesenteroides*, saf ve ko-kültür olarak büyütülmüşlerdir. *L. lactis* ve *Leu. mesenteroides* türlerinden oluşan ko-kültürler ile *L. lactis* ve *S. thermophilus* türlerinden oluşan ko-kültürler sırasıyla mezofilik ve termofilik starter ko-kültürleri temsil ettiği kabul edilmiştir. Saf ve ko-kültlerin metabolik kapasiteleri daha sonra dinamik metabolik ağ modelleme yaklaşımıyla kapsamlı olarak incelenmiştir. Dinamik modellerdeki substrat tüketim kinetiği, pH ve laktik asitin bir fonksiyonu olarak tanımlanmıştır. Kinetik parametreler, saf kültür deneyleri kullanılarak tahminlenmiş olup hem saf hem de ko-kültür modellerinde kullanılmıştır. Mezofilik ko-kültür modelleri, pH'ın mezofilik ko-kültür biyokütle dinamiğini etkileyen en önemli fermantasyon parametresi olduğunu gösterdi ve bu modeller, *Leu. mesenteroides* büyümesinin *L. lactis* tarafından nasıl baskılandığını açıkladı. Mezofilik ko-kültürlerin aksine, termofilik ko-kültürlerde en önemli fermantasyon parametresi sıcaklıktı. *L. lactis* ve *S. thermophilus* saf kültürlerinin fermantasyon sıcaklığı farklı olduğundan, termofilik ko-kültürler ortalama bir sıcaklıkta büyütüldü. Termofilik ko-kültürde her bir türe ait substrat tüketim hızları, sıcaklık farkını yansıtacak bir katsayı ile çarpıldı ve ancak bu katsayı çarpımından sonra termofilik ko-kültürler deneysel koşulları simüle edebildi. Ayrıca, ko-kültür modelleri ko-kültür içerisindeki türlere ait tüm ekstraselüler metabolit üretim/tüketim hızlarını tahminledi. Deneysel olarak gerçekleştirilemeyen bu tahminler laktik asit bakterileri arasındaki potansiyel metabolik etkileşimleri de göstermiş oldu.

ABSTRACT

METABOLIC NETWORK-BASED ANALYSIS OF CHEESE STARTER CULTURES AS A MICROBIAL COMMUNITY

There is almost no pure culture in nature, but rather microorganisms are open to interact with other organisms, and different species share the same habitat. Therefore, microbial community studies enable nature to be understood better. Cheese starter cultures as a microbial community have been studied in this thesis. For this purpose, dairy-origin lactic acid bacteria (LAB), *Lactococcus lactis* subsp. *cremoris*, *Lactococcus lactis* subsp. *lactis*, *Streptococcus thermophilus* and *Leuconostoc mesenteroides*, which are commonly used LAB species in cheese starter cultures, were grown in pure and co-cultures. The co-cultures composed of *L. lactis* and *Leu. mesenteroides* species and the co-cultures composed *L. lactis* and *S. thermophilus* species were assumed to represent mesophilic and thermophilic starter cultures, respectively. The metabolic capacities of the pure and co-cultures were then comprehensively investigated by the dynamic metabolic network modelling approaches in a quantitative manner. Substrate uptake kinetics in the dynamic models were defined as a function of pH and lactic acid. The kinetic parameters were estimated using the pure culture experiments, and they were used both in the pure and co-culture models. The mesophilic co-culture models showed that pH was the major fermentation parameter that effects the co-culture biomass composition, and the models explained the mechanisms behind the suppression of the growth of *Leu. mesenteroides* by *L. lactis* strains in mesophilic starter cultures. Unlike the mesophilic co-cultures, temperature was the major fermentation parameter in thermophilic co-cultures. Since the fermentation temperature of the *L. lactis* and *S. thermophilus* pure cultures were different, the thermophilic co-cultures were grown at an average fermentation temperature. The thermophilic co-culture models could simulate the fermentations only after the individual substrate uptake rates, which are the model constraints, were multiplied by a strain-specific correction coefficient reflecting the temperature difference. Furthermore, the co-culture models estimated the individual production/consumption profiles of the various extracellular metabolites, as well as the potential metabolic interactions between the LAB in the co-cultures, which could not be obtained experimentally.

CLAIM OF ORIGINALITY

In both artisanal and industrial fermentative foods, different types of microorganism coexist as a microbial community. Therefore, in order to get a better understanding of the food fermentation, they should be studied together as well. The metabolic network-based analysis which is one of the systems biology tools is a promising approach to investigate the metabolism of microbial communities in a holistic way. This thesis study focuses on the microbial communities of cheese starter cultures, and it handles the topic using the dynamic metabolic network modelling approach. Some noteworthy outputs of the study which are expected to contribute the related areas are as follows:

- Lactic acid bacteria commonly used in cheese starter cultures were investigated using metabolic network modelling. To this aim, dynamic genome-scale metabolic models were reconstructed at both single-species and co-culture level. Although there are several studies about the metabolic modelling of lactic acid bacteria at single-species level (Flahaut et al., 2013; Oliveira et al., 2005; Pastink et al., 2009; Teusink et al., 2006; Vinay-Lara et al., 2014), this study is the first study which models the different LAB composing a microbial consortia via dynamic co-culture metabolic models.
- Genome-scale metabolic model of *Leu. mesenteroides* subsp. *cremoris* which was one of the metabolic models used in the co-culture models, has been reconstructed for the first time within the scope of this thesis study.
- In order to estimate the model parameters and to then compare the *in-silico* and *in-vitro* results, comprehensive bioreactor experiments were carried out for this study. LAB were grown in chemically defined medium as pure and co-cultures. Concentration profiles of biomass, glucose, organic acids and amino acids were obtained for pure and co-cultures. Relative microbial abundance profiles of the co-cultures were also estimated using a molecular-based approach (qPCR).
- In addition to the compounds which were also obtained experimentally, the pure and co-culture models predicted the other extracellular compounds profiles including flavour metabolites.
- The co-culture models estimated the potential metabolic interactions between LAB used.

SYMBOLS

°C	: Degree Celsius
#	: number
μ	: growth rate
μ_{max}	: Maximum growth rate
CO_2	: Carbon dioxide
K_S	: Michaelis-Menten constant
mmol	: Millimole
N_2	: Nitrogen
O_2	: Oxygen
q_P	: Product rate
q_S	: substrate rate
S	: Stoichiometric matrix
v	: Reaction rate/flux distribution
v/v	: volume/volume
Z	: Objective function

ABBREVIATION

aa : Amino acids

Ac : Acetic acid

Ala : Alanine

Arg : Arginine

Asn : Asparagine

Asp : Aspartate

bp : Base pair

CDM : Chemically defined medium

CFU : Colony forming unit

Cit : Citric acid

COBRA : Constraint-based reconstruction and analysis

Cys : Cysteine

dFBA : Dynamic flux balance analysis

DOA : Dynamic optimization approach

DyMMM : Dynamic Multispecies Metabolic Modelling

EtOH : Ethanol

FBA : Flux balance analysis

For : Formic acid

FVA : Flux variability analysis

gDW : gram dry weight

Glc : Glucose

Gln : Glutamine

Glu : Glutamate

Gly : Glycine

GSMM : Genome-scale metabolic model

His : Histidine

HPLC : High performance liquid chromatography

Ile : Isoleucine

KEGG : Kyoto Encyclopedia of Genes and Genomes

l : Litre

LAB : Lactic acid bacteria

Lac : Lactic acid

LacH : Undissociated lactic acid

LB : Lower bound

Leu : Leucine

LLC : *Lactococcus lactis* subsp. *cremoris*

LLL : *Lactococcus lactis* subsp. *lactis*

LM : *Leuconostoc mesenteroides*

LP : Linear programming

Lys : Lysine

Met : Methionine

NLP : Nonlinear programming

OD : Optical density

ODE : Ordinary differential equation

Orn : Ornithine

PCR : Polymerase chain reaction

Phe : Phenylalanine

Pro : Proline

QP : Quadratic programming

qPCR : Quantitative polymerase chain reaction

rpm : Revolutions per minute

SBML : Systems biology markup language

Ser : Serine

ST : *Streptococcus thermophilus*

Thr : Threonine

Trp : Tryptophan

Tyr : Tyrosine

UB : Upper bound

Val : Valine

3MOB : 3-Methyl-2-oxobutanoate

3MOP : (S)-3-Methyl-2-oxopentanoate

4MOP : 4-Methyl-2-oxopentanoate

LIST OF FIGURES

Figure 1.1. Central carbon metabolism pathways of LAB 2
Figure 1.2. Methodology for constraint-based metabolic modelling 8
Figure 1.3. dFBA methodology with static optimization approach (SOA)..... 11
Figure 1.4. Microbial community metabolic modelling approaches. 12
Figure 1.5. Community flux balance analysis (cFBA) framework 14
Figure 1.6. Dynamic multi-species metabolic modelling framework for three-species microbial community..... 15
Figure 1.7. Overall design of the study..... 18
Figure 2.1. Dynamic co-culture metabolic modelling framework 33
Figure 3.1. Phosphoketolase pathway in the metabolic network of *Leu. mesenteroides* 40
Figure 3.2. Effect of glucose and citrate uptake rates on metabolite production profile and growth rate, obtained by model simulations..... 42
Figure 3.3. Flavour metabolite production associated with citrate metabolism..... 44
Figure 3.4. Respiration mechanisms mediated by menaquinone-8 and ubiquinone-8 in *Leu. mesenteroides.* 46
Figure 3.6. Representation of the utilization of commonly used carbon sources by *Leu. mesenteroides* 48
Figure 3.7. Effect of commonly used carbon sources on the metabolic products of *Leu. mesenteroides* in anaerobic condition predicted by the model..... 50
Figure 3.8. Pure culture batch profile of *Lactococcus lactis* subsp. *cremoris* (LLC).... 53
Figure 3.9. Pure culture batch profile of *Lactococcus lactis* subsp. *lactis* (LLL) 54
Figure 3.10. Pure culture batch profile of *Streptococcus thermophilus* (ST)..... 54
Figure 3.11. Pure culture batch profile of *Leuconostoc mesenteroides* (LM)..... 55
Figure 3.12. Comparative profiles of biomass (A), glucose (B), total lactic acid (C), pH and undissociated lactic acid (LacH) (D) of the pure cultures. 56
Figure 3.13. Batch profile of the co-culture comprised of *Lactococcus lactis* subsp. *cremoris* and *Leu. mesenteroides* (LLC-LM)..... 58
Figure 3.14. Batch profile of the co-culture comprised of *Lactococcus lactis* subsp. *cremoris*, *Lactococcus lactis* subsp. *lactis* and *Leu. mesenteroides* (LLC-LM) 58

Figure 3.15. Batch profile of the co-culture comprised of *Lactococcus lactis* subsp. *cremoris* and *S. thermophilus* (LLC-ST)..... 59
Figure 3.16. Batch profile of the co-culture comprised of *Lactococcus lactis* subsp. *cremoris, Lactococcus lactis* subsp. *lactis* and *S. thermophilus* (LLC-LLL-ST)..... 60
Figure 3.17. Comparative biomass, glucose and lactic acid profiles of pure and co-cultures. (A) Mesophilic co-cultures and pure cultures constituting the co-cultures, (B) thermophilic co-cultures and pure cultures constituting the co-cultures..... 61
Figure 3.18. Individual biomass profiles of the co-culture members in the two-species mesophilic co-culture (A), the three-species mesophilic co-culture (B), the two-species thermophilic-co culture (C) and the three-species thermophilic co-culture (D). 62
Figure 3.19. Comparative amino acids profiles of *L. lactis* subsp. *cremoris* (LLC), *L. lactis* subsp. *lactis* (LLL) and *Leu. mesenteroides* (LM), two species mesophilic co-culture (LLC-LM) and three-species mesophilic co-culture (LLC-LLL-LM)..... 64
Figure 3.20. Comparative amino acid profiles of *L. lacti*s subsp. *cremoris* (LLC), *L. lactis* subsp. *lactis* (LLL) and *S. thermophilus* (ST), two species thermophilic co-culture (LLC-ST) and three-species thermophilic co-culture (LLC-LLL-ST)..... 65
Figure 3.21. The route of the major part of ATP flux produced by minimal glucose uptake ($-V_{min}$)..... 70
Figure 3.22. Batch culture profiles of *L. lactis* subsp. *cremoris*. Solid lines denote model results simulated by dFBA, while points denote average values of two independent biological repetitions. Corresponding error bars are also given..... 70
Figure 3.23. Batch culture profiles of *L. lactis* subsp. *lactis*. Solid lines denote model results simulated by dFBA, while points denote average values of two independent biological repetitions. Corresponding error bars are also given..... 71
Figure 3.24. Batch culture profiles of *S. thermophilus*. Solid lines denote model results simulated by dFBA, while points denote average values of two independent biological repetitions. Corresponding error bars are also given..... 72
Figure 3.25. Batch culture profiles of *Leu. mesenteroides*. Solid lines denote model results simulated by dFBA, while points denote average values of two independent biological repetitions. Corresponding error bars are also given..... 72

Figure 3.26. *In-silico* and *in-vitro* biomass profiles of pure cultures in the early phase. Solid lines denote model results simulated by dFBA, while points denote average values of two independent biological repetitions. Corresponding error bars are also given. 73
Figure 3.27. Dynamic co-culture metabolic modelling structure 74
Figure 3.28. Computational and experimental mesophilic co-culture profiles. A) Two-species mesophilic co-culture comprised of *L. lactis* subsp. *cremoris* (LLC) and *Leu. mesenteroides* (LM). B) Three-species mesophilic co-culture comprised of *L. lactis* subsp. *cremoris* (LLC), *L. lactis* subsp. *lactis* (LLL) and *Leu. mesenteroides* (LM)..... 76
Figure 3.29. The growth performance of the *L. lactis* and *S. thermophilus* strains based on the experimental growth rate with respect to pH in pure and thermophilic co-cultures. Th2Sp and Th3Sp denote the two and three-species thermophilic co-cultures..... 78
Figure 3.30. Computational and experimental thermophilic co-culture profiles. A) Two-species thermophilic co-culture comprised of *L. lactis* subsp. *cremoris* (LLC) and *S. thermophilus* (ST). B) Three-species thermophilic co-culture comprised of *L. lactis* subsp. *cremoris* (LLC), *L. lactis* subsp. *lactis* (LLL) and *S. thermophilus* (ST)..... 79
Figure 3.31. Individual biomass abundance ratio of *L. lactis* subsp. *cremoris* (LLC) in two-species thermophilic co-culture. Solid lines and points denote the model and average experimental results respectively. 80
Figure 3.32. Individual flux rate profiles of *L. lactis* subsp. *cremoris* (blue line) and *Leu. mesenteroides* (red line) in two-species mesophilic co-culture. Negative and positive flux values show consumption and production respectively. 82
Figure 3.33. Individual flux rate profiles of *L. lactis* subsp. *cremoris* (blue line), *L. lactis* subsp. *lactis* (green line) and *Leu. mesenteroides* (red line) in three-species mesophilic co-culture. Negative and positive flux values show consumption and production respectively. 84
Figure 3.34. Individual flux rate profiles of *L. lactis* subsp. *cremoris* (blue line) and *S. thermophilus* (red line) in two-species thermophilic co-culture. Negative and positive flux values show consumption and production respectively. 85
Figure 3.35. Individual flux rate profiles of *L. lactis* subsp. *cremoris* (blue line), *L. lactis* subsp. *lactis* (green line) and S. thermophilus (red line) in three-species thermophilic co-culture. Negative and positive flux values show consumption and production respectively. 87

Figure 4.1. Relationship pattern of Prt+ and Prt- variants of *L. lactis* strains in a cheese starter culture in a complex medium. (a) The Prt+ variant supplies the surplus peptides and amino acids for Prt- variants, this has no negative effect on the Prt+ variant, (b) If the growth rate of the Prt- variant is higher than that of the Prt+, microbial abundance of the Prt- variant increases, and this commensal relationship eventually turns into the parasitism 91
Figure 4.2. The co-culture of *L. lactis* SK110 and *L. lactis* B1157 in a complex medium. The metabolisms of these two strains complete each other to produce the flavour metabolite, 3-methylbutanal. Arrows denote the enzymatic activity 92

LIST OF TABLES

Table 2.1. Chemically defined medium (CDM) composition used in this study. 20
Table 2.2. 16S rRNA specific qPCR primers 25
Table 2.3. The comparative reaction, metabolite and gene numbers of the genome-scale metabolic models used in this study. 28
Table 3.1. Essential amino acids obtained via *in-vitro* and *in-silico* analyses..... 36
Table 3.2. Experimental and computational reaction rates of the co-metabolism of citrate and glucose for anaerobic fermentation of *Leu. mesenteroides*. 38
Table 3.3. The yields and carbon balances of the pure cultures 52
Table 3.4. The co-culture compositions in this study. 57
Table 3.5. The yields and carbon balances of the co-cultures 60
Table 3.6. The strain specific parameters used in the substrate uptake kinetics..... 66
Table 3.7. Co-culture specific parameters, C_1 and C_2..... 74

1. INTRODUCTION

Milk has been processed by humankind for millennia, and cheese is one of the oldest fermented dairy foods (Salque et al., 2013). Production of fermentative foods including cheese is rarely based on single species but is rather a combination of different microorganism species as a microbial community. The community members either naturally exist together or are chosen species based on desired product quality. Starter cultures are essential for industrial fermentative food production as they start the fermentation and assure the desired and standard final product. Cheese starter cultures as a microbial community is the scope of this thesis, and metabolic characterization of cheese starter cultures is studied by metabolic network-based microbial community modelling. Compared to the microbial communities in nature, cheese starter cultures are less complex, and they are composed of a couple of lactic acid bacteria, which makes them a good standard for microbial community modelling. In this section, after a brief discussion about lactic acid bacteria and cheese starter cultures, the methodology and mathematics behind the metabolic network-based analyses will be discussed.

1.1. An Overview of Lactic Acid Bacteria and Cheese Starter Cultures

Lactic acid bacteria (LAB) are gram-positive, non-sporulating and facultative anaerobic or microaerophilic organisms, and their main fermentation product is lactic acid (Gaspar et al., 2013; Kleerebezem and Hugenholtz, 2003). The most known habitats of LAB are plants, dairy foods and mucosal surfaces such as the human gastrointestinal system (Kleerebezem and Hugenholtz, 2003; Makarova et al., 2006). LAB belong to the phylum Firmicutes, class Bacilli and order Lactobacillales (Gaspar et al., 2013). Although the most LAB are known as industrially significant and considered as GRAS (Generally Regarded As Safe) organisms, not all bacteria in the order Lactobacillales are industrially relevant and GRAS (Hatti-Kaul et al., 2018). Some industrially important LAB genera are *Lactococcus*, *Streptococcus*, *Leuconostoc*, *Lactobacillus*, *Enterococcus*, *Oenococcus* and *Pediococcus*. They are used in fermented food manufacturing and play an important role in human nutrition as probiotics (de Vos, 1996; Klaenhammer et al., 2008; Kleerebezem and Hugenholtz, 2003; Makarova et al., 2006). Among these organisms,

Lactococcus, *Streptococcus* and *Leuconostoc* species are commonly used in cheese production as starter culture (Cogan and Hill, 1993), which is the main focus of this thesis.

The main reason of the use of LAB in food manufacturing is their rapid lactic acid production during the fermentation, which extends the shelf life of the product as low pH prevents spoilage (de Vos, 1996; Kleerebezem and Hugenholtz, 2003). In addition to food safety and hygiene, lactic acid contributes to the final product characteristic such as texture (de Vos, 1996; Kleerebezem and Hugenholtz, 2003; Muñoz et al., 2011). There are two lactic acid production pathways in the LAB, which are the Embden–Meyerhof–Parnas (EMP) pathway and the phosphoketolase pathway (PKP) (Gaspar et al., 2013) (Fig. 1.1).

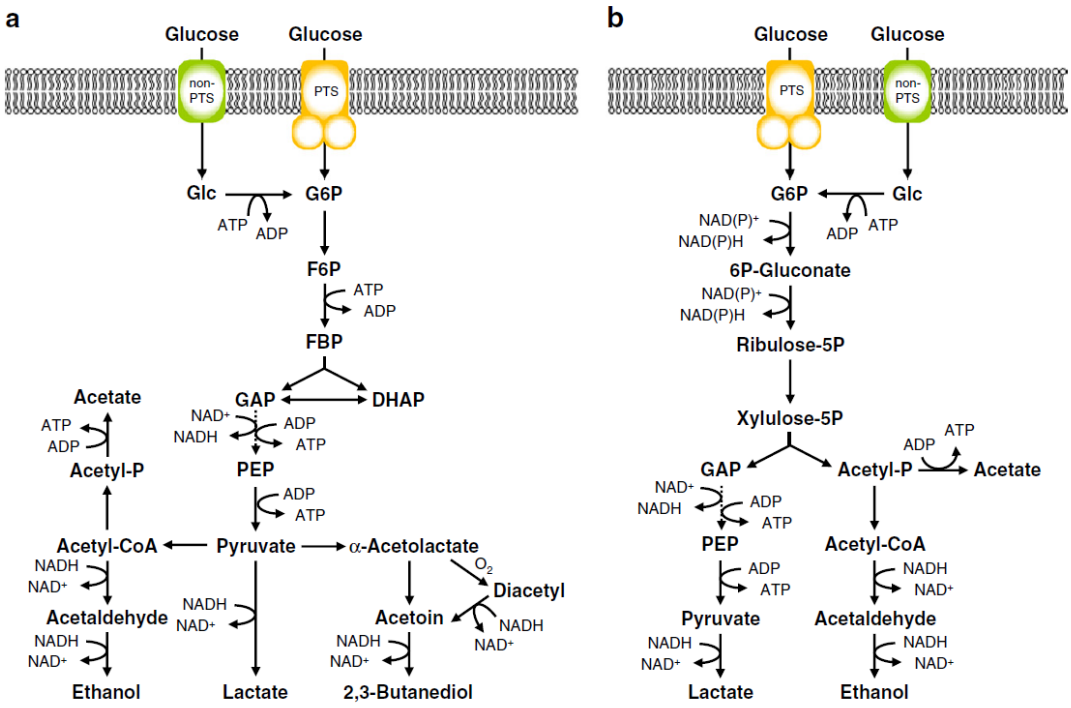

Figure 1.1. Central carbon metabolism pathways of LAB. (A) Embden–Meyerhof–Parnas (EMP) pathway, (B) phosphoketolase pathway (PKP). This figure was taken from (Gaspar et al., 2013)

While the only major product of homolactic fermentation is lactic acid, significant amount of other fermentation products such as formic acid, acetic acid, CO_2 and/or ethanol are also produced in heterolactic fermentation in addition to lactic acid (Gaspar et al., 2013; Kleerebezem and Hugenholtz, 2003). LAB having EMP pathway such as *Lactococcus lactis* and *Streptococcus thermophilus* might exhibit either homolactic or heterolactic fermentation (Giaretta et al., 2018), while only heterolactic fermentation is observed in LAB having PKP such as *Leuconostoc mesenteroides*, and the fermentation through PKP is also called obligate heterolactic fermentation (Ganzle, 2015). Although *L. lactis* and *S. thermophilus* are mostly known as homolactic fermentative species, they can switch to mixed-acid fermentation under some conditions such as the change of the carbon source and continuous cultures at low dilution rate (Flahaut et al., 2013; Giaretta et al., 2018). The redox balance plays an important role on the final product composition (Garrigues et al., 1997).

In homolactic fermentation through the EMP pathway, 1 mole of glucose is broken down into 2 moles of lactic acid, leading to the production of 2 moles of ATP. In obligate heterolactic fermentation, however, 1 mole of lactic acid is produced per 1 mole of glucose via the PKP, which yields only one ATP per glucose (Ganzle, 2015; Gaspar et al., 2013). In organisms with active PKP, lactic acid production acts as an ATP production source while ethanol production acts as redox balance under anaerobic conditions. Under cases of alternative electron sinks, such as aerobic conditions (Plihon et al., 1995) and co-metabolism of citrate (Schmitt and Divies, 1992), ethanol can be substituted by acetate, which yields extra ATP.

In traditional ways, cheese is made by LAB which are naturally present in milk or by the back-slopping technique, which is adding small portion of a previous batch of cheese to milk. In industrial cheese production, on the other hand, starter cultures, which are defined mixtures of purified and characterized LAB, are used to standardize the bulk production (Cogan and Hill, 1993; Leroy and De Vuyst, 2004; Powell et al., 2011). Acidification and flavour compound production are the main functions of the starter cultures in the cheese making. Lactic acid produced by LAB helps coagulation of the caseins in milk to form curd which affects the final moisture content of cheese, and consequently also affects the product texture (Powell et al., 2011). Low pH is the result of lactic acid production, and it prevents the growth of undesired microorganisms spoiling the milk fermentation or

pathogen organisms (Powell et al., 2011). Furthermore, LAB produce several flavour and aroma compounds that give the specific tastes of different cheeses (Smid and Kleerebezem, 2014; Smit et al., 2005; Yvon and Rijnen, 2001).

Cheese making is a multi-step process; in addition to milk fermentation carried out by starter LAB, during the ripening of cheese -and especially for artisanal cheeses- in the long term, other microorganisms such as non-starter LAB, propionic acid bacteria and even yeast might also contribute to the final form of the cheese (Blaya et al., 2018), but this study only focusses on the LAB used as starter cultures in industrial cheese production.

Cheese starter cultures are composed of different LAB changing according to cheese being made and they can be distinguished as mesophilic and thermophilic starter cultures (Cogan and Hill, 1993). Mesophilic starter cultures are used in the cheese productions requiring the moderate temperature (~30°C) such as Cheddar and Dutch type cheese (Cogan and Hill, 1993; Smid et al., 2014). Mesophilic starter cultures consist of *L. lactis* and *Leu. mesenteroides* strains in which main functions are acidification and flavour formation, respectively (Erkus et al., 2013; Smid et al., 2014). Thermophilic starter cultures are used in the cheese productions requiring higher temperature such as Swiss and Italian cheese and are dominated by *L. lactis* and *S. thermophilus* strains (Cogan and Hill, 1993; Powell et al., 2011). A successful cheese production with desired functions such as aroma and texture depend on the starter cultures being used. The metabolic capacity of the individual organisms in the starter cultures and their co-cultures should be well characterized. Therefore, metabolic network-based analyses, with the advent of the next generation sequencing technology, have been recently used for the characterization of LAB used in starter cultures (de Vos, 2011; Teusink et al., 2011; Teusink and Molenaar, 2017), which give a more holistic point of view than classical microbiological approaches to better understand both species and the co-culture level metabolism of cheese starter cultures.

1.2. Metabolic Network-Based Analysis of LAB

Understanding the metabolism of LAB may help to efficiently use them in the industry. Although the classical studies investigating LAB at external metabolite level give important insights for their metabolism, systems biology approaches (Kitano, 2002; Nielsen, 2017) are more promising to decipher the full metabolic potential of LAB at a genome scale. New generation sequencing technologies give an unprecedented view of the biodiversity and metabolic capacity of the microorganisms in food fermentation (Smid and Hugenholtz, 2010), and various studies investigating the genomic characterization of LAB strains have been published (Douillard and de Vos, 2014; Makarova et al., 2006; O'Sullivan et al., 2009; Siezen and Bachmann, 2008).

A metabolic network defines a set of biochemical reactions denoting interactions between compounds and their stoichiometry in the reactions. A metabolic network can be either a local pathway which consists of known reactions from literature, or a genome-scale metabolic network which is reconstructed using whole genome sequence. Finally, a genome-scale metabolic model (GSMM) systematizes the genome-scale metabolic network into a mathematical framework (Bordbar et al., 2014).

GSMMs are very useful tools to investigate the metabolic patterns and capacities of organisms, and they have already been developed for quite a number of LAB, such as probiotic strains *Lactobacillus plantarum* (Teusink et al., 2006), *Lactobacillus casei* (Vinay-Lara et al., 2014); dairy-origin strains *L. lactis* subsp. *lactis* (Oliveira et al., 2005), *L. lactis* subsp. *cremoris* (Flahaut et al., 2013), *S. thermophilus* (Pastink et al., 2009), *Leu. mesenteroides* (reconstructed for this study) and a plant-origin strain *Leu. mesenteroides* (Koduru et al., 2017). GSMMs are not only used to investigate the metabolic pattern of an organism, but also to compare the metabolic capacities of different organisms. The comparison of the dairy-origin LAB using GSMMs is also important for better understanding of the fermentation of the dairy foods where different LAB take part in co-culture.

The metabolic networks, thereby GSMMs, their reconstruction and metabolic network-based analyses for pure and microbial communities are discussed in the following sections.

1.2.1. Metabolic network reconstruction and constraint-based analysis of metabolic networks

As science continues to develop itself, collective scientific knowledge increases. Databases used in biotechnology collect such cumulative knowledge/data and share them with the researchers wishing to make further research. There are several online metabolic network databases such as KEGG (Goto et al., 1997), BIGG (King et al., 2015b), MetaCyc (Caspi et al., 2015), BRENDA (Scheer et al., 2010), ModelSEED (Henry et al., 2010), which store the data of metabolic pathways, their biochemical reactions and the genes/enzymes related to these reactions. And the online and offline tools such as ModelSEED (Henry et al., 2010) , AuReMe (Aite et al., 2018), CarveMe (Machado et al., 2018), Merlin (Dias et al., 2010) and RAVEN (Wang et al., 2018) gather the reactions from the databases mentioned above based on the genome annotation of the organism of interest to reconstruct metabolic network models.

The metabolic network models reconstructed by the reconstruction tools, which are also called draft metabolic network models, require additional manual curation. The manual curation of a draft metabolic network model is carried out according to experimental evidences, and some of the curation steps are adding extra reactions such as a species-specific biomass reaction and adding the reactions missed by the reconstruction tool. A protocol was published to reconstruct a high quality and robust genome-scale metabolic model (Thiele and Palsson, 2010), describing each step necessary to build a genome-scale metabolic model. A genome-scale metabolic model of *Leu. mesenteroides* ATCC 19254 was also reconstructed in this thesis study and reconstruction steps including manual curation were discussed in the following sections.

One important issue that is worth to mention is the synonym names used to refer to metabolic network models, and the most common ones are metabolic model, metabolic network model, genome-scale metabolic network model or genome-scale metabolic model, which denotes the metabolic model composed of all reactions encoded by whole genome, and constraint-based metabolic model. Flux balance analysis (FBA) is a constraint-based optimization method and it analyses a metabolic model in quantitative manner. FBA calculates the metabolic flux rates through a metabolic network, which

enables the prediction of, for instance, the growth rate of an organism or the production rate of an industrially important metabolite (Orth et al., 2010).

Methodology and mathematics behind the FBA were illustrated in Fig. 1.2 through a simple toy model. Metabolic reactions in the metabolic models are converted into a stoichiometric matrix in which rows and columns represent metabolites and reactions respectively (Fig. 1.2-D). FBA assumes steady-state conditions, which means that the concentrations of the metabolites in a cell are constant and the rate of change of the metabolites are zero over time (Bordbar et al., 2014; Maarleveld et al., 2013). At steady state, flux distribution vector (reaction rates of all reactions in the model, v) is determined by $S.v=0$, which defines a linear equation set (Fig. 1.2-F). As degrees of freedom is more than zero for this linear equation set, the flux distribution is estimated by linear programming (LP) (Fig. 1.2-G). The most common objective function (C^TV) of the linear optimization problem of $S.v=0$ is biomass production. Solution space of this optimization problem can be narrowed down by some constraints such as reaction boundaries (lower and upper bounds of the reactions, $LB \leq v \leq UB$ in Fig. 1.2-G) and experimentally obtained flux rates (Kauffman et al., 2003).

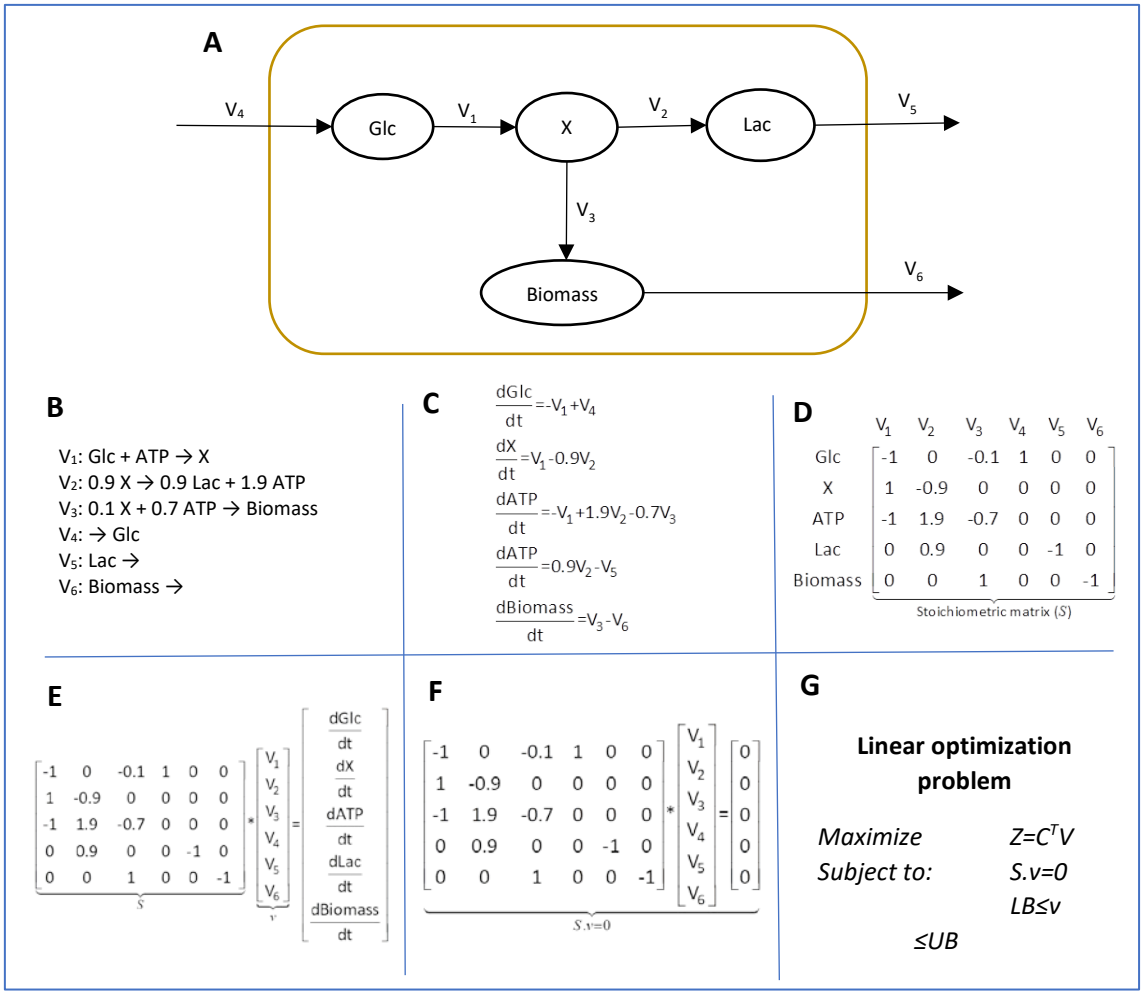

Figure 1.2. Methodology for constraint-based metabolic modelling. A) Toy model system comprising 6 reactions and 5 compounds. B) Reactions in the toy model. C) Differential mass balance equations. D) Stoichiometric matrix. E) Dynamic mass balance in matrix format. F) Steady-state mass balance in matrix format. G) Linear optimization problem.

Because of alternate optima, which means the existence of more than one optimal solution with the same objective value, the flux distribution estimated by FBA is actually only one solution assuring the maximized objective. Flux variability analysis (FVA) calculates the minimum and maximum values of all reaction rates (flux span) at the optimal objection function value (Mahadevan and Schilling, 2003). Mathematical description of the linear programming for FVA can be written as follows:

for i = 1 : # of reaction

Maximize and minimize	V_i
Subject to:	$S.v=0$
	$C^TV=Z_{obj}$
	$LB \leq V \leq UB$

Eq. 1.1

1.2.2. Dynamic flux balance analysis (dFBA)

Output of classical FBA is flux distribution, which is the reaction rates of an organism in steady-state conditions, and FBA simulations are compared with experimental flux values at steady-state conditions, such as production rate of a fermentation product and growth rate in continuous culture, to check for their predictive capacity. However, FBA cannot simulate the dynamics of metabolites such as changing metabolite concentrations in batch culture over time. Hence, to simulate the dynamic conditions such as batch fermentation cultures, dynamic flux balance analysis (dFBA) is applied. dFBA is a constraint-based metabolic network analysis, combining FBA and kinetic modelling (Watanabe et al., 2018). Compared to simplified unstructured models having limited predictive capacity (e.g. Monod model which relates the growth rate to the concentration of a single growth-limiting substrate), dFBA models can predict the dynamic profiles of concentrations of biomass and all metabolites in a system (Hoffner et al., 2013). There are two main dFBA approaches, which are dynamic optimization approach (DOA) and static optimization approach (SOA) (Mahadevan et al., 2002). In the DOA, optimization problem is solved over the entire time of batch to obtain flux and metabolite concentration profiles (Mahadevan et al., 2002). Formulation of DOA results in nonlinear programming (NLP), and it is given below (Kleessen and Nikoloski, 2012):

$$\textit{Maximize} \quad \int_{t_0}^{t_1} f(x)dx$$

$$\textit{Subject to:} \quad \frac{dX}{dt} = S.v$$
$$v_{\min} \le v \le v_{\min}$$
$$x_{\min} \le x \le x_{\min}$$
$$X(t_0) = X_0$$

Eq. 1.2.

where *V, X* and X_0 are the vectors of reaction fluxes, metabolite concentrations and initial concentrations of the metabolites over time, respectively. Compared to SOA, DOA is rarely used because of the intractability of NLP (Gomez et al., 2014).

SOA divides the batch time into several time intervals and solves the optimization problem (i.e. classical FBA) for each time interval, which means SOA applies several LPs to estimate the process dynamics (Mahadevan et al., 2002). Simulation methodology of dFBA with SOA is illustrated in Fig. 1.3 for a model constrained by a substrate uptake kinetics, which is a function of metabolite concentration. In each time interval (i.e. each iteration for the numeric solution of ODE set), substrate uptake rates constraining the metabolic model change based on the substrate uptake kinetics, which is the function of metabolite (substrate and/or product) concentration. Subsequently, metabolic model embedded into dynamic mass balance equations (ODE set) estimates the flux distribution, and this flux distribution is used in ODE set to calculate the biomass and metabolite concentrations for each time interval.

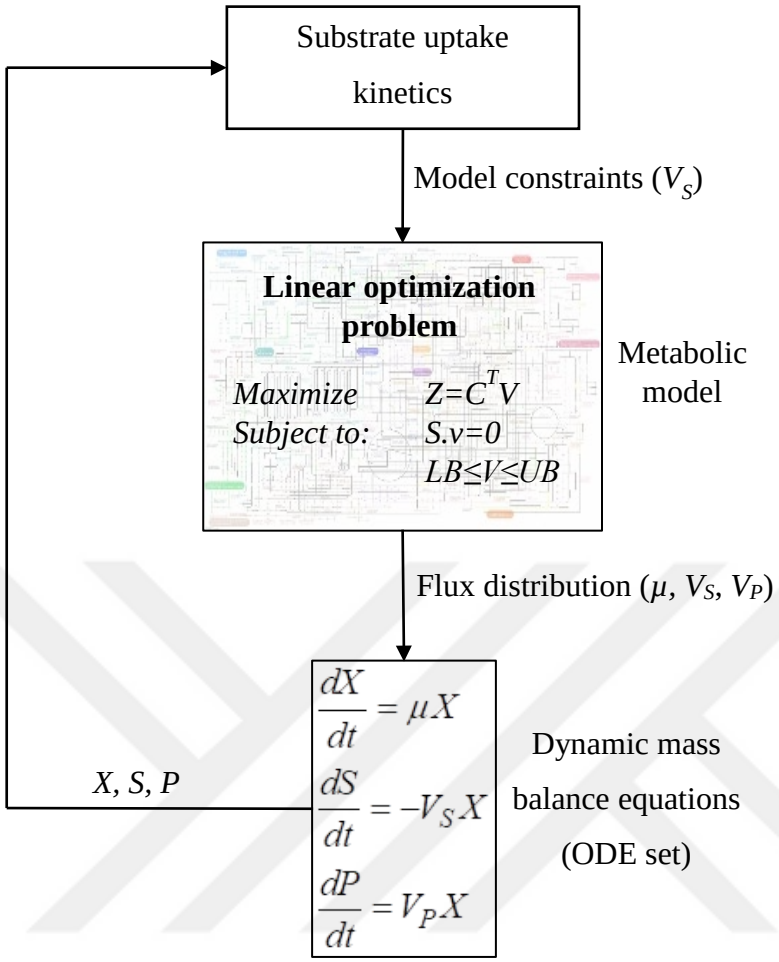

Figure 1.3. dFBA methodology with static optimization approach (SOA). *X*, *S* and *P* denote concentrations of biomass, substrates and products. (Note that: the term "*S*" in the metabolic model box represents stoichiometric matrix as mentioned in the text above)

1.2.3. Microbial community metabolic modelling

There are basically two approaches for metabolic network-based analysis of microbial communities, which are (i) supra-organism metabolic modelling approach that evaluates a whole microbial community as a single organism and (ii) multi-species metabolic modelling approach that considers individual microorganisms in the consortia and their metabolic interactions (Fig. 1.4).

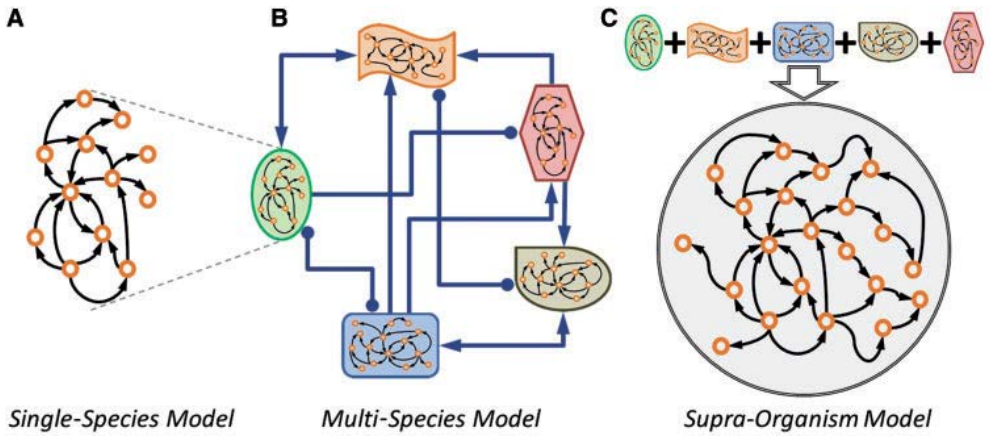

Figure 1.4. Microbial community metabolic modelling approaches. (A) Single-species metabolic models represent the set of biochemical reactions. (B) Multi-species metabolic models integrate the individual metabolic networks and their interactions. (C) supra-organism metabolic models have single metabolic network reconstructed using metagenome sequencing. This figure was taken from (Borenstein, 2012).

1.2.3.1. Supra-organism metabolic modelling

Supra-organism metabolic modelling takes whole microbial community as a single organism, which is also called pan-organism (Borenstein, 2012; Hanemaaijer et al., 2015; Succurro and Ebenhoh, 2018). This approach is used for complex microbial communities such as gut and soil microbiota, and metagenomic data is used to reconstruct the supra-organism metabolic network. Metagenomics defines the investigation of genetic material of microbial communities, and metagenomic data is obtained from entire genome of a microbial community using next generation sequencing technology and bioinformatics tools (Wooley et al., 2010). In the first supra-organism metabolic model in literature (Rodríguez et al., 2006), the authors reconstructed a single stoichiometric matrix including the most common fermentative pathways such as lactate, acetate, ethanol, CO_2, propionate, butyrate and H_2 production pathways, which are catalysed by a mixed culture and biomass production of mixed culture. Others (Greenblum et al., 2012) used metagenomic data of human gut microbiome to reconstruct community-level metabolic networks, and they identified topological differences of these metabolic networks belonging to different people groups having obesity and inflammatory bowel disease. In another study (Tobalina et al., 2015), meta-proteomic data was used instead of meta-

genomics to reconstruct context-specific metabolic network of a naphthalene degrading bacterial community, and FBA was applied for the context-specific metabolic network reconstructed.

Although supra-organism metabolic models are able to better understand community-level metabolic capacity of a microbial community, these models do not consider the metabolic behaviours of community members and their interactions.

1.2.3.2. Multi-species metabolic modelling

Compared to the microbial communities reconstructed as supra-organism metabolic models, microbial communities reconstructed as multi-species metabolic models are less complex in terms of number of involved microorganism types, and such microbial communities are mostly called co-cultures, which can be also grown in laboratory conditions. Unlike supra-organism modelling, multi-species metabolic modelling allows compartmentalized metabolic network, and metabolic networks of the individual organisms are integrated to reconstruct a multi-species metabolic model (Biggs et al., 2015; Gamboa-Rueda et al., 2015). Multi-species metabolic modelling approach can be separated into two sub-approaches, which are multi-species metabolic modelling under steady-state and dynamic conditions. If a co-culture grows under steady-state conditions, there is a metabolic dependency such as mutualism or cross-feeding among the co-culture members, and the first sub-approach is based on this fact. Community flux balance analysis (cFBA) (Khandelwal et al., 2013) integrates the genome-scale metabolic networks of individual community members, and it is formulated such that exchange reactions of the individual organisms are combined to allow metabolic interaction between organisms and environment (Fig. 1.5.). cFBA assumes balanced growth rates of individual organisms because of metabolic dependency between organisms. Hence, individual-level and community-level growth rates are equal, which is also single objective function. In addition to individual and community level metabolic capacity investigation, cFBA enables the prediction of the effect of the relative microbial abundance on community growth.

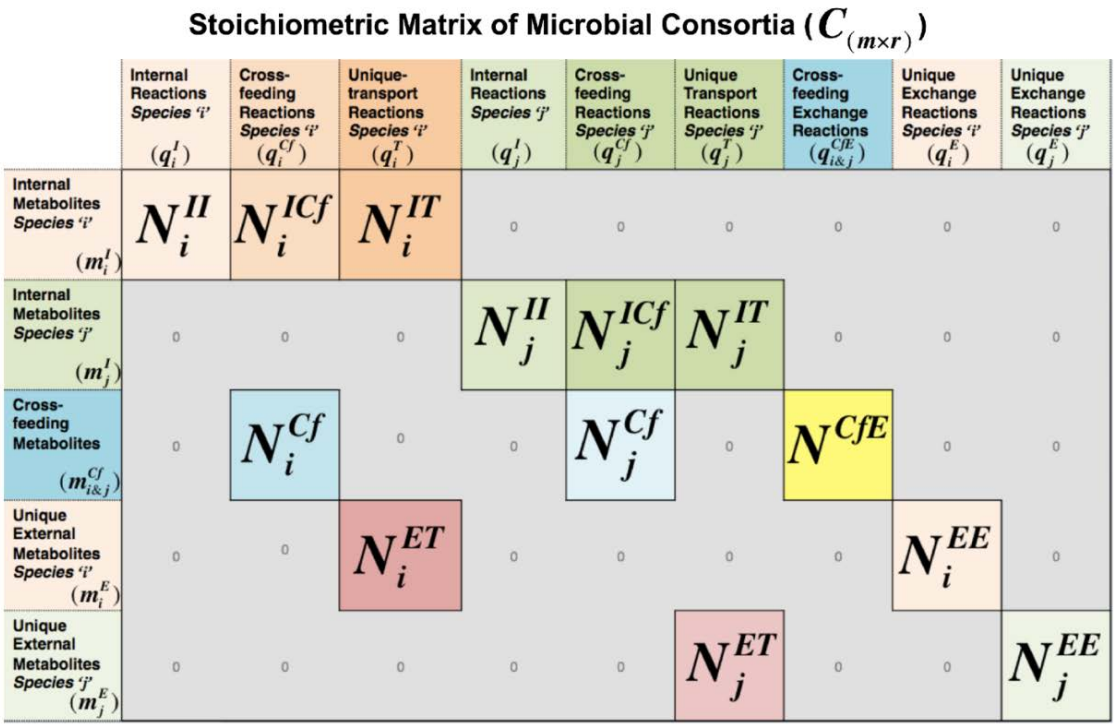

Figure 1.5. Community flux balance analysis (cFBA) framework. cFBA integrates the stoichiometric matrices of individual organisms to reconstruct a community model. This figure was taken from (Khandelwal et al., 2013)

Another steady-state multi-species metabolic modelling framework is OptCom (Zomorrodi and Maranas, 2012). OptCom is suitable for well-characterized communities and it enables to simulate the different types of metabolic interactions such as mutualism, commensalism, parasitism and competition. OptCom applies bilevel optimization, where inner optimization is maximization of growth of individual organisms and, outer optimization is maximization of community growth.

The dynamic multi-species metabolic modelling (DyMMM) or dynamic co-culture metabolic modelling is basically dFBA framework with static optimization approach, which is extended for microbial communities (Henson and Hanly, 2014). The dynamic multi-species metabolic modelling framework is illustrated for three-species co-culture in Fig. 1.6. Like dFBA, output of the DyMMM framework is the dynamic biomass and metabolite concentration profiles, which can be both species and community-level concentrations. Because metabolites consumed and produced are shared by all

community members, DyMMM allows metabolic interactions such as competition and cross-feeding. In this approach, individual metabolic models are constrained by individual substrate uptake kinetics, which are a function of community level metabolite concentrations. After the independent solution of the individual models by FBA, flux distributions are used in dynamic mass balance equations. Every iteration for the solution of the ODE set in dynamic mass balance equations gives new set of metabolite concentrations, which are subsequently used in substrate uptake kinetics (Fig. 1.6.). The dynamic multi-species metabolic modelling approach was used before in several studies (Hanemaaijer et al., 2017; Hanly and Henson, 2011; Zhuang et al., 2011; Zhuang et al., 2012).

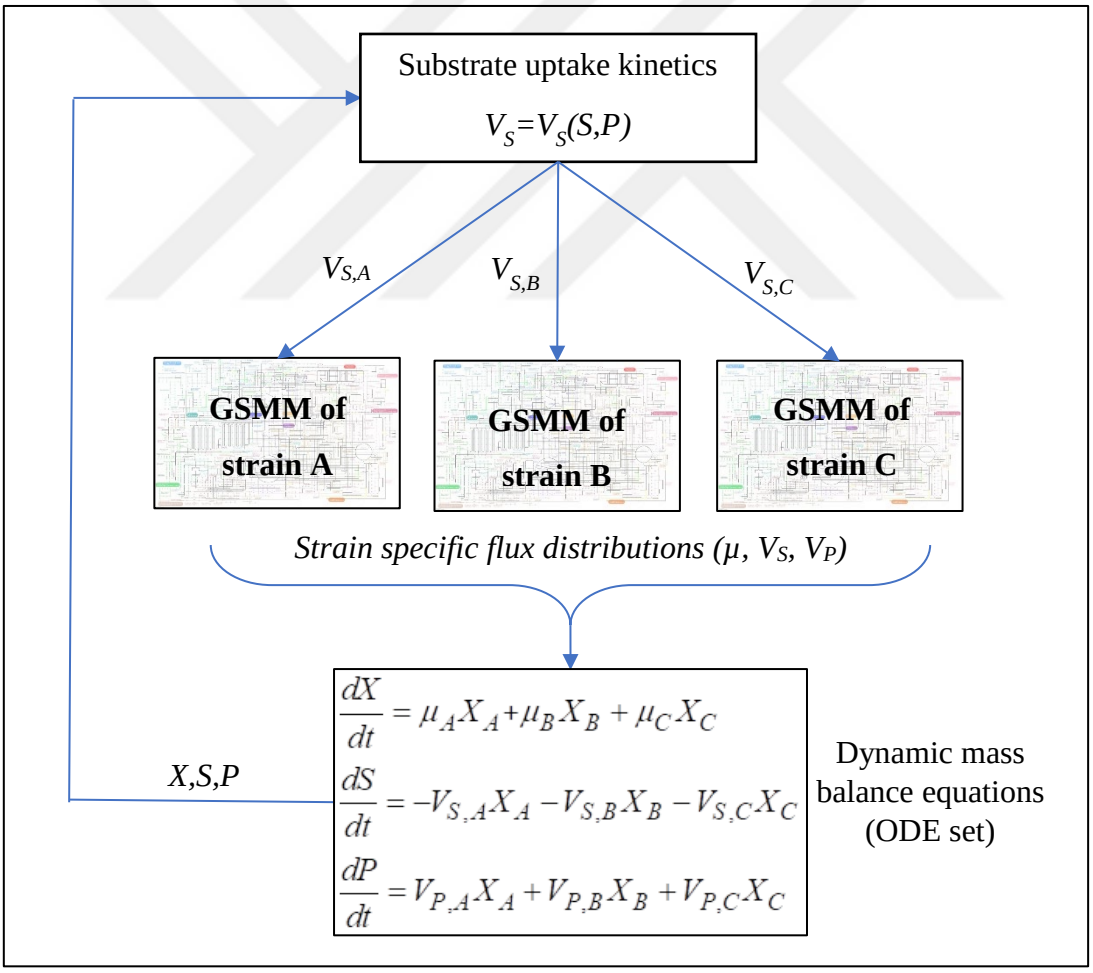

Figure 1.6. Dynamic multi-species metabolic modelling framework for three-species microbial community. *X*, *S*, *P* denote concentrations of biomass, substrates and

products; and μ, V_S and V_P denote growth, substrate uptake and product production rates, respectively.

1.3. Aim and Overall Design of This Study

The Monod model relates the microbial growth rate (μ) to the concentration of a single growth-limiting substrate (S) with the parameters μ_{max} and K_S (Monod, 1949) as shown in Eq. 1.3.

$$\mu = \frac{\mu_{\max} S}{K_S + S} \qquad \text{Eq. 1.3.}$$

The Luedeking-Piret model is based on the product formation which is proportional to growth, and it relates product rate (q_P) to growth rate (μ) with a linear equation with the parameters A and B (Luedeking and Piret, 1959) as shown in Eq. 1.4.

$$q_p = A\mu + B \qquad \text{Eq. 1.4.}$$

Both the Monod and the Luedeking-Piret models are commonly used for the unstructured modelling of LAB fermentations, and they can explain the fundamental relationships between microbial growth, substrate consumption and product formation. Modified versions of the Monod and the Luedeking-Piret models applied to LAB fermentation, for example a model considering inhibitory compounds, can be found elsewhere (Bouguettoucha et al., 2011). On the other hand, the dynamic genome-scale metabolic models have a more comprehensive predictive capacity compared to the simple microbial kinetic models such as the Monod and the Luedeking-Piret models. A dynamic genome-scale metabolic model considers the entire metabolic stoichiometry and enables to relate all the substrates and products not only to growth but also to each other.

This thesis study aims for a better understanding of the dynamics in the LAB fermentations and metabolic capacities of cheese starter cultures at both single species and co-culture level using metabolic network-based analysis. To that end, LAB commonly used in cheese starter cultures were grown in a batch bioreactor, and experimental results were used to estimate the parameters of the dynamic metabolic models. Taking advantage of the dynamic metabolic modelling, it aimed to obtain more data on the fermentations, which previously could not be obtained by the experimental methods used. The individual compound profiles of LAB in the co-cultures, which also enables to estimate the potential metabolic interactions among LAB in the co-cultures, were also predicted by the metabolic models.

This study was designed in two parts: experimental and computational (Fig. 1.7.). The experimental part consists of bioreactor experiments of both pure and co-cultures and subsequent experimental analyses, while the computational part consists of reconstruction and analysis of dynamic metabolic models for pure and co-cultures.

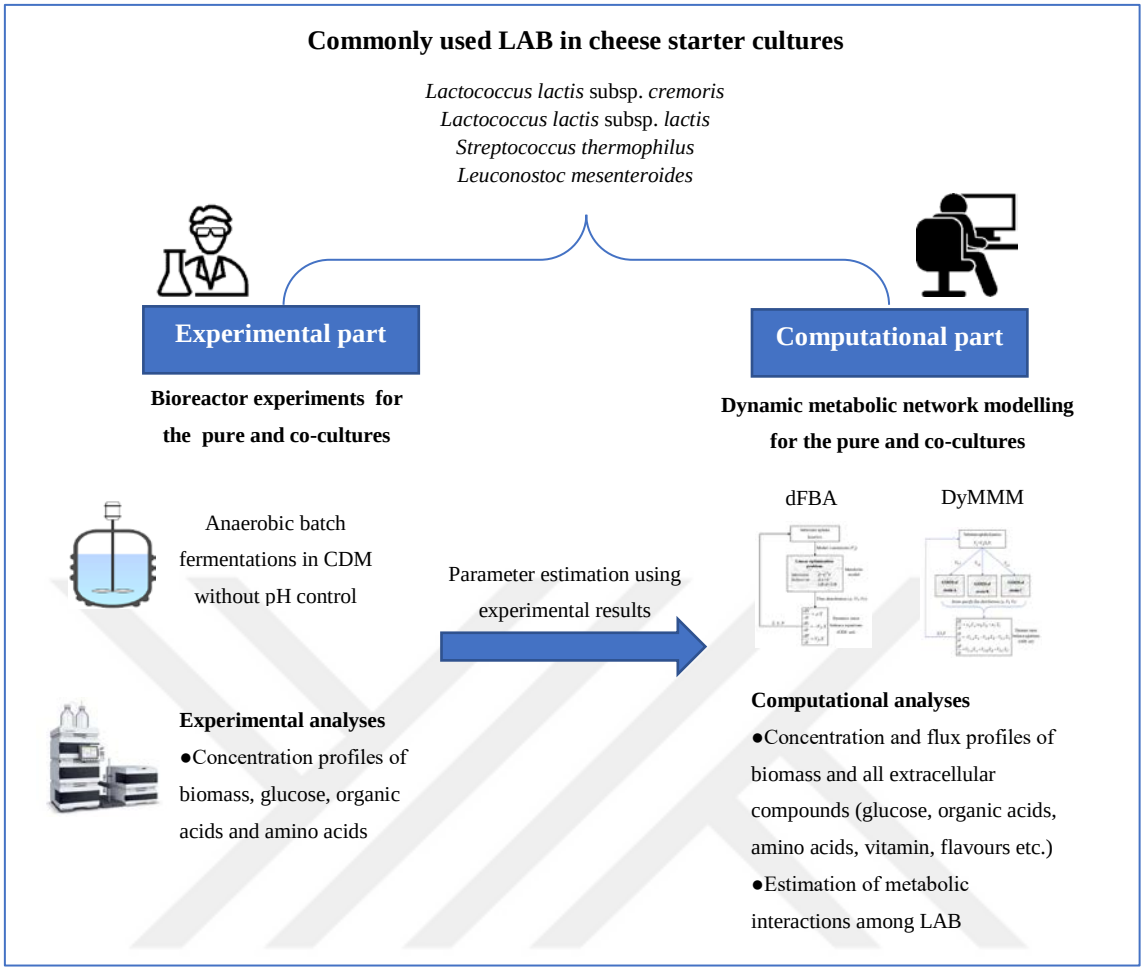

Figure 1.7. Overall design of the study. dFBA: dynamic flux balance analysis, DyMMM: dynamic multi-species metabolic modelling.

In the experimental part, LAB species of *L. lactis* subsp. *cremoris*, *L. lactis* subsp. *lactis*, *Leu. mesenteroides* and *S. thermophilus*, which are commonly used LAB in cheese starter cultures, were grown in pure and co-cultures in batch cultures with chemically defined medium under anaerobic conditions. The co-cultures composed of *L. lactis* and *Leu. mesenteroides* species and the co-cultures composed of *L. lactis* and *S. thermophilus* species were assumed to represent mesophilic and thermophilic starter cultures, respectively. In bioreactor experiments, pH was not controlled to mimic cheese fermentation by starter cultures in which pH was allowed to follow its natural course (Bachmann et al., 2009; Cogan et al., 2007). Biomass, glucose as a carbon source, organic acids and amino acids concentration profiles of the pure and co-cultures and relative

microbial abundance profiles of the co-cultures were obtained experimentally. Relative microbial abundance in a microbial community gives important insights about the community dynamics such as suppression or domination of the individual organisms and related changes in the medium composition. With classical microbiological methods, relative microbial abundance is obtained by counting the colony forming units (CFU) of survived microorganisms on agar plate with a selective growth medium (Bellengier et al., 1997). Yet, the microorganisms used in this study are phylogenetically very close species, which are hardly distinguished using a selective medium. Thus, a molecular-based method (i.e. qPCR) was employed instead of CFU-based methods to estimate the relative abundance ratio.

In the computational part, pure and co-culture experiments were then simulated by metabolic network-based analyses. Pure cultures were simulated by dFBA, while co-cultures were simulated by the dynamic multi-species metabolic modelling approach. Undissociated lactic acid which is the protonated form of lactic acid and increasingly formed by low pH, was the rate limiting compound for all batches. Therefore, the substrate uptake kinetics in the dynamic models was defined with an empirical equation as a function of undissociated lactic acid. Strain-specific parameters used in substrate uptake kinetics were estimated using pure culture experiments and they were also used in dynamic co-culture models. Furthermore, a genome-scale metabolic model of dairy-origin *Leu. mesenteroides*, which was also used in co-culture models, was reconstructed for the first time in this study. From genome sequences to manual curation of the metabolic model, all steps of the genome-scale metabolic model reconstruction were also discussed for this study.

2. MATERIALS AND METHODS

2.1. Organisms and Growth Medium

Lactic acid bacteria used in this study were *Lactococcus lactis* subsp. *cremoris* MG1363, *Lactococcus lactis* subsp. *lactis* IL1403, *Streptococcus thermophilus* LMG 18311 and *Leuconostoc mesenteroides* subsp. *cremoris* ATCC 19254, which are dairy-origin lactic acid bacteria used in several experimental and metabolic network-based studies (Flahaut et al., 2013; Oliveira et al., 2005; Pastink et al., 2009; Solopova et al., 2012). The organisms were stored at -80°C in M17 medium (Terzaghi and Sandine, 1975) for *L. lactis* and *S. thermophilus* strains and in MRS medium (De Man et al., 1960) for *Leu. mesenteroides*, and both media were supplemented with 0.5% glucose and 15% glycerol. Chemically defined medium (CDM) described elsewhere (Otto et al., 1983) and modified by others (Poolman and Konings, 1988) was used for the preparation of the inoculum and for the fermentation cultures (Table 2.1), and the CDM was filter-sterilized with 0.22 µm filters. This CDM was firstly described for *L. lactis* and then used for several LAB in literature with original recipe or by omitting some components based on the minimal requirements of related microorganism (Kim et al., 2012; Letort and Juillard, 2001).

Table 2.1. Chemically defined medium (CDM) composition used in this study.

	(g/L)		(g/L)
Main Ingredients		DNA precursor mix	
Glucose	10	Adenine	0.01
K_2HPO_4	2.5	Guanine	0.01
KH_2PO_4	3	Xanthine	0.01
Na-acetate	1	Uracil	0.01
$(NH_4)_3$-citrate	0.6	Vitamins	
Ascorbic acid	0.5	Pyridoxamine-HCl	0.005
Amino acids		D-biotin	0.01
Alanine	0.24	6,8-thioctic acid	0.0025
Arginine	0.125	Pyridoxine-HCl	0.002

Table.2.1. (Continued)

Asparagine	0.35	Nicotinic acid	0.001
Aspartate	0.46	Ca-(D+) pantothenate	0.001
Cysteine	0.25	Riboflavin	0.001
Glutamate	0.4	Thiamin-HCl	0.001
Glutamine	0.39	Vitamin B_{12}	0.001
Glycine	0.175	Na-4-aminobenzoate	0.01
Histidine	0.15	Orotic acid	0.005
Isoleucine	0.21	2-deoxythymidine	0.005
Leucine	0.475	Inosine	0.005
Lysine	0.44	Folic acid	0.001
Methionine	0.125	Trace metals	
Phenylalanine	0.275	$MgCl_2 \times 6\ H_2O$	0.2
Proline	0.675	$CaCl_2 \times 2\ H_2O$	0.05
Serine	0.34	$MnSO_4$ x H_2O	0.028
Threonine	0.225	$FeCl_2 \times 4\ H_2O$	0.005
Tryptophan	0.05	$ZnSO_4 \times 7\ H_2O$	0.005
Tyrosine	0.29	$CoCl_2 \times 6\ H_2O$	0.0025
Valine	0.325	$CuSO_4 \times 5\ H_2O$	0.0001

2.2. Fermentation Conditions

Stocked *L. lactis* and *S. thermophilus* strains were transferred to M17 agar plates including 0.5 % glucose, and stocked *Leu. mesenteroides* was transferred to MRS agar plates including 0.5 % glucose to obtain single colonies for inoculum preparation. Agar plates of *L. lactis*, *S. thermophilus* and *Leu. mesenteroides* strains were kept in incubator at 30°C, 37°C and 30°C, respectively. Single colonies of *L. lactis* and *S. thermophilus* strains were observed on agar plates after overnight incubation, while single colonies of *Leu. mesenteroides* were observed after two overnight incubations. The single colonies were then transferred to 50 ml inoculation medium in 50-ml falcon tubes and incubated in static culture with the same temperatures of the agar plates mentioned above.

Bioreactor experiments required for the study of genome-scale metabolic model reconstruction of *Leu. mesenteroides* was carried out in a 5-liter bioreactor (Minifors HT, Switzerland), while other pure and co-culture experiments of *L. lactis*, *S. thermophilus* and *Leu. mesenteroides* strains were carried out in 1-liter bioreactors (Biostat Q, B. Braun Biotech International).

2.2.1. Fermentation conditions for the study of the genome-scale metabolic network reconstruction of *Leu. mesenteroides*

Leu. mesenteroides was fermented under anaerobic conditions in a 5-liter stirred tank bioreactor (Minifors HT, Switzerland) with a working volume of 3 litters. Fermentation medium was deoxygenized with filter-sterilized pure N_2 supply before inoculation, and anaerobic condition was maintained by filter-sterilized pure N_2 supply with 0.5 vvm during fermentation. The bioreactor was inoculated with 2% (v/v) inoculum culture grown till late exponential phase. Anaerobic fermentation was carried out at constant temperature (30°C) with 100 rpm mixing rate and without pH control (starting pH: 6.8).

2.2.2. Fermentation conditions for the pure and co-cultures

Pure and co-culture fermentations were carried out under anaerobic conditions in a 1-litre stirred tank bioreactor (Biostat Q, B. Braun Biotech International) with a working volume of 0.6 litres at constant temperature and without pH control (initial pH: 6.8). Pure cultures of *L. lactis*, *Leu. mesenteroides* and *S. thermophilus* strains were fermented at 30°C, 30°C and 37°C, respectively, while mesophilic co-cultures comprised of *L. lactis* and *Leu. mesenteroides* strains and thermophilic co-cultures comprised of *L. lactis* and *S. thermophilus* strains were grown at 30°C and 33°C, respectively. Fermentation medium was deoxygenized with filter-sterilized pure N_2 supply before inoculation and there was no gas supply after inoculation. Maintenance of the anaerobic conditions was assumed with slow mixing (50 rpm). For both pure and co-cultures, the bioreactor was inoculated with 2% (v/v) inoculum culture grown till late exponential phase. Starting biomass compositions of the co-cultures were 1:1 (OD:OD) and 1:1:1 (OD:OD:OD) for two and

three-species co-cultures respectively. For each different batch experiments (pure and co-cultures), two independent culture replicates were run.

2.3. Experimental Analyses

2.3.1. Analysis of biomass and extracellular compounds

Biomass concentration was determined using optical density (OD) measurements of fermentation culture at 600 nm, which was then correlated with corresponding biomass dry weight (gDW) values via a calibration graph. Based on this, one unit of optical density at 600 nm was taken to be equivalent to 0.37 g dry cell weight/l for all species, since they had similar OD/gDW slopes. Culture samples were centrifuged at 10000g for 10 minutes to separate biomass and supernatant, and cell free supernatant was used for glucose, organic acid and amino acid analyses.

Glucose concentration was determined by reducing sugar analysis (Miller, 1959). Organic acid (lactic, formic, acetic and citric acids) concentrations were determined using HPLC with anion exchange column (IC-Pak Ion exclusion column (7 µm, 7.8 x 300 mm, Waters)) and UV detector with 2 mM H_2SO_4 as mobile phase and with 0.5 ml/min flow rate.

Amino acids were quantified using HPLC with pre-column derivatization using phenyl isothiocyanate (PITC), following a modified version of the method described in literature (Shi et al., 2013). HPLC (LC20AD, Shimadzu) was equipped with a UV detector (254 nm) and XSelect HSS C18 column (5 µm, 4.6 mm x 250 mm, Waters) maintained at 36°C. Two mobile phases (0.1 M pH 6.5 sodium acetate buffer solution: acetonitrile (97:3(v/v)) and acetonitrile: water (4:1(v/v)) are used, at 0.9 ml/min.

Undissociated lactic acid concentration increases with decreasing pH, and it is calculated via Henderson–Hasselbalch equation (Bouguettoucha et al., 2011) described in Eq. 2.1.

$$[LacH] = \frac{[Lac]}{1 + \exp(pH - pKa)} \qquad \text{Eq. 2.1}$$

where [*LacH*], [*Lac*] and *pKa* are undissociated lactic acid concentration, total lactic acid concentration and logarithmic acid dissociation constant, respectively, and pKa is 3.86 for lactic acid (https://pubchem.ncbi.nlm.nih.gov/compound/Lactic-acid).

CO_2 production of *L. lactis* and *S. thermophilus* strains showing homolactic fermentation pattern was assumed to be negligibly small compared to the total carbon outflow under anaerobic conditions as also stated in the literature (Jensen et al., 2001). Molar concentrations of ethanol and CO_2 produced by *Leu. mesenteroides* were estimated based on the rate of glucose consumption following the stoichiometry observed in heterolactic fermentation of *Leu. mesenteroides* under anaerobic conditions with glucose as the only carbon source (Dols et al., 1997; Schmitt et al., 1992; Starrenburg and Hugenholtz, 1991), and this ratio was taken as rates of glucose:ethanol:CO_2 = 1:1:1. For citrate and glucose co-metabolism of *Leu. mesenteroides*, production of one mole CO_2 was also considered per one mole citrate consumed.

2.3.2. Carbon balance

The carbon balance was determined based on the sum of overall biomass produced and extracellular compounds consumed or produced (glucose, organic acids, ethanol and CO_2) (see Appendix H for detailed carbon balance calculation).

2.3.3. Estimation of the relative microbial abundance in co-cultures

Quantitative-PCR (qPCR) method was employed for quantifying relative microbial abundance ratios of different bacterial strains during co-culturing. The gene-copy number ratios were assumed to be the biomass ratios of individual organisms, and individual biomass concentration profiles of co-cultures were calculated based on the gene-copy numbers. Total cell dry weight concentrations of the co-cultures were multiplied by the relative microbial abundance ratios to estimate the individual biomass concentrations.

DNA extraction was done using peqGOLD Bacterial DNA Kit (Peqlab, VWR, Vienna, Austria), according to manufacturer protocol, from 3 ml of culture. Isolated gDNA samples were quantified by absorbance at 260 nm wavelength using Nanodrop spectrophotometer (Nanodrop 2000) and diluted to give same concentrations. Dynamic strain abundances of individual members in co-cultures were determined by Q-RT-PCR using the primers given in Table 2.2 that are specific to target genomes and iTaq Universal SYBR Green Supermix (Biorad, CA, USA). Primer designs of *S. thermophilus* LMG 18311 and *Leu. mesenteroides* ATCC 19254 were done using Primer3 (version 0.4.0) (Koressaar and Remm, 2007; Untergasser et al., 2012) and NetPrimer (PREMIER Biosoft International, Palo Alto, CA) online tools. The following PCR protocol was used for all samples: initial denaturation at 95°C for 5 minutes, 40 cycles of 95°C for 15 seconds, 62°C for 30 seconds and a melting curve analysis with 0.5°C increments/5 second from 65°C to 95°C using CFX96 Touch Real-Time PCR Detection System (BioRad, CA, USA).

Table 2.2. 16S rRNA specific qPCR primers

	Forward primer sequences (5'-3')	**Reverse primer sequences (5'-3')**	**PCR product size (bp)**	**References**
***L. lactis* subsp. *cremoris* MG1363**	GTGCTTGCACCAA TTTGAA	GGGATCATCTTT GAGTGAT	163	(Pu et al., 2002)
***L. lactis* subsp. *lactis* IL1403**	GTACTTGTACCGA CTGGAT	GGGATCATCTTT GAGTGAT	163	(Pu et al., 2002)
***S. thermophilus* LMG 18311**	CGGGTGAGTAACG CGTAGGT	CGCCTAGGTGA GCCATTACC	177	This study
***Leu. mesenteroides* ATCC 19254**	CCGCATCTTCACG GGTATTT	AGTTTCGGCGAA GGTACGAA	173	This study

2.3.4. Analyses of essential amino acid requirements for *Leu. mesenteroides*

Essential amino acid requirements of *Leu. mesenteroides* were determined by amino acid omission experiments, which is crucial for the metabolic network model reconstruction of *Leu. mesenteroides*. Centrifuged inoculum culture was washed twice and re-suspended with sterile pure water with 0.9 % NaCl. CDM broth with all amino acids (reference

culture) and CDM broths with omitted individual amino acids were inoculated (2 % v/v) using the amino acid-free inoculum culture. They were incubated at 30ºC for 48 hours in static cultures. The OD of the cultures at 600 nm was then measured as an indication for growth. All experiments were repeated at least twice.

2.4.Computational Analyses

2.4.1. Genome Annotation

Leu. mesenteroides subsp. *cremoris* ATCC 19254 was sequenced as part of the Human Microbiome Project (Human Microbiome Project, 2012a; Human Microbiome Project, 2012b). The complete genome sequence of *Leu. mesenteroides* subsp. *cremoris* ATCC 19254 (GenBank accession number GCA_000160595.1) is available online at National Center for Biotechnology Information (NCBI) (http://www.ncbi.nlm.nih.gov). The genome sequence was imported into the RAST server (http://rast.nmpdr.org/) for gene calling and annotation (the statistics for the genome and annotation of *Leu. mesenteroides* ATCC 19254 can be found in Appendix F).

2.4.2. Reconstruction of *Leu. mesenteroides* genome-scale metabolic network model

A genome-scale metabolic draft model for *Leu. mesenteroides* subsp. *cremoris* ATCC 19254 was generated using the ModelSEED database (Henry et al., 2010). The genome of *Leu. mesenteroides* ATCC 19254 was also uploaded to the following databases in order to recover the functions missing in the ModelSEED annotation: (i) MetaDraft (B.G. Olivier, 2018. [Online], https://systemsbioinformatics.github.io/metadraft) which generates genome-scale metabolic draft models based on existing well-curated models, (ii) a KEGG based database BlastKOALA (http://www.kegg.jp/blastkoala/) which gives genome annotations and related functions of the genome and (iii) TransportDB 2.0 (www.membranetransport.org/) which lists membrane transport proteins. Experimental and literature-based studies were used for the manual curation of the draft model (see the https://github.com/ozcanemrah for the complete reaction list and related gene-reaction

associations). The biomass composition of *Leu. mesenteroides* used for the biomass reaction in the reconstructed model was obtained from the literature. Protein, lipid, DNA, RNA and polysaccharide contents as major biopolymers and compositions of building blocks such as amino acids, nucleotides and fatty acids forming these biopolymers are based on species or strain specific data (Bang et al., 2017; Harney et al., 1967; Tracey and Britz, 1989), while other minor compositions are based on the data of phylogenetically close LAB (Flahaut et al., 2013; Oliveira et al., 2005; Pastink et al., 2009; Teusink et al., 2006; Vinay-Lara et al., 2014) (see the Appendix A for the details of biomass composition of *Leu. mesenteroides*). The values of growth associated maintenance (GAM, K_x) and non-growth associated maintenance (NGAM, m_{atp}) were calculated via Pirt Equation ($\sum q_{ATP,i} - K_X \mu - m_{ATP} = 0$) using the experimental data (Dols et al., 1997) that estimates the rates of energy synthesis (q_{ATP}) with respect to growth rates (μ) for various sugar sources for *Leu. mesenteroides* in batch cultures (see Appendix B). Consequently, 30.651 mmol/gDW and 0.51 mmol/gDW/h were used as GAM and NGAM values for this study.

2.4.3. GSMMs used in this study

GSMMs of *Leu. mesenteroides* ATCC 19254, *L. lactis* subsp. *cremoris* MG1363 (Flahaut et al., 2013) and the revised version of *S. thermophilus* LMG 18311 (Pastink et al., 2009), which were the same strains as used in experiments, were used in this study.

The GSMM of *L. lactis* subsp. *cremoris* MG1363 (Flahaut et al., 2013) was used to simulate the experimental data of both *L. lactis* subsp. *cremoris* and *L. lactis* subsp. *lactis*. Apart from the use of strain specific parameters, the exchange reactions of arginine, glutamine, histidine, isoleucine, leucine, methionine and valine were constrained as the model can only consume these amino acids for the simulation of *L. lactis* subsp. *lactis*, because *L. lactis* IL1403 is known to be unable to synthesize these amino acids (Aller et al., 2014; Cocaign-Bousquet et al., 1995; van Niel and Hahn-Hägerdal, 1999).

The revision of the GSMM of *S. thermophilus* LMG 18311 (Pastink et al., 2009) was carried out with following steps: the draft GSMM of *S. thermophilus* LMG18311 was reconstructed using genome sequence of *S. thermophilus* LMG 18311 (Bolotin et al.,

2004) (GenBank accession number GCA_000011825.1) by MetaDraft (B.G. Olivier 2018. [Online], https://systemsbioinformatics.github.io/metadraft). MetaDraft is fully compliant with and takes full advantage of the latest model encoding and storage standards in systems biology. New reaction set was compared with the reactions of original model, and only the reactions missed by the original model were added to the revised GSMM of *S. thermophilus* LMG18311 (See https://github.com/ozcanemrah for the revised *S. thermophilus* model in SBML format). The comparative reaction, metabolite and gene numbers of the GSMMs used were given in the Table 2.3.

Table 2.3. The comparative reaction, metabolite and gene numbers of the genome-scale metabolic models used in this study.

GSMM	Reaction number	Metabolite number	Gene number	Reference
L. lactis	754	650	518	(Flahaut et al., 2013)
S. thermophilus	829	886	429	Modified version of (Pastink et al., 2009)
Leu. mesenteroides	1088	1129	559	This study

2.4.4. Flux balance analysis for GSMM of *Leu. mesenteroides*

Metabolic flux distributions were estimated via flux balance analysis (FBA) (Orth et al., 2010) and flux variability analysis (FVA) (Mahadevan and Schilling, 2003). Biomass production was maximized as the objective function in FBA to obtain the metabolic flux distributions by constraining the carbon source and amino acid uptake rates to fixed and maximal values, respectively. Manual curation of the draft model and all constraint-based metabolic flux analyses were performed using COBRA Toolbox (Schellenberger et al., 2011) in MATLAB environment with Gurobi6 (http://www.gurobi.com) as the optimization solver.

2.4.5. The dynamic flux balance analysis (dFBA) for pure cultures

Static optimization-based dFBA approach, which is based on dividing the batch time into several time intervals and estimating the flux distribution by FBA for each time interval (Mahadevan et al., 2002) was applied for the pure culture of *L. lactis* subsp. *cremoris*, *L. lactis* subsp. *lactis*, *S. thermophilus* and *Leu. mesenteroides*. dFBA solves a set of ordinary differential equations (ODE) numerically, and reaction rates such as growth rate (μ), glucose and amino acid utilization rates (V_{Glc}, V_{aa}) and lactic acid production rate (V_{Lac}) in the ODE set (Eq. 2.2) are estimated by classical FBA for each iteration of the numeric solution.

$$\frac{d[biomass]}{dt} = \mu[biomass]$$
$$\frac{d[Glc]}{dt} = -V_{Glc}[biomass]$$
$$\frac{d[aa]}{dt} = -V_{aa}[biomass]$$
$$\frac{d[Lac]}{dt} = V_{Lac}[biomass]$$
$$\frac{d[other\ compounds]}{dt} = V_{other\ compounds}[biomass] \qquad \text{Eq. 2.2}$$

In Eq. 2.2, [*Glc*], [*aa*] and [*Lac*] are concentrations of glucose, amino acids and lactic acid respectively, while [*other compounds*] are the concentration of other extracellular compounds, which are formic acid, acetic acid, citric acid, ethanol, CO_2, nucleic acids, vitamins and flavour metabolites. Since the unit of flux rate values was mmol/gDW/h, all concentrations predicted by dFBA were in the unit of mmol/L, and they were converted to g/L, which is the unit of experimentally obtained concentrations. Dynamic concentration profiles of biomass and extracellular compounds simulated by dFBA were then compared with experimental data.

Glucose and amino acid uptake rates (V_{Glc} and V_{aa}) were used as constraints for GSMMs, and both glucose and amino acids uptake kinetics were defined as an empirical function of undissociated lactic acid concentration (Eq. 2.3).

$$V_i \leq -V_{\max,i} \exp(-K_{LacH,i}[LacH]) - V_{\min,i} \qquad \text{Eq. 2.3}$$

where *i* denotes the indices for glucose or amino acids, *V* is the uptake rate of glucose or amino acids, V_{max}, V_{min} and K_{LacH} are the parameters that denote maximum uptake rate, minimum uptake rate and undissociated lactic acid constant, respectively. In each time interval (i.e. one iteration of dFBA) glucose and amino acid uptake rates were calculated from the lactic acid concentration and used as flux constraints for the model; in return, the lactic acid concentration is updated by the calculated fluxes. Substrate uptake kinetics defined in Eq.2.3 only constrains maximum uptake rates. This means that the models can consume the corresponding substrates in less amounts, or they can even produce the related compounds.

Assuming *pH* to be linearly correlated with lactic acid concentration, [*LacH*] term in Eq. 2.1 can be written as in Eq. 2.4.

$$[LacH] = \frac{[Lac]}{1+\exp(C_1[Lac]+C_2)} \qquad \text{Eq. 2.4}$$

The constants C_1 and C_2 in Eq. 2.4 were estimated by non-linear regression of experimental [*LacH*] and [*Lac*] values using CFTool, which is a MATLAB application for fitting curves and surfaces to data (The MathWorks™).

Hence, combining Eq. 2.3 and Eq. 2.4, substrate uptake kinetics used in dFBA is shown in Eq. 2. 5.

$$V \leq -V_{\max} \exp(-K_{LacH} \frac{[Lac]}{1+\exp(c_1[Lac]+c_2)}) - V_{\min} \qquad \text{Eq. 2.5}$$

In addition to substrate uptake kinetics constraining the GSMMs in dFBA, the yield of lactic acid produced per glucose consumed, ($Y_{[Lac]/[Glc]}$) was also used as a reaction ratio constraint between glucose consumption and lactic acid production rates in GSMMs of *L. lactis* and *S. thermophilus*, which assures *in-silico* homolactic fermentation as observed in experiments.

A set of metabolic fluxes that are required for the solution of the ODE set were obtained by two sequential optimizations. First one is a linear programming (LP) problem estimating the flux distribution with maximization of the growth rate, and the second optimization is a quadratic programming (QP) problem minimizing Euclidean norm, the sum of squares of absolute fluxes. QP applied in the flux analyses as a secondary optimization after LP is based on the principle of minimal use of enzyme resources achieving the primary objective (Ozcan and Cakir, 2016; Tarlak et al., 2014).

2.4.6. Parameter estimation

The parameters used in the substrate uptake kinetics were dynamically estimated using MEIGO optimization tool (Egea et al., 2014) in MATLAB, minimizing the optimization problem defined in Eq. 2.6.

$$\min_{p} J = \sum_{j=1}^{n} \sum_{i=1}^{t} (y_j(p, t_i) - y_{ji}^{\text{experimental}})^2 \qquad \text{Eq. 2.6}$$

subject to the system dynamics (Eq. 2.7) and parameter bounds (Eq. 2.8):

$$\frac{dy_i}{dt} = V(y_i, p)[biomass] \qquad \text{Eq. 2.7}$$

$$p_{i,\min} \leq p_i \leq p_{i,\max} \qquad \text{Eq. 2.8}$$

where *n* is the number of dependent variables (concentrations of biomass, glucose, lactic acid and amino acids), *t* is time, *y* is the matrix of dependent variables, *V* is reaction rates, and *p* is parameters. Reaction rates at each iteration of the algorithm were calculated by the GSMM constrained by glucose and amino acid utilization rates. LSQNONLIN, which is a MATLAB algorithm solving non-linear least squares problems (The MathWorks^{TM}), was used as the local solver in the optimization problem solved by MEIGO Toolbox.

2.4.7. Dynamic co-culture metabolic modelling

Dynamic co-culture metabolic modelling, also called dynamic multi-species metabolic modelling, used in this study is a dFBA framework adapted for co-cultures. Common metabolic pool, which is comprised of the compounds of fermentation medium and the compounds produced by the organisms, is shared by the organisms in the co-cultures, which allows the *in-silico* metabolic interactions such as competition and cross feeding. This framework was used before in several studies (Hanemaaijer et al., 2017; Hanly and Henson, 2011; Zhuang et al., 2011; Zhuang et al., 2012). Similar to dFBA for pure cultures, substrate uptake kinetics defined in Eq. 2.5 was used to constrain the models, which means total lactic acid produced by the individual members of the co-cultures affects the individual substrate uptake rates. The parameters that were estimated using pure culture experiments and then used in pure culture dFBA, were also used in dynamic co-culture metabolic modelling. Dynamic co-culture metabolic modelling framework is illustrated in Fig. 2.1.

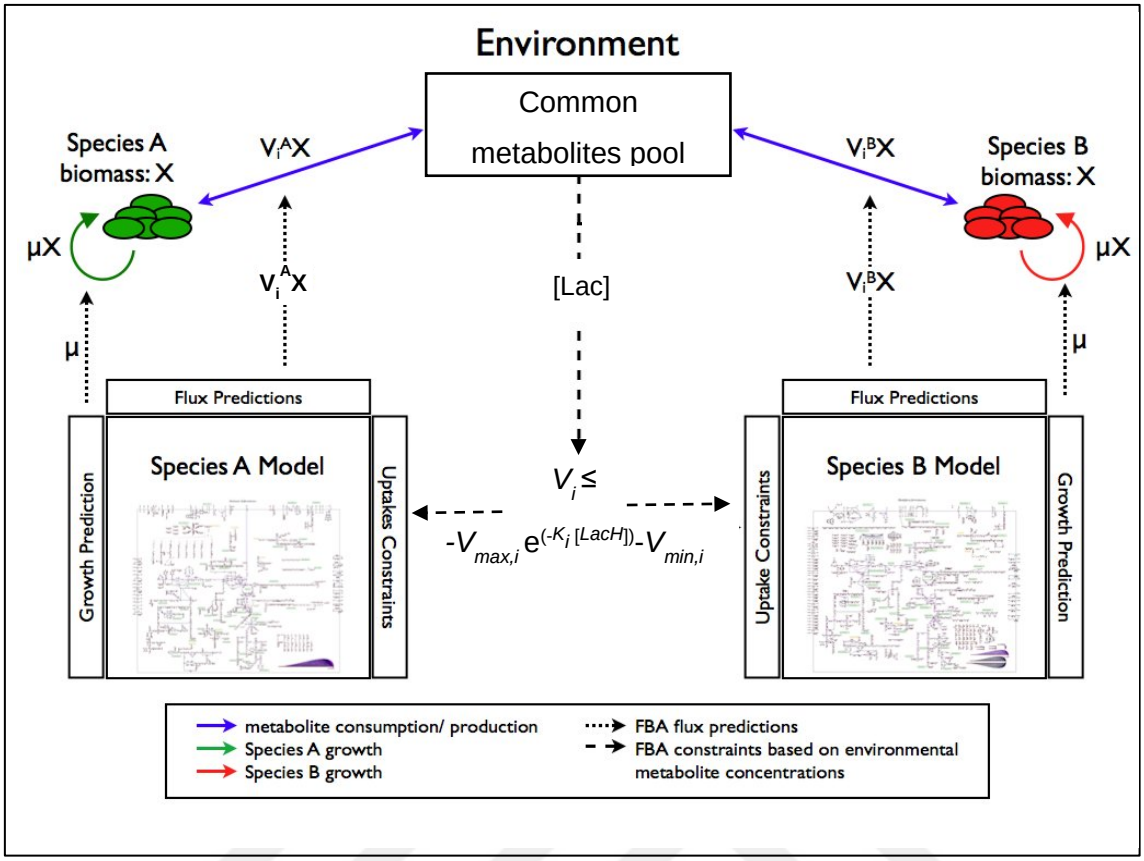

Figure 2.1. Dynamic co-culture metabolic modelling framework. Lactic acid from common metabolites pool changes the individual substrate uptake rates for each time interval. The figure was adapted from (Zhuang et al., 2011).

The ODE set in dynamic co-culture metabolic modelling is shown in Eq. 2.9. Solving this ODE set gives *in-silico* individual biomass and co-culture level compound concentration profiles during the batch fermentations.

$$\frac{d[biomass]_i}{dt} = \mu_i [biomass]_i$$
$$\frac{d[Glc]}{dt} = \sum_{i=1}^{\#\text{ of organism}} \left(-\left(V_{Glc}\right)_i [biomass]_i \right)$$
$$\frac{d[aa]}{dt} = \sum_{i=1}^{\#\text{ of organism}} \left(-\left(V_{aa}\right)_i [biomass]_i \right)$$
$$\frac{d[Lac]}{dt} = \sum_{i=1}^{\#\text{ of organism}} \left(\left(V_{lactic\ acid}\right)_i [biomass]_i \right)$$
$$\frac{d[other\ compounds]}{dt} = \sum_{i=1}^{\#\text{ of organism}} \left(\left(V_{other\ compounds}\right)_i [biomass]_i \right) \qquad \text{Eq. 2.9}$$

Similar to dFBA for pure cultures, the metabolic flux distributions required for the solution of the ODE set were obtained by two sequential optimizations, which was applied for the individual models separately for each iteration.

In pure and co-culture modelling, both LP and QP problems were solved by COBRA Toolbox (Schellenberger et al., 2011) in MATLAB environment with Gurobi6 (http://www.gurobi.com) as the optimization solver. The ODE sets on Eq. 2.2 and Eq. 2.9 were solved by ode45, which is a MATLAB function solving ODEs numerically based on the Runge-Kutta method. Finally, experimentally obtained initial biomass and compound concentrations were used as initial conditions for the solution of ODE sets.

3. RESULTS AND DISCUSSION

Results of this thesis were given under three parts, which are “genome-scale metabolic network model of *Leu. mesenteroides*”, “overview of the pure and co-culture batch results” and “the dynamic metabolic network modelling of pure and co-cultures”. In the first part, reconstruction and validation of a genome-scale metabolic model of *Leu. mesenteroides*, which was later used in the co-culture metabolic modelling, is discussed. In the second part, results of the pure and co-culture batch experiments (e.g. batch biomass and compound profiles, yields, carbon balances) are given. Finally, in the last part, reconstruction and computational analysis of the pure and co-culture metabolic models are discussed, and the computational results are compared with the experimental results. The co-culture fermentation dynamics affecting the biomass composition of the co-cultures and the potential metabolic interactions between LAB in the co-cultures estimated by the co-culture models are also discussed in the last part.

3.1. Genome-Scale Metabolic Network Model of *Leu. mesenteroides*

3.1.1. Model reconstruction and validation

The draft metabolic model initially reconstructed by the automatic reconstruction tools (see Materials and Methods) was subsequently manually curated using our experimental data and literature-based results. After adding the species-specific biomass reaction, amino acid requirements were predicted by the draft model using FBA, through maximizing the growth rate while consecutively constraining the individual amino acid uptake rates to zero. Amino acid requirements predicted by the draft model were then compared with the experimental results, and inconsistencies between *in-silico* and *in-vitro* results were used to manually curate the draft model (Table 3.1).

Table 3.1. Essential amino acids obtained via *in-vitro* and *in-silico* analyses. R: required for growth, NR: not required for growth.

	Experimental results* **(OD at 600 nm)**	**Draft model**	**Curated model**
Control	1.310	NR	NR
Alanine	1.187	R	NR
Arginine	0.060	NR	NR
Aspartate	1.204	NR	NR
Asparagine	1.258	R	NR
Cysteine	0.158	R	R
Glutamate	1.237	NR	NR
Glutamine	1.239	NR	NR
Glycine	1.253	NR	NR
Histidine	0.203	NR	NR
Isoleucine	0.089	NR	NR
Leucine	0.124	NR	NR
Lysine	0.068	R	R
Methionine	0.163	R	R
Phenylalanine	1.136	R	NR
Proline	1.266	NR	NR
Serine	1.251	NR	NR
Threonine	0.829	NR	NR
Tryptophan	0.082	NR	NR
Tyrosine	1.228	R	NR
Valine	0.093	NR	NR
Prediction ratio by models		12/20	16/20

*Data shown are the averages of three repetitive cultures. Maximal optical densities observed were classified as amino acid required for growth (OD<0.20) and amino acid not required for growth (OD>0.20).

Although there was no growth without alanine, asparagine, phenylalanine and tyrosine *in-silico*, *Leu. mesenteroides* grew without these amino acids *in-vitro*. This indicated that biosynthesis pathways of these amino acids were not complete or not available in the genome annotation of *Leu. mesenteroides* ATCC 19254. Therefore, the required reactions for the biosynthesis of alanine, asparagine, phenylalanine and tyrosine were added to the draft model based on the biosynthesis mechanisms observed on previous LAB metabolic models (Flahaut et al., 2013; Oliveira et al., 2005; Pastink et al., 2009; Teusink et al., 2006).

Arginine, tryptophan and the branched-chain amino acids (leucine, isoleucine and valine) were not essential according to the computational analysis with the draft model, however, they were identified as essential amino acids based on our experimental results. This unexpected result may be explained by the feedback inhibition of the synthesis of some amino acids in the presence of other amino acids, which was also reported in literature (Teusink et al., 2005). In that study, for example, although the complete pathway for tryptophan synthesis existed in genome annotation, no growth was observed when tryptophan was omitted from the medium, and a reasonable growth was observed when other aromatic amino acids (tyrosine or phenylalanine) were also omitted. This indicated that the presence of phenylalanine and tyrosine in the medium could inhibit the synthesis of tryptophan (Teusink et al., 2005). *In-silico* growth was observed with not only individual omission of the branched-chain amino acids (leucine, isoleucine and valine), but also simultaneous omission of these three amino acids. On the other hand, there was no *in-silico* growth with omission of glutamine and glutamate together, which shows that glutamate and glutamine are not synthesized individually but compensate each other if needed.

Glucose 6-phosphate dehydrogenase (G6PDH) of *Leu. mesenteroides* can utilize either NAD and NADP, and this unusual dual coenzyme specificity of the G6PDH from *Leu. mesenteroides* was reported by several studies (Cosgrove et al., 1998; Levy, 1989; Levy et al., 1983; Naylor et al., 2001; Olive et al., 1971). Only NADP-specific G6PDH existed in the draft metabolic model, and it caused excessive production of NADPH, which was re-oxidized by biologically irrelevant ways in the network. Thus, NAD-specific G6PDH reaction was added to the draft model. In the final model, NADH generated by the NAD-

specific G6PDH and NADPH generated by the NADP-specific G6PDH were re-oxidized in the reductive steps of heterolactic fermentation and biosynthesis of lipids, respectively.

Upon manual curation, the final metabolic model contained 1129 metabolites and 1088 reactions governed by 559 genes and is named as *iLM.c559*. The reconstructed model is available in SBML format at https://github.com/ozcanemrah.

After manual curation, the model was compared with our anaerobic experimental data for validation (Table 3.2). Experimental results showed a typical heterolactic fermentation pattern; half of the carbon sources consumed were converted to lactate, and the rest of the carbon sources were converted to ethanol, acetate and CO_2 (see Appendix C for the batch fermentation data). The consistency between experimental and computational growth rates provided a validation of the reconstructed genome-scale metabolic model, iLM.c559. It also showed that the calculated values of the energetic parameters (GAM and NGAM) used in the model were acceptable for *Leu. mesenteroides*.

Table 3.2. Experimental and computational reaction rates of the co-metabolism of citrate and glucose for anaerobic fermentation of *Leu. mesenteroides*. The objective function (growth rate) flux value was obtained by FBA, and minimum and maximum *in-silico* flux values of production rates were obtained by FVA. Reaction rates for the experimental values were calculated for the exponential phase of batch fermentation (2-14 h). Uptake rates of amino acids obtained by experimental analysis were constrained as maximum uptake rates of amino acids in the model. See the Appendix D for the maximum amino acid uptake rates used.

Reaction	***In-vitro* reaction rates (mmol/gDW/h)**	***In-silico* reaction rates (mmol/gDW/h)**
Glucose uptake rate	5.03	5.03 (1)
Citrate uptake rate	1.17	1.17 (1)
Lactate production rate	5.29	4.80-5.80
Ethanol production rate	5.03(2)	3.85-4.43
Acetate production rate	1.53	1.38-1.76
CO_2 production rate	6.20(2)	5.88-6.94

Table. 3.2. (Continued)

Flavour metabolite [3] production rate	NM	0-0.77
Growth rate (1/h)	0.15	0.14

(1) Constrained value
(2) Ethanol and CO_2 were not measured experimentally, but they were calculated based on experimental consumption rates (see Experimental Procedures).
(3) Flavour metabolites: the summed production rates of acetyl, diacetyl, 2,3-Butandiol, 4-Methyl-2-oxopentanoate (4MOP), (S)-3-Methyl-2-oxopentanoate (3MOP) and 3-Methyl-2-oxobutanoate (3MOB)
- **NM: not measured**

3.1.2. Model-based investigation of heterolactic fermentation and flavour metabolism in *Leu. mesenteroides* in anaerobic conditions

The reconstructed metabolic model showed that heterolactic fermentation of *Leu. mesenteroides* is governed by energy and redox balances, as stated by several studies (Koduru et al., 2017; Plihon et al., 1995; Schmitt et al., 1992). Glucose is metabolized through PKP where one glucose 6-phosphate is broken down into two branches resulting in equal molar of glyceraldehyde 3-phosphate and acetyl phosphate. When glucose is the sole carbon source, the branch where glyceraldehyde 3-phosphate is converted into lactate is redox balanced and produces ATP required for the cell, while on the other branch, acetyl-phosphate is converted into ethanol resulting in NADH oxidation or into acetate by acetate kinase resulting in ATP (Fig. 3.1).

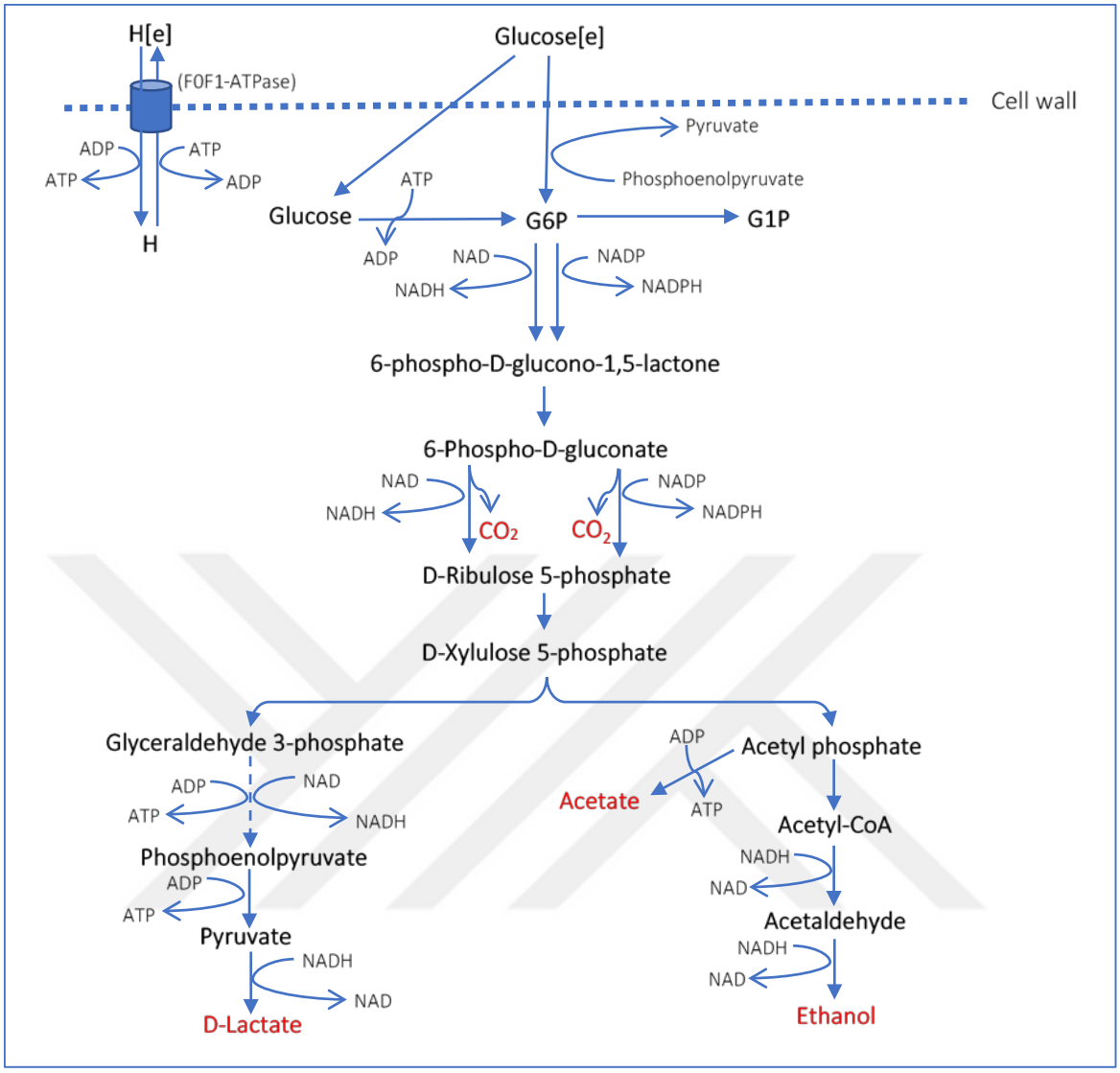

Figure 3.1. Phosphoketolase pathway in the metabolic network of *Leu. mesenteroides*. Metabolites represented by red colour are major external metabolites produced. G6P: D-Glucose 6-phosphate, G1P: D-Glucose 1-phosphate.

The conversion of acetyl-phosphate into acetate or ethanol is governed by the redox balance and ATP requirement of the cell. At first, the reconstructed model was used to simulate this phenomenon under glucose-only anaerobic conditions. Product formation rates were calculated as a function of increase in the glucose consumption rates (Fig. 3.2-A). The model predicted that glucose -as the only carbon source- was converted to lactate, ethanol and CO_2 with almost equal glucose:product molar ratio of glucose:CO_2:lactate:ethanol:acetate =1:1:1:1:0 (Fig. 3.2-A). This ratio was also observed

by several experimental studies for the anaerobic fermentation of *Leu. mesenteroides* (Bourel et al., 2003; LevataJovanovic and Sandine, 1996; Plihon et al., 1995).

When citrate was used as the sole carbon source, *in-silico* growth was not observed, which is also consistent with an experimental study (Starrenburg and Hugenholtz, 1991). Furthermore, the co-metabolism of citrate and glucose under anaerobic conditions was simulated by the metabolic model by changing citrate rates at a fixed glucose consumption rate (Fig. 3.2-B). Because citrate acts as an electron acceptor, *in-silico* growth was stimulated by the co-utilization of citrate, again in agreement with the experimental studies associated with the citrate consumption of *Leu. mesenteroides* (Schmitt et al., 1992; Starrenburg and Hugenholtz, 1991). Conversion of pyruvate to lactate and acetyl-CoA to ethanol leads to the oxidation of NADH. In flux predictions, citrate contributes to the pyruvate pool through oxaloacetate decarboxylase (Fig. 3.3), which is also stated in literature (LevataJovanovic and Sandine, 1996). The pyruvate derived from citrate utilization increased the lactate production, which led to an increase in the oxidation of NADH. Therefore, the cell needed to make less ethanol for the oxidation of NADH, and hence some part of acetyl-phosphate could be converted to acetate by acetate kinase resulting in additional ATP production. Stimulation of growth could be explained by the increase in available ATP through acetate production. The increased lactate production with increased citrate, as well as the decreased ethanol formation, in our model prediction is consistent with the studies of (Schmitt et al., 1992) and (Schmitt and Divies, 1992) respectively. In addition to indirect contribution of citrate to acetate production by acetate kinase (rxn00225 in Fig. 3.1), citrate also directly contributes to the acetate pool by citrate oxaloacetate-lyase (rxn00265 in Fig. 3.3).

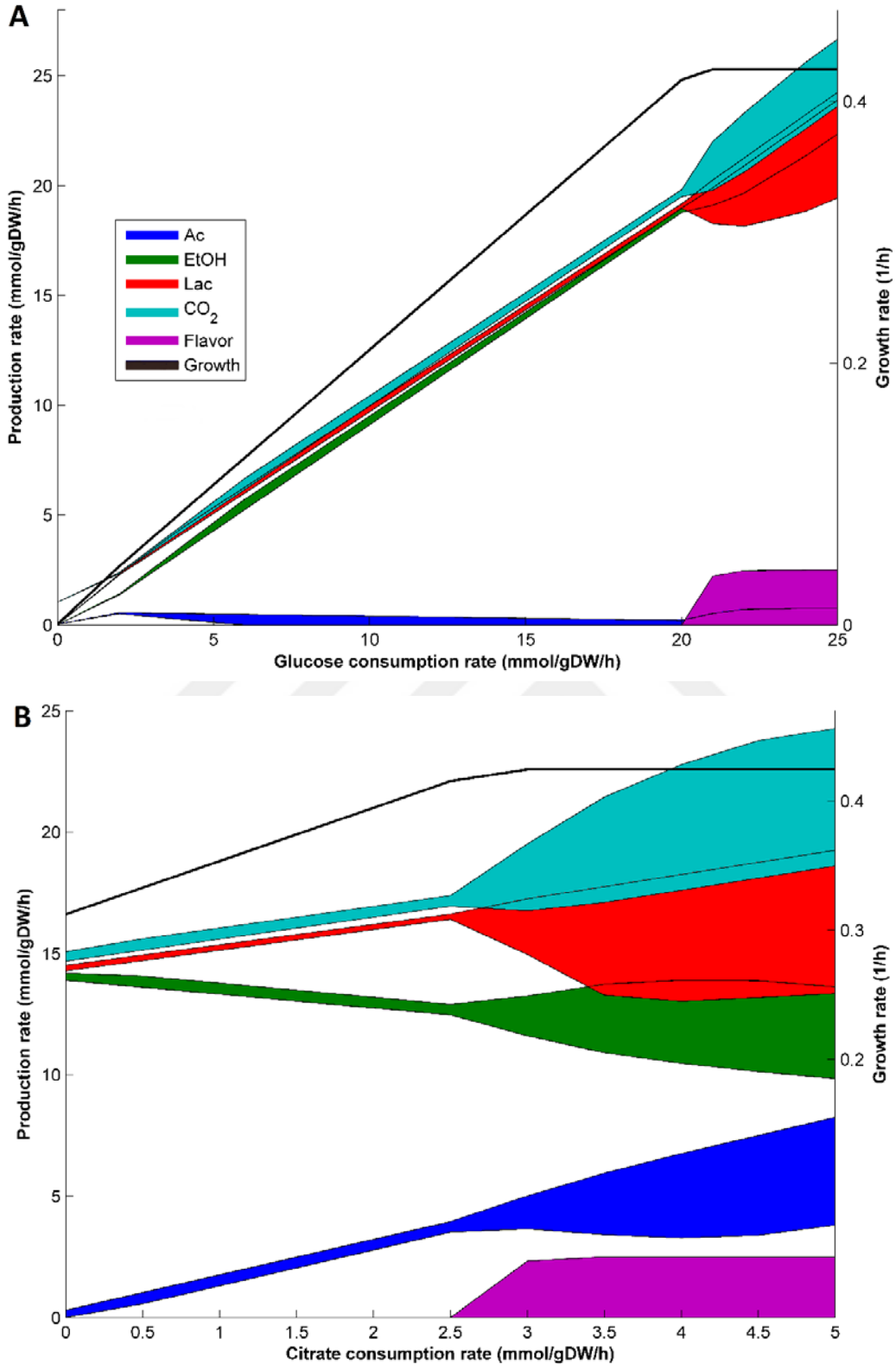

Figure 3.2. Effect of glucose and citrate uptake rates on metabolite production profile and growth rate, obtained by model simulations. Width of the flux profiles denotes flux

span obtained by FVA. **(A)** Product profiles with respect to glucose consumption rate when glucose is the sole carbon source, **(B)** Product profiles with co-metabolism of citrate and glucose. Glucose is fixed to a constant consumption rate (15 mmol/gDW/h) for this analysis. Maximum uptake rates of amino acids were constrained to 0.2 mmol/gDW/h for (A) and (B). Flavour: the summed rates of acetyl, diacetyl, 2,3-Butandiol, 4-Methyl-2-oxopentanoate (4MOP), (S)-3-Methyl-2-oxopentanoate (3MOP) and 3-Methyl-2-oxobutanoate (3MOB)

Citrate utilization leads to the production of flavour metabolites in *Leu. mesenteroides* (LevataJovanovic and Sandine, 1996; Schmitt et al., 1992; Starrenburg and Hugenholtz, 1991). In our model, flavour metabolites produced following the routes seen in Fig. 3.3 are acetoin, diacetyl, 2,3-butanediol, 4-methyl-2-oxopentanoate (4MOP), (S)-3-methyl-2-oxopentanoate (3MOP) and 3-methyl-2-oxobutanoate (3MOB), the last three of which are associated with amino acid metabolism. Flavour metabolite production was observed with not only co-metabolism of citrate and glucose (Fig. 3.2-B), but also with glucose as the only carbon source (Fig 2-A). However, significant production was only observed when the growth rate could not increase anymore due to amino acid limitation. Because of excess carbon and ATP, the flux span of products obtained by FVA widens after this point. Whereas minimum flux values of lactate and acetate production decreased, maximum flux values of flavour metabolites production increased. This result shows that the cell can divert the carbon sources to flavour production when it has no growth requirements (carbon or ATP) anymore. The amount of molar carbon required to reach the maximal growth rate, and hence flavour formation, was lower when glucose and citrate were co-metabolized compared to sole glucose consumption (Fig. 3.2). This may indicate how citrate can be advantageous for flavour production.

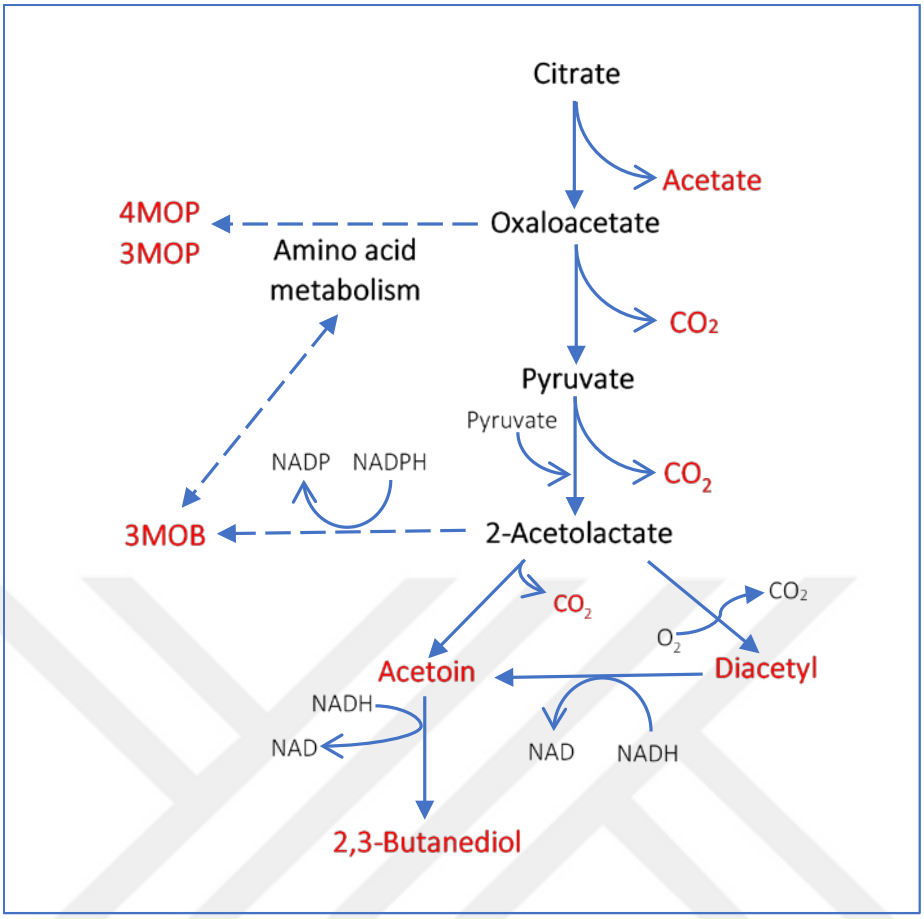

Figure 3.3. Flavour metabolite production associated with citrate metabolism. Metabolites represented by red colour are external metabolites produced. 4MOP: 4-Methyl-2-oxopentanoate, 3MOP: (S)-3-Methyl-2-oxopentanoate and 3MOB: 3-Methyl-2-oxobutanoate

In line with our model predictions, the production of aromatic compounds was favored over the synthesis of other metabolites from citrate during the stationary phase (LevataJovanovic and Sandine, 1996). Moreover, a recent study about the aroma formation from a citrate-consuming dairy *Lactococcus lactis* at near-zero growth rates points out that some particular LAB can survive in long periods of nutrient limitation, as in the case of cheese ripening, and these LAB still contribute to the flavour formation (van Mastrigt et al., 2018). We therefore investigated the flavour metabolite production during co-metabolism of citrate and glucose at low growth rates *in-silico*: growth rate was fixed to near-zero values, and flux distributions were calculated constraining carbon and

nitrogen sources to low values to mimic nutrient limitation conditions, with the maximization of ATP production as the objective function. As expected, production of total flavour metabolites linearly increased, and acetate and lactate production decreased with decreasing growth rate (data not shown).

3.1.3. Metabolic shift and stimulation of growth in *Leu. mesenteroides* under aerobic conditions

Although acetate production by acetate kinase supplies ATP for the cell, significant amount of acetyl-phosphate is converted into ethanol to balance the redox state of the cell by producing NAD under anaerobic conditions. The bottleneck of obligate heterolactic *Leu. mesenteroides* due to energy and redox state could be overcome by aerobic fermentation. The reconstructed metabolic model was used to simulate aerobic conditions on growth and product formation characteristics of the organism. Simulation results showed that oxygen acted as another electron acceptor for *Leu. mesenteroides*, and NADH was oxidized by aerobic fermentation, which is also observed in the respiration of some LAB (Pedersen et al., 2012). The membrane-associated mechanisms of *Leu. mesenteroides* suggested by the metabolic model for aerobic conditions is illustrated in Fig. 3.4. Then, the protons extruded by the respiratory mechanism could be utilized by the F0F1-ATPase to generate ATP. In this two-step mechanism, NADH is not oxidized by oxygen directly, but rather NADH is oxidized by menaquinone or ubiquinone, which are re-oxidized by oxygen. This mechanism is also observed in some LAB (Pedersen et al., 2012), and it is different from that of NADH oxidases (NOX) that oxidize NADH directly using oxygen .

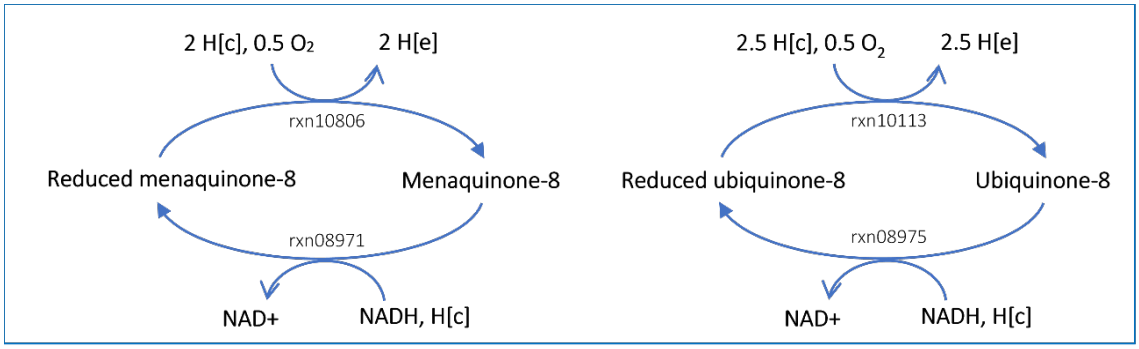

Figure 3.4. Respiration mechanisms mediated by menaquinone-8 and ubiquinone-8 in *Leu. mesenteroides.*

Thus, under aerobic conditions, the requirement of ethanol production for re-oxidation of NADH decreases and acetate production increases. This phenomenon causes a metabolic shift between ethanol and acetate production and stimulates the cell growth (Fig. 3.5) due to ATP production by acetate kinase and F0F1-ATPase. Hence, the stoichiometric ratio of glucose:ethanol:acetate could be summarized as 1:1:0 and 1:0:1 for anaerobic and fully aerobic fermentation of *Leu. mesenteroides* respectively, which is also reported by several experimental studies associated with *Leu. mesenteroides* (Bourel et al., 2003; Dols et al., 1997; Plihon et al., 1995). The same simulation also showed that increasing oxygen uptake rates had minimal effect on lactate and CO_2 production rates (Fig. 3.5), in agreement with an experimental study (Plihon et al., 1995).

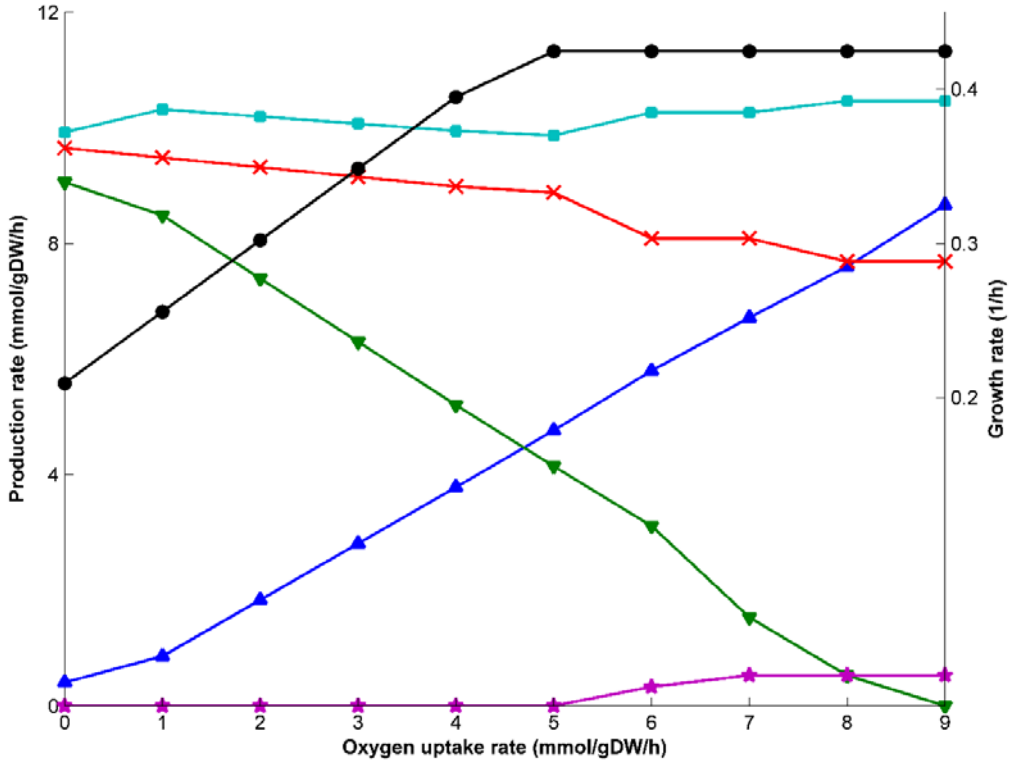

Figure 3.5. Model predictions on the metabolic shift between ethanol and acetate production by increasing oxygen uptake rate. Glucose uptake rate as only carbon source was fixed to 10 mmol/gDW/h, and maximum uptake rates of amino acids were fixed to 0.2 mmol/gDW/h. Growth, ●; CO_2, ■; lactate, ✕; acetate, ▲; ethanol, ▼; flavour, ★

The model also predicted flavour production with increasing oxygen uptake rate (Fig. 3.5), but similar to the simulations in anaerobic conditions, significant amount of flavour metabolites production was observed only after the oxygen-induced growth increase saturated. Flux span patterns obtained by FVA (see Appendix E) was also similar to the co-metabolism of glucose and citrate in anaerobic condition, which was discussed above.

3.1.4. Effect of different carbon sources on growth profiles in *Leu. mesenteroides*

In addition to aerobic fermentation, another strategy to overcome the energy and redox state bottleneck in *Leu. mesenteroides* could be the use of different carbon sources. For

this purpose, growth and product profiles were simulated by the model for commonly used mono and disaccharides as carbon sources, the utilization mechanisms of which were illustrated in Fig. 3.6. Although lactose utilization is considered as weak in *Leu. mesenteroides* ATCC 19254 (LevataJovanovic and Sandine, 1996) and mannitol production via fructose utilization is absent in the genome of *Leu. mesenteroides* ATCC 19254, the metabolic model includes the complete mechanism of the lactose and fructose utilization (Fig. 3.6). The latter is because an experimental study (Carvalheiro et al., 2011) reported that *Leu. mesenteroides* ATCC 19254 produced mannitol through the consumption of fructose, suggesting that this strain has a mannitol dehydrogenase activity. Furthermore, the model does not consider the dextran production through sucrose utilization due to the lack of related enzymes in *Leu. mesenteroides* subsp. *cremoris*. Dextran production was observed in *Leu. mesenteroides* subsp. *dextranicum* and subsp. *mesenteroides* strains (Naessens et al., 2005). A study investigating different *Leuconostoc* strains also stated that the strains identified as *Leu. mesenteroides* subsp. *cremoris* (20 of 60 *Leuconostoc* strains examined) did not produce dextran (LevataJovanovic and Sandine, 1996).

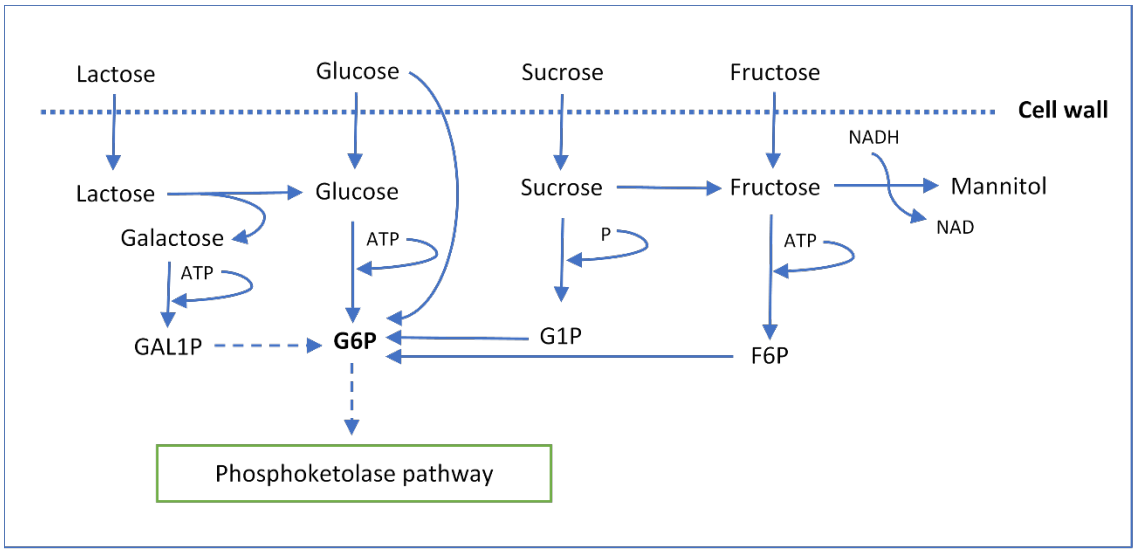

Figure 3.6. Representation of the utilization of commonly used carbon sources by *Leu. mesenteroides*. G6P: Glucose 6-phosphate, G1P: Glucose 1-phosphate, F6P: Fructose 6-phosphate, GAL1P: Galactose 1-phosphate

Consumption rates of monosaccharides (glucose and fructose) were fixed to twice the disaccharides (sucrose and lactose) consumption rates to simulate the equivalent carbon utilization rates. Another constraint was applied for the ethanol production in fructose growth by fixing its rate to zero according to the experimental study (Dols et al., 1997) because it was necessary for the simulation of non-zero mannitol production by fructose utilization. The model predicted the oxidation of NADH by mannitol production since the oxidation route via ethanol production was inactive in the fructose fermentation. The usage of significant amounts of the fructose for mannitol production led to the decrease in growth rate compared to other carbon sources. On the other hand, the growth was stimulated with the utilization of sucrose as a carbon source (Fig. 3.7) because less ATP was consumed per equivalent carbon utilization rate compared to the other carbon sources (Fig. 3.6). A decrease and increase of growth on fructose and sucrose, respectively, is consistent with literature (Dols et al., 1997). Although the consumed ATP per equivalent carbon utilization rate was the same for glucose and lactose, *in-silico* growth rate decreased with lactose utilization due to the difference in transport systems of these two sugar sources. Lactose is transferred by proton symport, which is the only transport mechanism for lactose in the model, whereas glucose is transferred by a phosphotransferase system (PTS), which is energetically more advantageous. Our model explains the reason behind this advantage. F0F1-ATPase is a membrane-bound enzyme that pumps out the intracellular proton using ATP in anaerobic conditions in LAB for pH homeostasis (Konings, 2002), and F0F1-ATPase in our model also has the same task for anaerobic conditions. Contrary to the proton symport used as a lactose transport system, the PTS, used as a glucose transport system in the model, does not introduce intracellular proton. Hence, F0F1-ATPase spent less ATP to pump protons out.

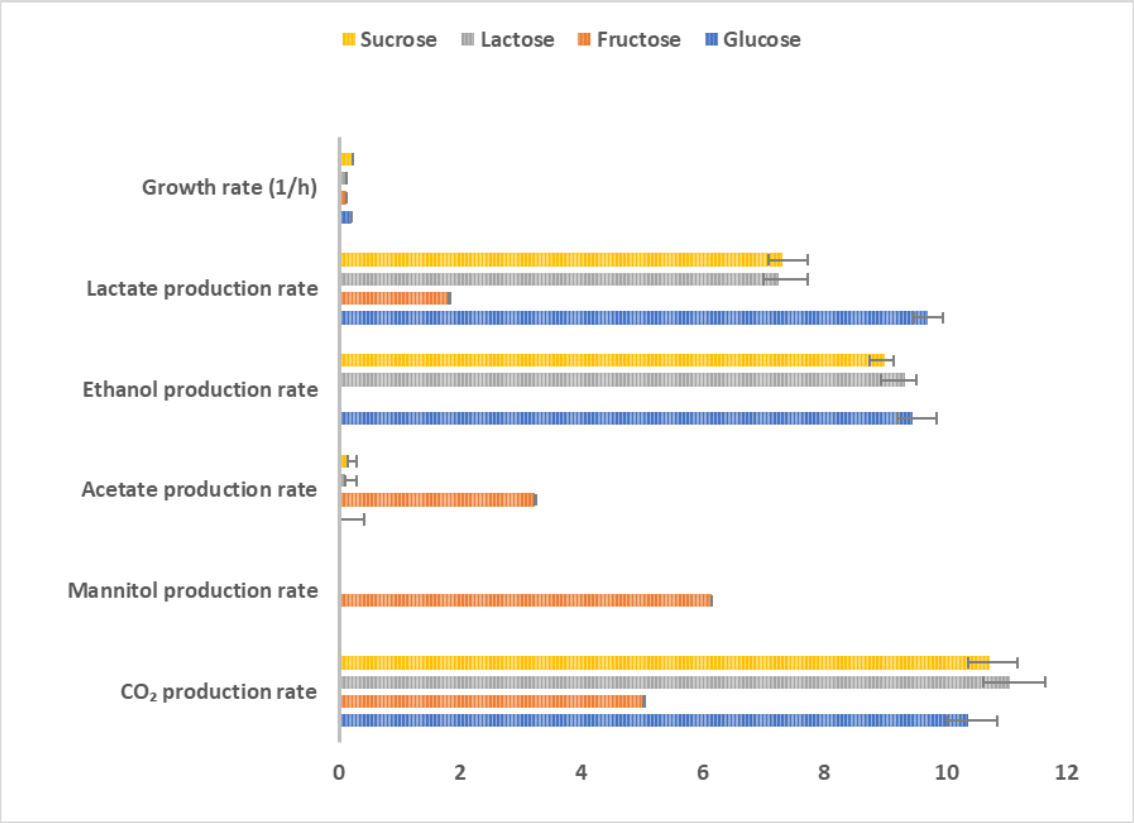

Figure 3.7. Effect of commonly used carbon sources on the metabolic products of *Leu. mesenteroides* in anaerobic condition predicted by the model. Uptake rates of monosaccharides (glucose and fructose) and disaccharides (lactose and sucrose) were constrained to 10 and 5 mmol/gDW/h respectively (without citrate uptake), and maximum uptake rates of amino acids were constrained to 0.2 mmol/gDW/h. Ethanol production via fructose fermentation was fixed to zero (Dols et al., 1997). Error bars denote flux span obtained by FVA

3.1.5. Comparison of the GSMMs *of Leu. mesenteroides* subsp. *cremoris* and *Leu. mesenteroides* subsp. *mesenteroides*

Although our model is the first GSMM of dairy-origin *Leu. mesenteroides* subsp. *cremoris* ATCC 19254, it is the second *Leu. mesenteroides* reconstruction in the literature after the plant-origin *Leu. mesenteroides* subsp. *mesenteroides* ATCC 8293 (Koduru et al., 2017). In terms of their genome sizes, the two subspecies are the most distinct ones among 17 subspecies (Chun et al., 2017). The plant-origin subspecies has the biggest

genome size among 17 subspecies (2.08 Mb) whereas the cheese-origin subspecies has the lowest genome size (1.74 Mb). The difference is also reflected in the number of genes. The subspecies reconstructed and analysed in this work has around 300 genes less than the plant-origin subspecies. Genome comparison of dairy-origin *Leu. mesenteroides* ATCC 19254 and plant-origin *Leu. mesenteroides* ATCC 8293 show significant differences in the metabolism of the two, which include sucrose and amino acid metabolism in particular. (See Appendix G for the comparison of sucrose metabolism).

Our individual amino acid omission experiments showed that the absence of histidine causes weak growth and eight amino acids (arginine, cysteine, isoleucine, leucine, lysine, methionine, tryptophan and valine) are required for the growth of the dairy-origin strain *Leu. mesenteroides*. However, only two amino acids (glutamine and valine) are essential for a plant-origin *Leu. mesenteroides* (Koduru et al., 2017). The amino acid auxotrophy differences between dairy and plant-origin *Leu. mesenteroides* supports the hypothesis in a study which, by stating the difference in amino acid auxotrophies for the dairy and plant-origin lactic acid bacterium *Lactococcus lactis*, proposes that dairy strains originate from the plant niche (Bachmann et al., 2012). In that study, plant-origin *L. lactis* strains propagated for 1000 generations in milk were adapted to milk environment, and they were able to use the milk proteins as a source of amino acids. Genome sequences of these strains revealed point mutations in loci related to amino acid biosynthesis (Bachmann et al., 2012).

Upon simulation of our model, we realized an important difference in the redox state of the two models: In the plant-derived model, glucose 6-phosphate dehydrogenase (G6PDH) and phosphogluconate dehydrogenase (GND) reactions of PKP produce only NADPH, which is re-oxidized via futile cycles not related with PKP, and NADH oxidized in ethanol production is also produced by futile cycles not related with PKP. But in our model, both G6PDH and GND have dual coenzyme specificity, and NADH and NADPH produced in PKP were re-oxidized in the reductive steps of heterolactic fermentation and biosynthesis of lipid, respectively. Finally, the metabolic model reconstructed in this study additionally incorporated the citrate utilization and citrate related flavour metabolism, which was not considered in the plant-origin *Leu. mesenteroides* model. This allowed us to investigate the role of citrate metabolism and oxygen uptake on flavour formation.

3.2. Overview of The Pure and Co-Culture Batch Results

The pure and co-cultures were grown in 1-litre batch bioreactor under anaerobic conditions, without pH maintenance and using chemically defined medium. Biomass, glucose, organic acids and amino acids concentrations were obtained using the hourly basis fermentations samples.

3.2.1. Pure Culture Batch Profiles

Pure cultures of *L. lactis*, *S. thermophilus* (ST) and *Leu. mesenteroides* (LM) strains were fermented in batch cultures until stationary phase. Although *L. lactis* subsp. *cremoris* (LLC) and *L. lactis* subsp. *lactis* (LLL) reached the stationary phase at the same time (Fig. 3.8. and Fig. 3.9), the biomass yield of *L. lactis* subsp. *cremoris* was higher than *L. lactis* subsp. *lactis* (Table 3.3). *S. thermophilus* showed rapid growth and reached the stationary phase at 4th hour (Fig 3.10), while *Leu. mesenteroides* showed slower growth and reached the stationary phase at around 22nd hour (Fig. 3.11). *L. lactis* and *S. thermophilus* species showed homolactic fermentation in which main fermentation product was lactic acid, while *Leu. mesenteroides* being obligate heterolactic lactic acid bacterium (Chun et al., 2017; Garvie, 1986) produced CO_2 and ethanol in addition to lactic acid. The difference between homolactic and heterolactic fermentation could also be explained by the yield of lactic acid produced per glucose consumed, of which *Leu. mesenteroides* had the minimum yield among all strains (Table 3.3).

Table 3.3. The yields and carbon balances of the pure cultures

	$Y_{X/S}$, Biomass yield (g Biomass/ g Glc)*	**$Y_{P/S}$, Lactic acid yield (g Lac/ g Glc)**	**Carbon balance (%)**
L. lactis* subsp. *cremoris	0.186±0.001	0.841±0.007	93.06±0.95
L. lactis* subsp. *lactis	0.171±0.001	0.833±0.000	91.99±0.24

Table 3.3. (Continued)

S. thermophilus	0.183±0.006	0.865±0.010	101.64±1.65
Leu. mesenteroides	0.068±0.006	0.487±0.037	94.05±6.39

*Since glucose consumption continued after growth inhibition, biomass yields were based on exponential growth phase.

Low pH as a result of increasing organic acid, especially lactic acid, caused growth inhibition for all batches. Therefore, glucose was not consumed completely due to the pH inhibition on growth for all batches. But, after growth inhibition, glucose consumption and lactic acid production slightly continued, and the yield of lactic acid produced per glucose consumed was almost constant during all batches (Table 3.3).

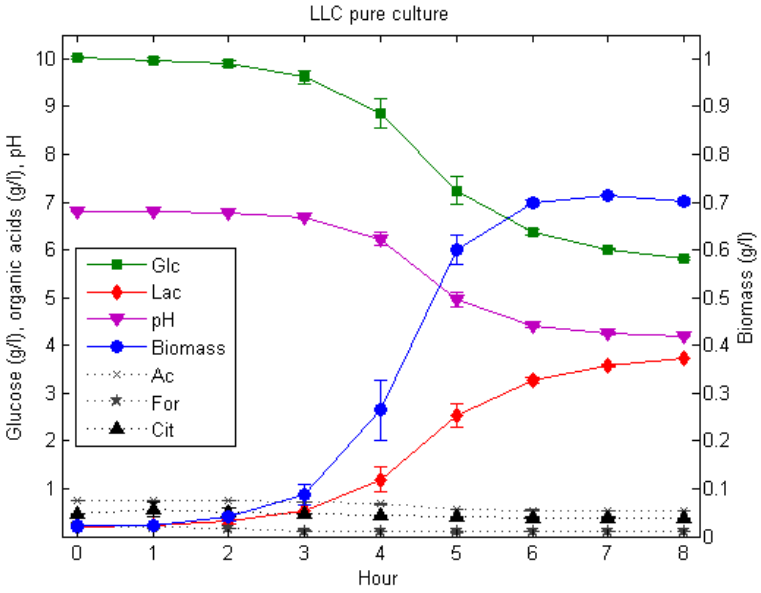

Figure 3.8. Pure culture batch profile of *Lactococcus lactis* subsp. *cremoris* (LLC). Points denote average values of two independent biological repetitions. Corresponding error bars are also given.

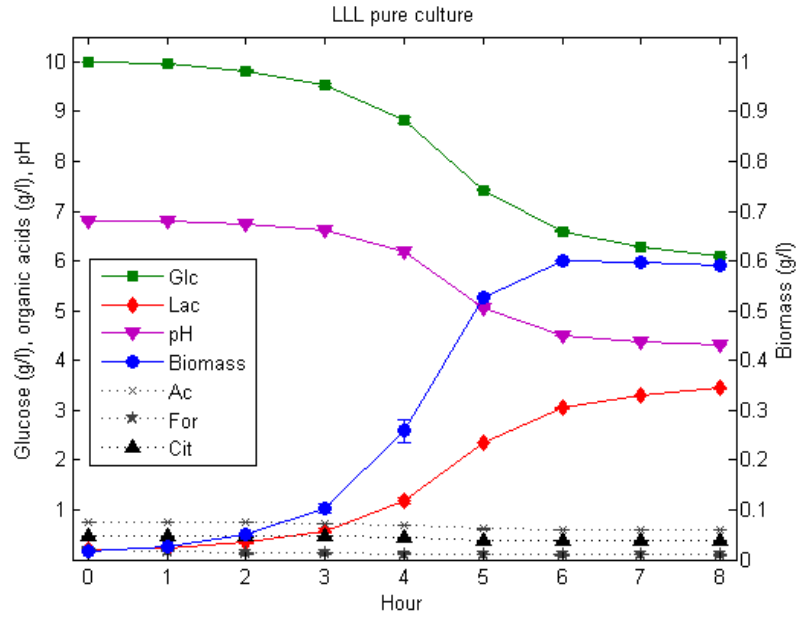

Figure 3.9. Pure culture batch profile of *Lactococcus lactis* subsp. *lactis* (LLL). Points denote average values of two independent biological repetitions. Corresponding error bars are also given.

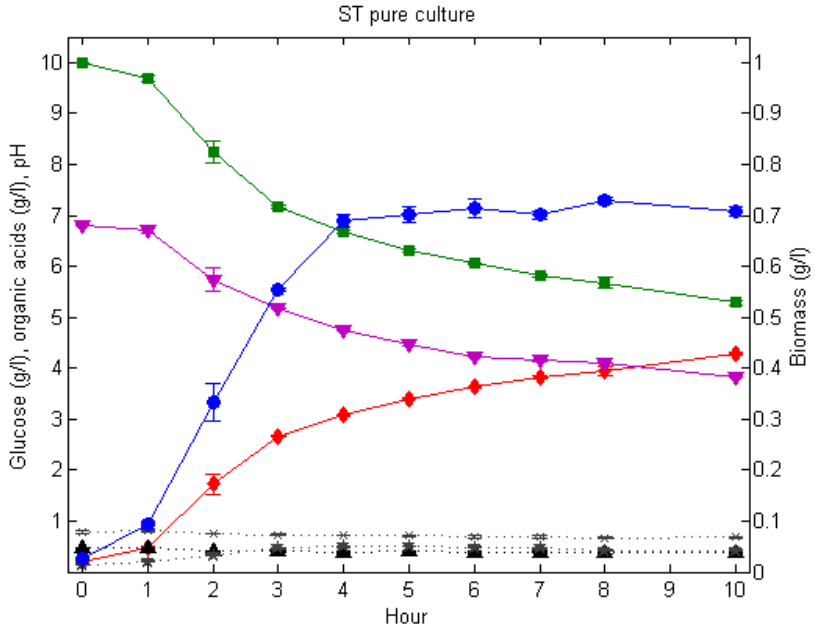

Figure 3.10. Pure culture batch profile of *Streptococcus thermophilus* (ST). Points denote average values of two independent biological repetitions. Corresponding error

bars are also given. Glucose, ■; lactic acid, ♦; pH, ▼; biomass, ●; acetic acid, ×; formic acid, ★; citric acid, ▲

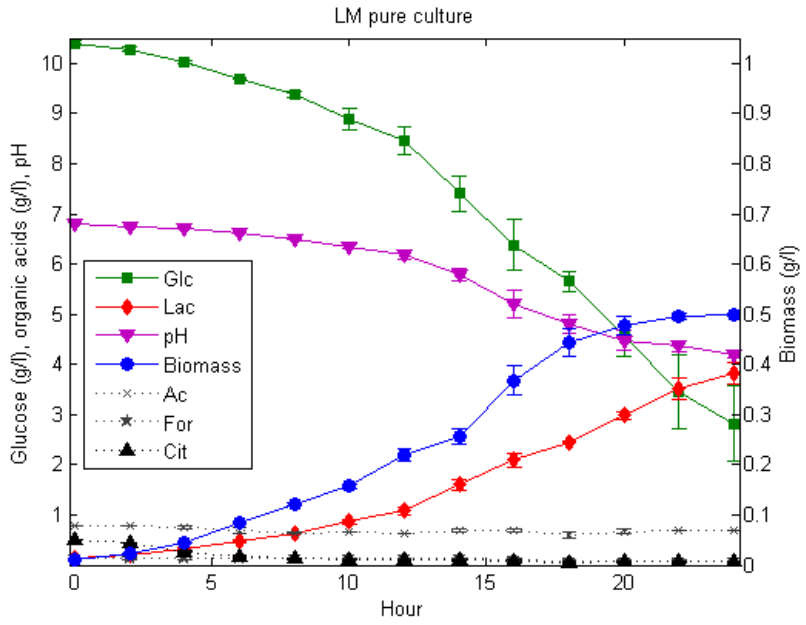

Figure 3.11. Pure culture batch profile of *Leuconostoc mesenteroides* (LM). Points denote average values of two independent biological repetitions. Corresponding error bars are also given.

Acetic acid and formic acid concentrations were observed to be slightly decreased in batches of *Lactococcus* species and *Leu. mesenteroides*. This unexpected result might be due to their concentrations being lower than detectable range of HPLC. On the other hand, formic acid production was observed in *S. thermophilus* until stationary phase (Fig. 3.10). But omitting acetic and formic acid did not change the carbon balance significantly (data not shown). Furthermore, citrate was not consumed significantly in *L. lactis* and S. *thermophilus* strains, while *Leu. mesenteroides*, which is known as citrate consumer lactic acid bacteria (Smid and Kleerebezem, 2014), consumed all citrate before the stationary phase (Fig. 3.11).

Fig. 3.12 shows biomass, glucose, lactic acid and pH profiles of the pure cultures, which enables to see a comparative picture of the pure cultures. Undissociated lactic acid, which

is the main inhibitory component of lactic acid fermentation, is increasingly formed by low pH (Bouguettoucha et al., 2011), and it is calculated as given Eq. 2.1. The undissociated lactic acid is the important component for the metabolic modelling study part (section 3.3) and undissociated lactic acid profiles of the pure cultures are also given in the Fig. 3.12-D.

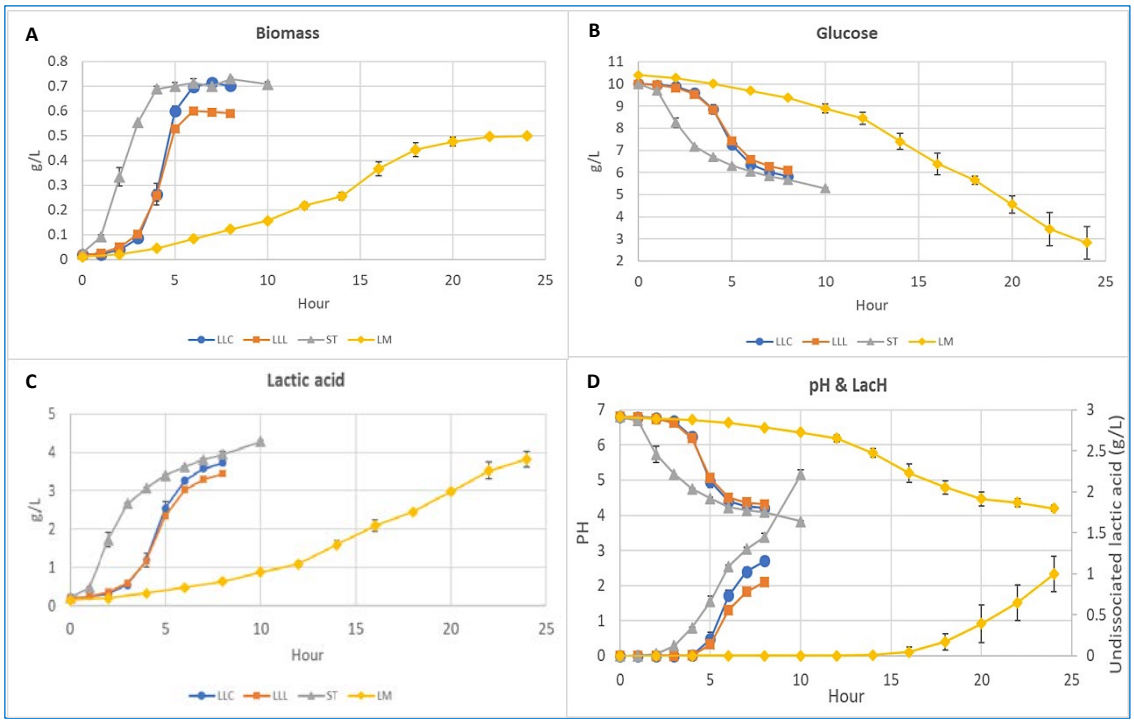

Figure 3.12. Comparative profiles of biomass (A), glucose (B), total lactic acid (C), pH and undissociated lactic acid (LacH) (D) of the pure cultures.

3.2.2. Co-Culture Batch Profiles

The co-cultures composed of *L. lactis* and *Leu. mesenteroides* species and the co-cultures composed *L. lactis* and *S. thermophilus* species were assumed to represent mesophilic and thermophilic starter cultures respectively. The co-culture compositions used in this thesis are given in Table 3.4.

Table 3.4. The co-culture compositions in this study.

Co-culture	Composition
Two-species mesophilic co-culture	*L. lactis* subsp. *cremoris* - *Leu. mesenteroides*
Three-species mesophilic co-culture	*L. lactis subsp. cremoris* - *L. lactis* subsp. *lactis*- *Leu. mesenteroides*
Two-species thermophilic co-culture	*L. lactis* subsp. *cremoris* - *S. thermophilus*
Three-species thermophilic co-culture	*L. lactis* subsp. *cremoris*- *L. lactis* subsp. *lactis*- *S. thermophilus*

Total biomass, glucose, organic acids and pH profiles of co-cultures are illustrated in Fig. 3.13-3.16. As it can been seen in Table 3.5, both biomass and lactic acid yields of co-cultures are between the yields of pure cultures that constitute the related co-cultures. This result showed that co-cultures did not create an advantage or disadvantage compared to pure cultures in terms of the yields. The fact that higher or lower fermentation yields of a co-culture than that of the pure cultures constituting the pure culture could strictly point out an interaction among the microorganisms. However, in this study, the intermediate fermentation yields of the co-culture do not prove a metabolic interaction. Potential metabolic interactions will be investigated via metabolic modelling analyses in section 3.3.4.

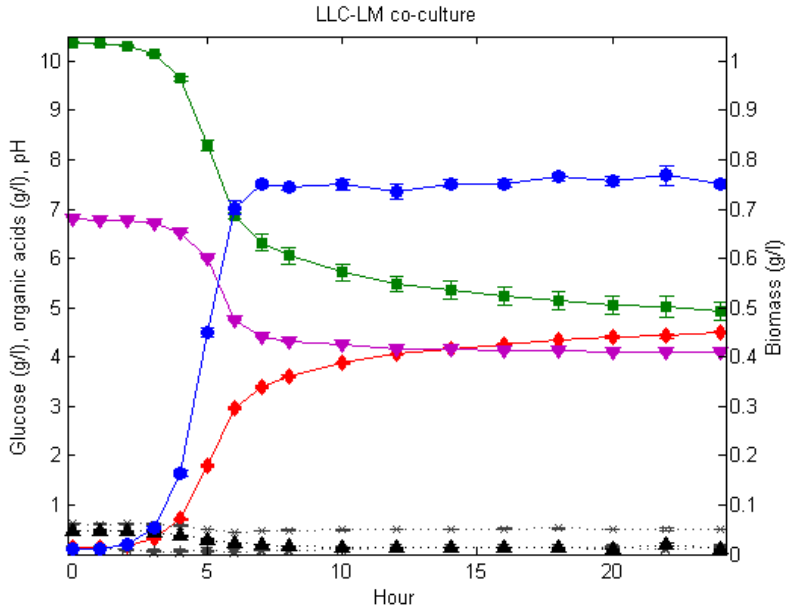

Figure 3.13. Batch profile of the co-culture comprised of *Lactococcus lactis* subsp. *cremoris* and *Leu. mesenteroides* (LLC-LM). Points denote average values of two independent biological repetitions. Corresponding error bars are also given. Glucose, ■; lactic acid, ♦; pH, ▼; biomass, ●; acetic acid, ×; formic acid, ★; citric acid, ▲

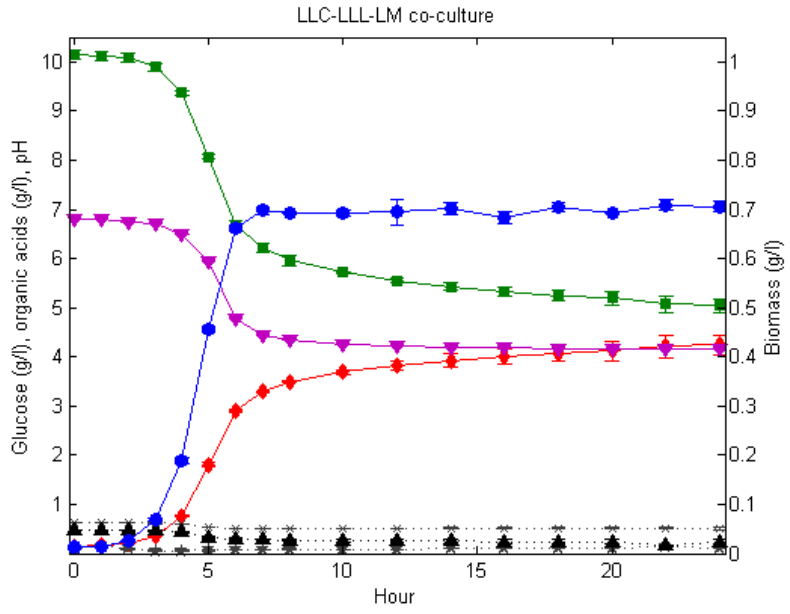

Figure 3.14. Batch profile of the co-culture comprised of *Lactococcus lactis* subsp. *cremoris*, *Lactococcus lactis* subsp. *lactis* and *Leu. mesenteroides* (LLC-LM). Points

denote average values of two independent biological repetitions. Corresponding error bars are also given. Glucose, ■; lactic acid, ♦; pH, ▼; biomass, ●; acetic acid, ×; formic acid, ★; citric acid, ▲

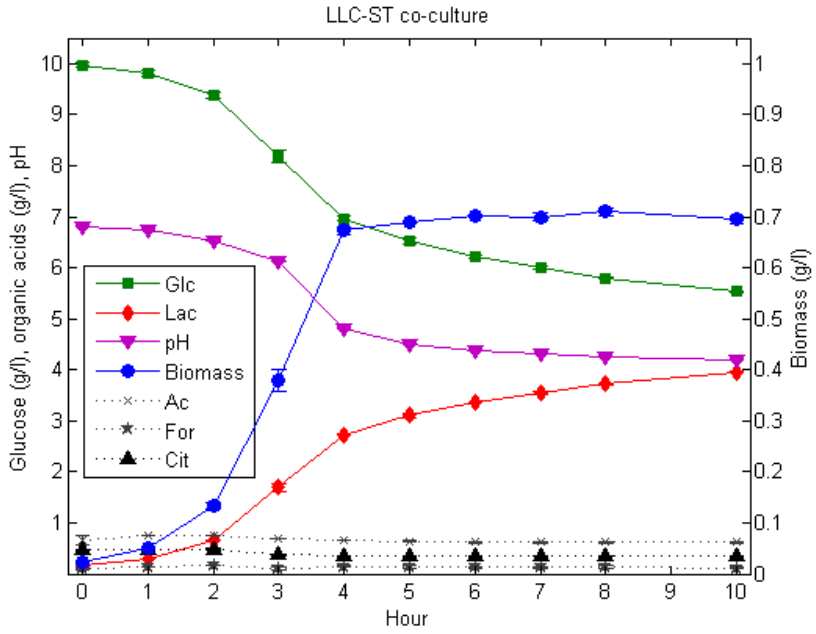

Figure 3.15. Batch profile of the co-culture comprised of *Lactococcus lactis* subsp. *cremoris* and *S. thermophilus* (LLC-ST). Points denote average values of two independent biological repetitions. Corresponding error bars are also given.

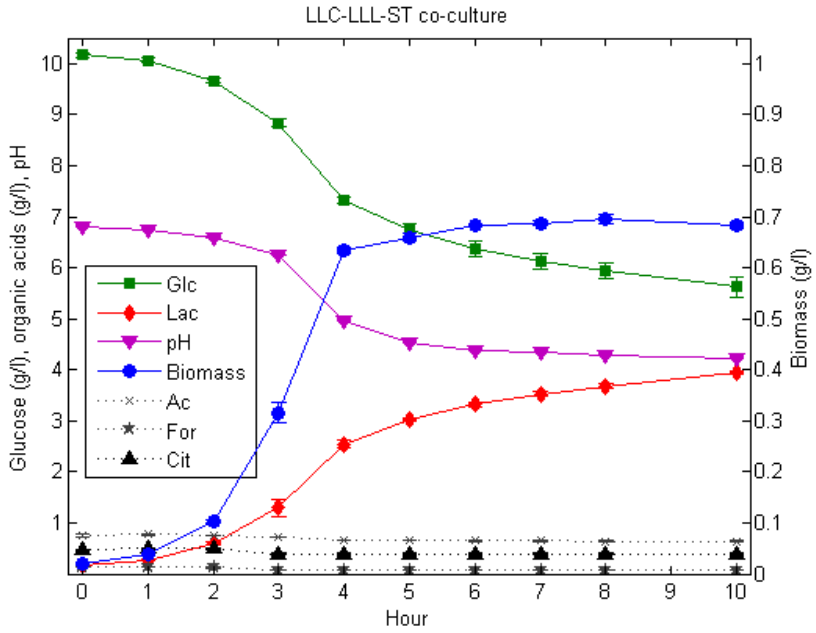

Figure 3.16. Batch profile of the co-culture comprised of *Lactococcus lactis* subsp. *cremoris*, *Lactococcus lactis* subsp. *lactis* and *S. thermophilus* (LLC-LLL-ST). Points denote average values of two independent biological repetitions. Corresponding error bars are also given.

Table 3.5. The yields and carbon balances of the co-cultures

	$Y_{X/S}$, Biomass yield (g Biomass/ g Glc) *	**$Y_{P/S}$, Lactic acid yield (g Lac/ g Glc)**	**Carbon balance (%)**
LLC-LM	0.182±0.005	0.805±0.026	87.77±2.79
LLC-LLL-LM	0.173±0.006	0.802±0.031	88.36±2.94
LLC-ST	0.181±0.001	0.855±0.011	98.67±3.49
LLC-LLL-ST	0.175±0.005	0.826±0.031	93.58±2.56

*Since glucose consumption continued after growth inhibition, biomass yields were based on exponential growth phase.

Among all pure and co-cultures, only carbon balances of mesophilic co-cultures were calculated as less than 90% (Table 3.5). Ethanol and CO_2 produced by *Leu. mesenteroides* in pure culture were calculated based on the glucose consumption (see methods), and

since individual glucose consumption of *Leu. mesenteroides* could not be measured in co-cultures experimentally, ethanol and CO_2 were not considered in the carbon balance of mesophilic co-cultures.

In addition of the yield comparison of pure and co-cultures, biomass, glucose and lactic acid profiles were also compared in Fig. 3.17. This results also showed that biomass, glucose and lactic acid profiles of co-cultures were located between the pure culture profiles.

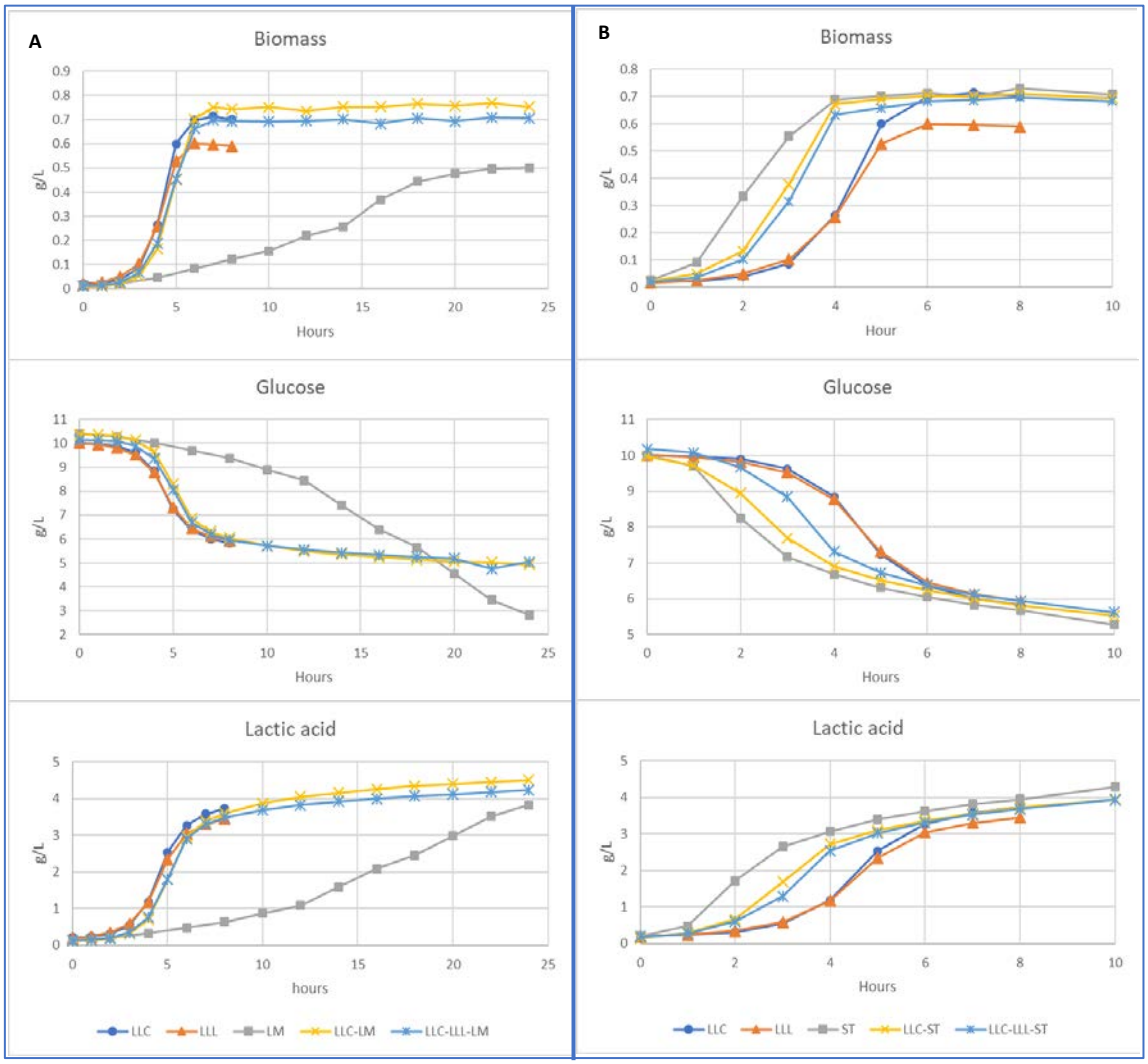

Figure 3.17. Comparative biomass, glucose and lactic acid profiles of pure and co-cultures. (A) Mesophilic co-cultures and pure cultures constituting the co-cultures, (B) thermophilic co-cultures and pure cultures constituting the co-cultures

3.2.3. Individual biomass profiles in the co-cultures

Relative microbial abundance in a microbial community gives important insights about the community dynamics such as suppression or domination of the individual organisms and related changes in the medium composition. Because the microorganisms used in this study are phylogenetically very close species that are hardly distinguished using classical microbiological methods such as colony counting on selective medium, we employed a molecular-based method, qPCR, to estimate relative abundance ratio (see Section 2.3.3).

In all co-cultures, the domination of *L. lactis* subsp. *cremoris* was observed (Fig. 3.18). The final biomass concentration of *Leu. mesenteroides* in mesophilic co-cultures was far lower than the final biomass concentration of *Leu. mesenteroides* in pure culture. Low *Leu. mesenteroides* abundance, in other words the domination of *L. lactis* strains, in mesophilic co-cultures also explained the similar biomass, glucose and lactic acid profiles between pure culture of *L. lactis* strains and mesophilic co-cultures seen in Fig. 3.17-A.

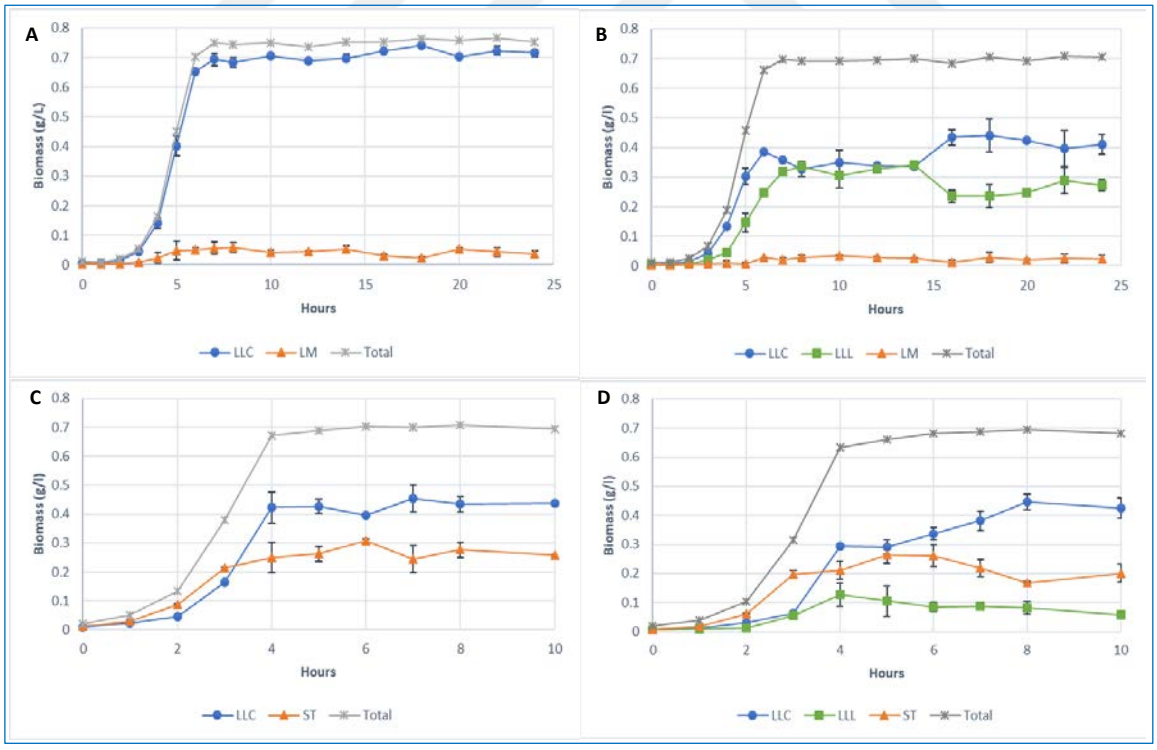

Figure 3.18. Individual biomass profiles of the co-culture members in the two-species mesophilic co-culture (A), the three-species mesophilic co-culture (B), the two-species thermophilic-co culture (C) and the three-species thermophilic co-culture (D).

Similar to mesophilic co-cultures, the final biomass concentration of *L. lactis* subsp. *cremoris* was higher than other co-culture members in the thermophilic co-cultures, although *S. thermophilus* dominated the co-cultures in the early phase of the batches (Fig. 3.18-C, Fig. 3.18-D).

The dynamics behind the biomass compositions in the co-cultures is discussed in Section 3.3 through the co-culture metabolic models.

3.2.4. Amino acid profiles of pure and co-cultures

Amino acid profiles of the pure and co-cultures are given in Fig. 3.19 and Fig. 3.20 comparatively. Since the chromatographic peaks of glutamine/glycine and alanine/proline pairs were overlapped, the profiles of these amino acids were given as a summation, while amino acid profiles of histidine and cysteine could not be detected by the methods used.

Amino acid consumption profiles of pure cultures were mostly coupled with the biomass profiles, except some amino acids such as isoleucine and leucine in *S. thermophilus* pure culture, in which consumption trends continued after stationary phase. We also observed production of some amino acids in pure cultures, and these were methionine and tyrosine in *L. lactis* subsp. *cremoris* and *S. thermophilus* pure cultures, aspartate in *L. lactis* subsp. *lactis* pure culture and asparagine in *Leu. mesenteroides* pure culture. On the other hand, asparagine, serine and threonine profiles in the *L. lactis* subsp. *lactis* pure culture, and asparagine and aspartate profiles in the *Leu. mesenteroides* pure culture showed increasing trend at the early phase of the culture and these amino acids started to be consumed afterwards.

Due to low microbial abundance of *Leu. mesenteroides* in mesophilic co-cultures, amino acid profiles of two-species mesophilic co-culture showed similar profiles to that of *L. lactis* subsp. *cremoris* pure culture. But, unlike *L. lactis* subsp. *cremoris* pure culture, aspartate and tryptophan showed increasing trends in two-species mesophilic co-culture, which might be due to the possible contribution of *Leu. mesenteroides*. Although we observed a general similarity between the amino acid profiles of the two and three-species

mesophilic co-cultures especially before stationary phase, the effects of *L. lactis* subsp. *lactis* on the three-species co-culture were also observed. For instance, methionine consumption was observed in three-species co-culture in parallel with the need of *L. lactis* subsp. *lactis* observed in pure culture. Furthermore, the final concentrations of some amino acids in the three-species mesophilic co-culture such as lysine, phenylalanine and serine were higher than the two-species mesophilic co-culture (Fig. 3.19).

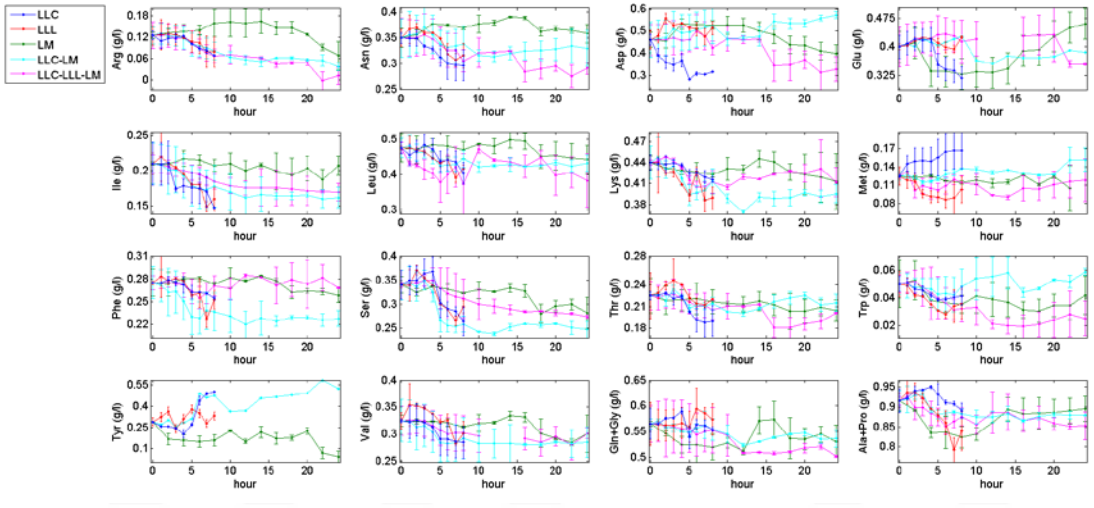

Figure 3.19. Comparative amino acids profiles of *L. lactis* subsp. *cremoris* (LLC), *L. lactis* subsp. *lactis* (LLL) and *Leu. mesenteroides* (LM), two species mesophilic co-culture (LLC-LM) and three-species mesophilic co-culture (LLC-LLL-LM).

Final aspartate concentration of the two-species thermophilic co-culture and the final phenylalanine concentration of the two and three-species thermophilic co-cultures were respectively higher and lower than the pure cultures of the strains constituting the co-cultures. The profiles of the other amino acids in the thermophilic co-cultures were between the amino acid profiles of the pure cultures. Similar to the three-species mesophilic co-culture, an effect of *L. lactis* subsp. *lactis* on the amino acid profiles of the three-species thermophilic co-culture was observed. For instance, the final aspartate concentrations increased in three-species thermophilic co-culture compared to two-species thermophilic co-culture, because of the aspartate production of *L. lactis* subsp. *lactis* (Fig. 3.20).

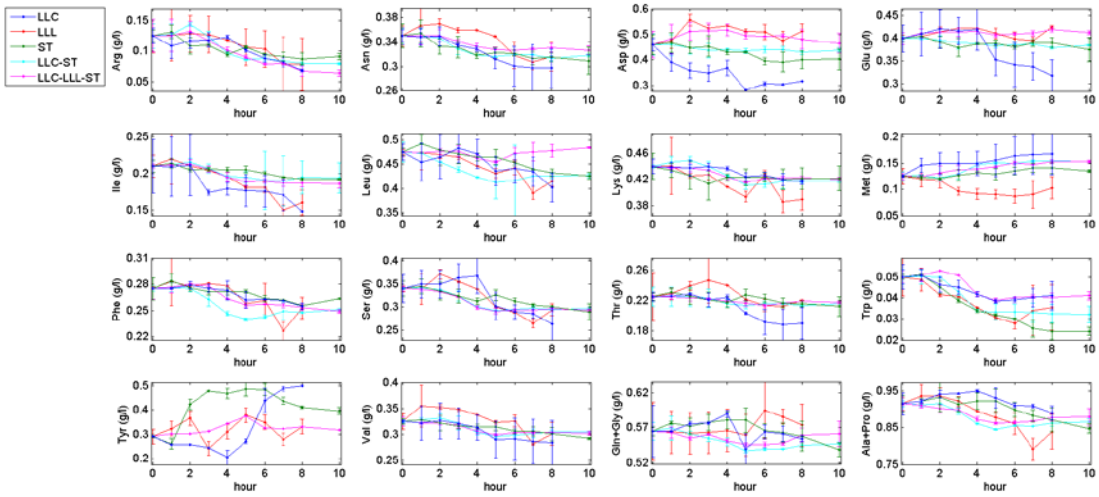

Figure 3.20. Comparative amino acid profiles of *L. lactis* subsp. *cremoris* (LLC), *L. lactis* subsp. *lactis* (LLL) and *S. thermophilus* (ST), two species thermophilic co-culture (LLC-ST) and three-species thermophilic co-culture (LLC-LLL-ST).

3.3. The Dynamic Metabolic Network Modelling of Pure and Co-Cultures

3.3.1. Parameter estimation

To mimic the cheese fermentation, pH was not controlled for all batches. Low pH as a result of increasing organic acid, especially lactic acid, concentration caused growth inhibition for all batches. Consequently, glucose and amino acids were not consumed completely for all batches. The main inhibitory component of lactic acid fermentation is the undissociated form of lactic acid, which is increasingly formed by low pH (Bouguettoucha et al., 2011). Compared to the dissociated form, the undissociated lactic acid is soluble within the cytoplasmic membrane and acidifies the cytoplasm (Gatje and Gottschalk, 1991; Mcdonald et al., 1990), which disturbs proton motive force and the related nutrient transport (Kashket, 1987; Konings, 2002). Hence, glucose and amino acid uptake kinetics used in the dynamic metabolic models were defined with an empirical equation (Eq. 2.3), which is a function of undissociated lactic acid, as glucose and amino acids were not the rate limiting compounds.

The strain specific parameters estimated by the dynamic parameter estimation approach (see methods) and used in substrate uptake kinetics were listed in Table 3.6.

In substrate uptake kinetics, V_{max} and V_{min} define the maximum and minimum utilization rate before and after the low pH conditions respectively, while $K_{[LacH]}$ defines the effect of undissociated lactic acid on the rate. The bigger $K_{[LacH]}$ is, the earlier the inhibition for the rate is. In the dynamic parameter estimation, computational and experimental concentration values are compared such that the errors arising from computational and experimental reaction rate comparison are minimized. Experimental concentration values are the direct results of bioanalyses such as HPLC, while experimental reaction rate values are calculated using these experimental concentration values in relatively large time intervals, which might miss some dynamics for the system. Hence, although the dynamic parameter estimation is computationally a time-consuming process (i.e. days), it was still preferred in this study for a more realistic parameter estimation.

Table 3.6. The strain specific parameters used in the substrate uptake kinetics. The same parameters were used in both pure and co-culture models. The units of V_{max} and V_{min} are mmol/gDW/h, while the unit of $K_{[LacH]}$ is $mmol^{-1}$.

		LLC	LLL	ST	LM			LLC	LLL	ST	LM
Glc	V_{max}	21.405	22.675	35.883	14.645	**Thr**	V_{max}	0.200	0.066	0.010	0.087
	$K_{[LacH]}$	0.182	0.129	0.752	0.178		$K_{[LacH]}$	0.272	0.063	0.250	0.138
	V_{min}	0.196	0.001	1.294	0.474		V_{min}	0.002	0.001	0.004	0.006
Arg	V_{max}	0.217	0.139	0.118	0.031	**Trp**	V_{max}	0.048	0.078	0.138	0.060
	$K_{[LacH]}$	0.140	0.124	0.235	0.064		$K_{[LacH]}$	0.210	0.500	0.358	0.052
	V_{min}	0.003	0.001	0.002	0.000		V_{min}	0.003	0.001	0.007	0.002
Asn	V_{max}	0.328	0.144	0.292	-0.072	**Tyr**	V_{max}	-0.051	0.000	-0.165	0.070
	$K_{[LacH]}$	0.280	0.183	0.591	0.083		$K_{[LacH]}$	0.173	0.112	0.100	0.056
	V_{min}	0.002	0.001	0.006	0.000		V_{min}	0.000	-0.001	0.000	0.000
Asp	V_{max}	0.403	-0.400	0.240	0.083	**Val**	V_{max}	0.410	0.393	0.200	0.092
	$K_{[LacH]}$	0.312	0.216	0.321	0.161		$K_{[LacH]}$	0.260	0.323	0.100	0.139
	V_{min}	0.003	-0.001	0.001	0.005		V_{min}	0.003	0.001	0.004	0.000
Glu	V_{max}	0.210	0.000	0.173	0.030	**Gln**	V_{max}	0.150	0.150	0.080	0.080
	$K_{[LacH]}$	0.286	0.390	0.755	0.272		$K_{[LacH]}$	0.240	0.340	0.500	0.160
	V_{min}	0.001	-0.001	0.005	0.000		V_{min}	0.005	0.003	0.003	0.001

Table 3.6. (Continued)

Ile	V_{max}	0.214	0.334	0.232	0.071	**Gly**	V_{max}	0.150	0.150	0.080	0.080
	$K_{[LacH]}$	0.130	0.261	0.211	0.221		$K_{[LacH]}$	0.240	0.340	0.500	0.160
	V_{min}	0.001	0.001	0.013	0.000		V_{min}	0.005	0.003	0.003	0.001
Leu	V_{max}	0.380	0.599	0.219	0.050	**Ala**	V_{max}	0.150	0.350	0.100	0.080
	$K_{[LacH]}$	0.175	0.400	0.534	0.052		$K_{[LacH]}$	0.200	0.200	0.400	0.160
	V_{min}	0.010	0.001	0.012	0.006		V_{min}	0.005	0.003	0.003	0.001
Lys	V_{max}	0.129	0.194	0.219	0.193	**Pro**	V_{max}	0.150	0.150	0.100	0.080
	$K_{[LacH]}$	0.123	0.385	0.428	0.333		$K_{[LacH]}$	0.200	0.200	0.400	0.160
	V_{min}	0.000	0.001	0.001	0.002		V_{min}	0.005	0.003	0.002	0.001
Met	V_{max}	-0.015	0.170	-0.053	0.010	**His**	V_{max}	0.120	0.120	0.100	0.080
	$K_{[LacH]}$	0.450	0.151	0.265	0.294		$K_{[LacH]}$	0.200	0.200	0.400	0.160
	V_{min}	-0.001	0.001	-0.003	0.001		V_{min}	0.005	0.003	0.003	0.001
Phe	V_{max}	0.141	0.157	0.116	0.065	**Cys**	V_{max}	0.200	0.200	0.100	0.050
	$K_{[LacH]}$	0.180	0.321	0.229	0.227		$K_{[LacH]}$	0.150	0.150	0.450	0.160
	V_{min}	0.001	0.005	0.001	0.000		V_{min}	0.005	0.003	0.020	0.001
Ser	V_{max}	0.364	0.168	0.238	0.090	**Cit**	V_{max}				12.00
	$K_{[LacH]}$	0.135	0.122	0.210	0.217		$K_{[LacH]}$				20.00
	V_{min}	0.006	0.001	0.003	0.000		V_{min}				0.020
							C_1	-0.112	-0.124	-0.147	-0.105
							C_2	5.382	5.728	6.924	5.531

Because the HPLC peaks of glutamine and glycine, alanine and proline were overlapped, and also histidine and cysteine could not be detected by the current HPLC method used, these six amino acids were not considered in dynamic parameter estimation analysis. Since lack of the experimental evidence, the parameters used for the uptake kinetics of these six amino acids were chosen with the following criteria: A moderate value was chosen for the $K_{[LacH]}$ values which was in the range of $K_{[LacH]}$ values estimated by the dynamic parameter estimation analysis for the corresponding strain, while V_{max} and V_{min} values were chosen as much as minimum. All chosen parameters were aimed not to limit the *in-silico* growth.

Citrate was not consumed significantly by pure cultures of *L. lactis* and S. *thermophilus* strains, while *Leu. mesenteroides*, which is known to be a citrate consumer lactic acid

bacteria (Smid and Kleerebezem, 2014), consumed all citrate before the stationary phase. Although the undissociated lactic acid was not the rate limiting compound for the citrate uptake rate in pure culture of *Leu. mesenteroides*, as the citrate was consumed before the undissociated lactic acid reached the rate limiting concentrations, citrate consumption by *Leu. mesenteroides* in the co-cultures was affected by acidic conditions. Hence, the substrate uptake kinetics defined in Eq. 2.5 was also used for citrate uptake, and the parameters used was estimated by manually fitting, changing the kinetic parameters until the simulation agreed most with the experimental data.

Finally, the batch specific parameters C_1 and C_2 in the substrate uptake kinetics were estimated by the non-linear regression of experimental [*LacH*] and [*Lac*] values using Eq. 2.4. Through the parameters C_1 and C_2, the effect of pH was also considered in the substrate uptake kinetics.

3.3.2. Dynamic flux balance analysis (dFBA) for pure cultures

The GSMM of *L. lactis* (Flahaut et al., 2013), the revised GSMM of *S. thermophilus* (Pastink et al., 2009) and the GSMM of *Leu. mesenteroides* reconstructed in this thesis study were used for dFBA. Dynamically changing glucose and amino acid uptake rates of the GSMMs were constrained using the substrate uptake kinetics in Eq. 2.5 and the parameters listed in Table 3.6. Non-growth associated maintenance (NGAM) of *L. lactis* and *Leu. mesenteroides* models were fixed to 0.92 and 0.51 mmol/gDW/h respectively. The NGAM value of *L. lactis* was reported in the in the original model study (Flahaut et al., 2013), while the NGAM value of *Leu. mesenteroides* was calculated for this study (see Appendix B). Since NGAM of *S. thermophilus* model was not reported in the original model study (Pastink et al., 2009), the NGAM of *S. thermophilus* was fixed to 0.7 mmol/gDW/h, which is the average of the values used for the two other microorganisms.

Although *L. lactis* and *S. thermophilus* are mostly known as homolactic fermentative species, as also observed in our experiments, they can switch to mixed-acid fermentation in some conditions such as change of carbon source and continuous cultures at low dilution rate (Flahaut et al., 2013; Giaretta et al., 2018). Apart from glucose and amino acids uptake constraints, the experimental lactic acid yield (the ratio of lactic acid

production and glucose consumption rates) was also used as another constraint for GSMMs of *L. lactis* and *S. thermophilus*, which assured the homolactic fermentation observed in *L. lactis* and *S. thermophilus* strains. Without the lactic acid yield constraint, *L. lactis* and *S. thermophilus* models showed mixed acid fermentation, which produced acetic acid, formic acid and/or ethanol instead of lactic acid, as previously reported in the GSMM study of *Lactobacillus plantarum* (Teusink et al., 2006) and *L. lactis* (Flahaut et al., 2013; Oliveira et al., 2005). The reason behind the mixed acid fermentation preference of the models with biomass optimization is extra ATP gain with acetic acid production, and re-oxidization of NADH through formic acid and ethanol production in mixed acid fermentation, which is re-oxidized though lactic acid production in homolactic fermentation. GSMM of *Leu. mesenteroides* did not need the lactic acid yield constraint, as the organism is an obligate heterolactic fermentative lactic acid bacterium that uses phosphoketolase pathway and produces lactic acid and ethanol in anaerobic fermentation for ATP production and re-oxidation of NADH respectively.

Biomass and extracellular metabolites profiles of the pure cultures of *L. lactis*, *S. thermophilus* and *Leu. mesenteroides* strains were then simulated by dFBA, and the model results were compared with experimental results (Fig. 3.22-3.25). Pure culture dFBA results showed that the models fitted closely to the experimental data, except for some amino acids.

As discussed in Section 3.2., the experiments showed that glucose consumption slightly continued at the stationary phase where growth was inhibited by low pH. But in the dFBA models, growth was non-zero as substrate consumption continued, because of the fact that growth rate was maximized as an objective function and it was proportional with substrate uptake rates. On the other hand, we could simulate the experimental stationary phase by dFBA models although glucose consumption continued. As pH decreases, undissociated lactic acid concentration ([*LacH*]) increases, and exponential term of substrate uptake kinetics (i.e. $-V_{\max} \exp(-K_{LacH}[LacH]) - V_{\min}$, Eq. 2.3) goes to zero, and the substrate uptake rate converges to the term "$-V_{min}$". Therefore, at low pH, glucose uptake rate in the models was almost equal to the $-V_{min}$ value (table 3.6), and the major part of the ATP produced with minimum glucose uptake flux ($-V_{min}$) was used in non-growth associated maintenance, which was already constrained with a constant value (Fig 3.22).

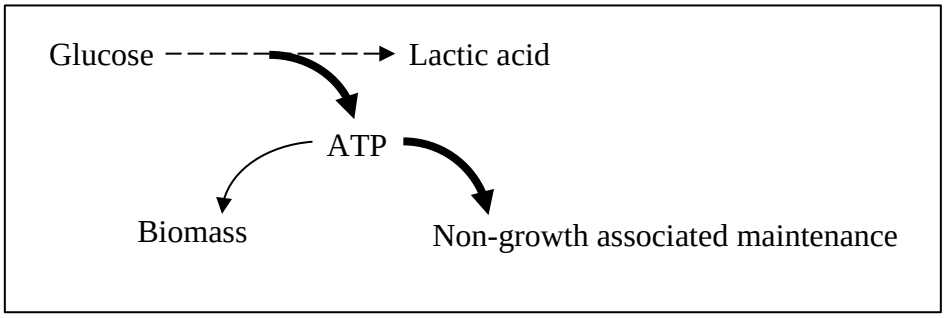

Figure 3.21. The route of the major part of ATP flux produced by minimal glucose uptake ($-V_{min}$).

But we still observed an increasing trend on *in-silico* biomass profile at stationary phase in *S. thermophilus* model, because V_{min} value of this strain was high enough to produce ATP satisfying both NGAM and significant growth rate (Fig. 3.25).

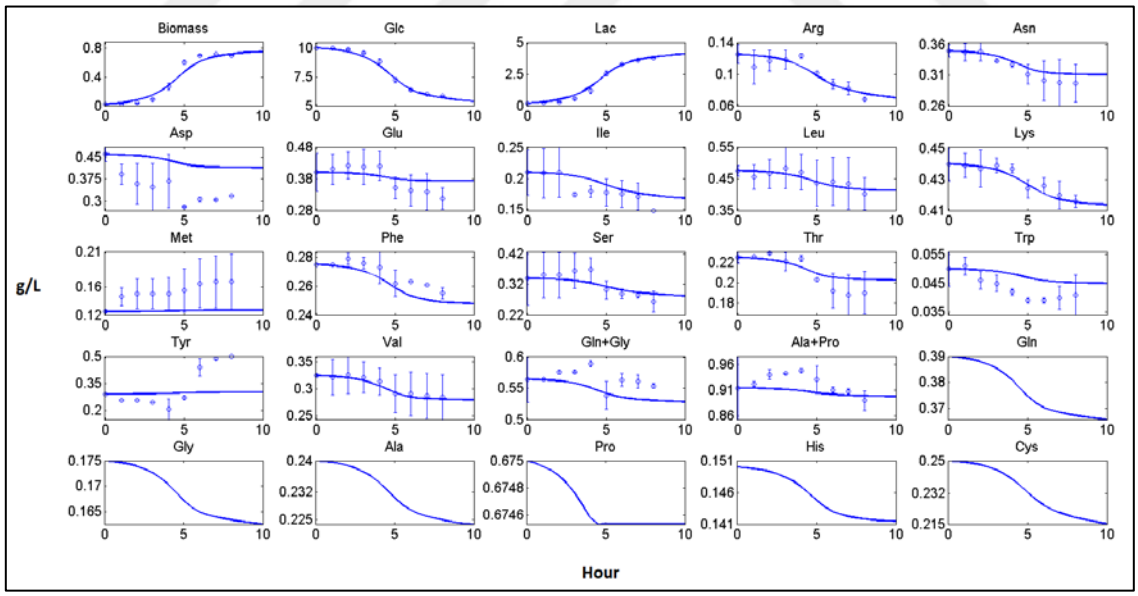

Figure 3.22. Batch culture profiles of *L. lactis* subsp. *cremoris*. Solid lines denote model results simulated by dFBA, while points denote average values of two independent biological repetitions. Corresponding error bars are also given.

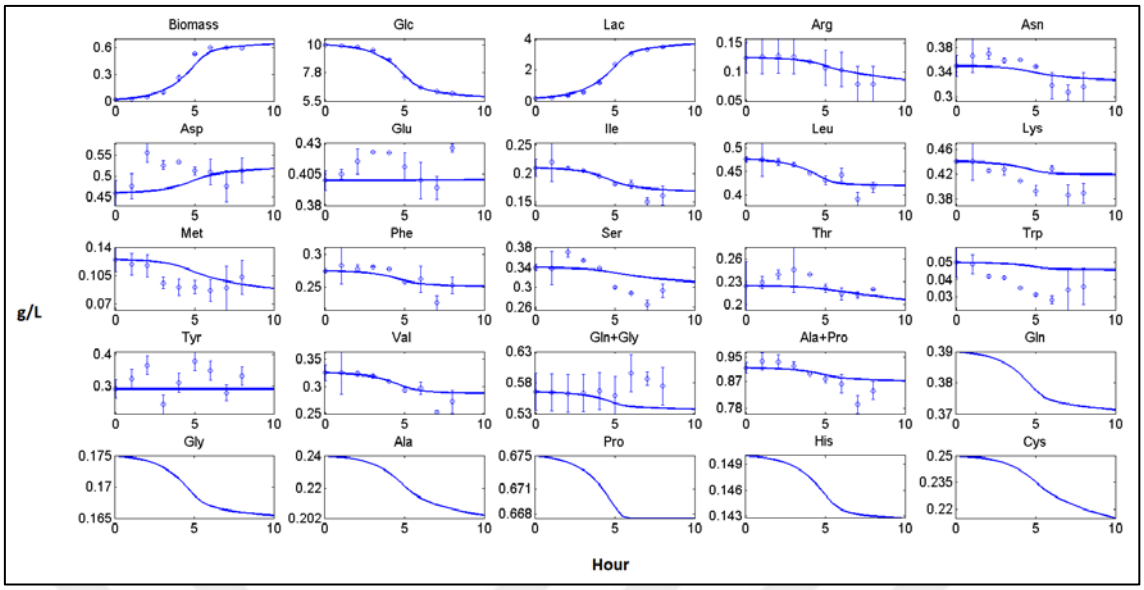

Figure 3.23. Batch culture profiles of *L. lactis* subsp. *lactis*. Solid lines denote model results simulated by dFBA, while points denote average values of two independent biological repetitions. Corresponding error bars are also given.

Amino acids profiles of the pure cultures were mostly coupled with biomass profiles (Fig. 3.22-3.25). For some amino acids such as aspartate in the LLC culture, the models underestimated the experimental profiles because substrate uptake rates were constrained as maximum uptake rates (e. i. the constraints were fixed to only lower bound of the exchange reactions), which allowed the models to consume the corresponding substrates in less amounts, or they can even produce the related compounds, if required. The underestimated *in-silico* amino acid profiles showed that the models used less amino acids than that observed in the experiments. Excess amino acids that could not be predicted by the models might be used in other metabolisms not considered by these models, such as protein production of secondary metabolism.

Methionine and tyrosine were experimentally produced in *L. lactis* subsp. *cremoris* and *S. thermophilus* batches. These amino acids were underestimated by the *L. lactis* model as the production of these amino acids dramatically decreased the growth. On the other hand, aspartate and asparagine were experimentally produced by *L. lactis* subsp. *lactis* and *Leu. mesenteroides* respectively, and the models of these species could simulate the productions.

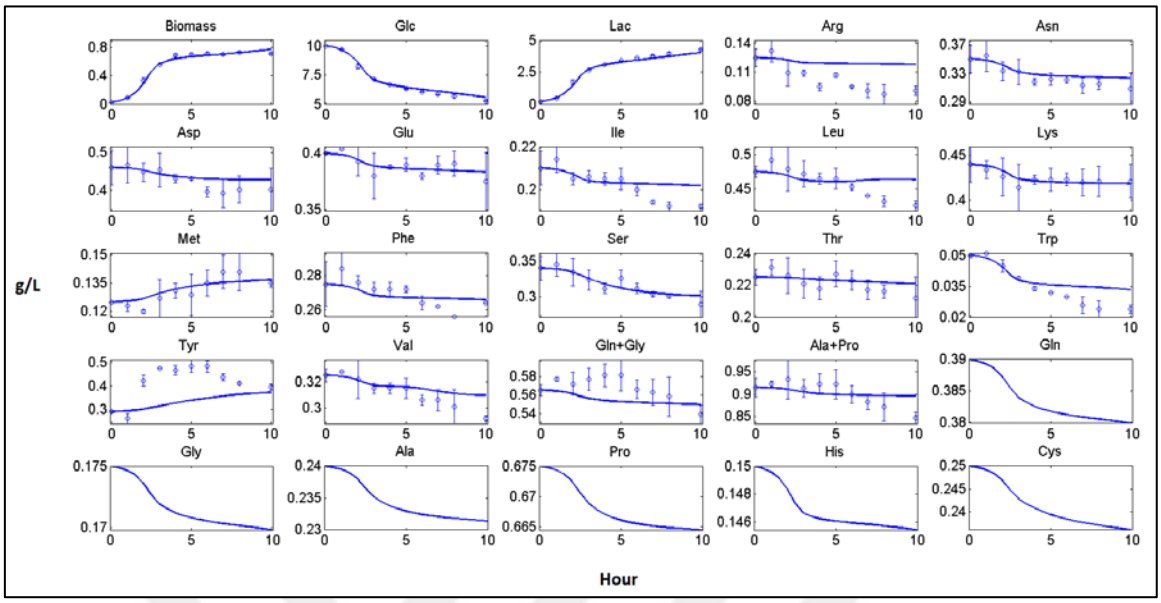

Figure 3.24. Batch culture profiles of *S. thermophilus*. Solid lines denote model results simulated by dFBA, while points denote average values of two independent biological repetitions. Corresponding error bars are also given.

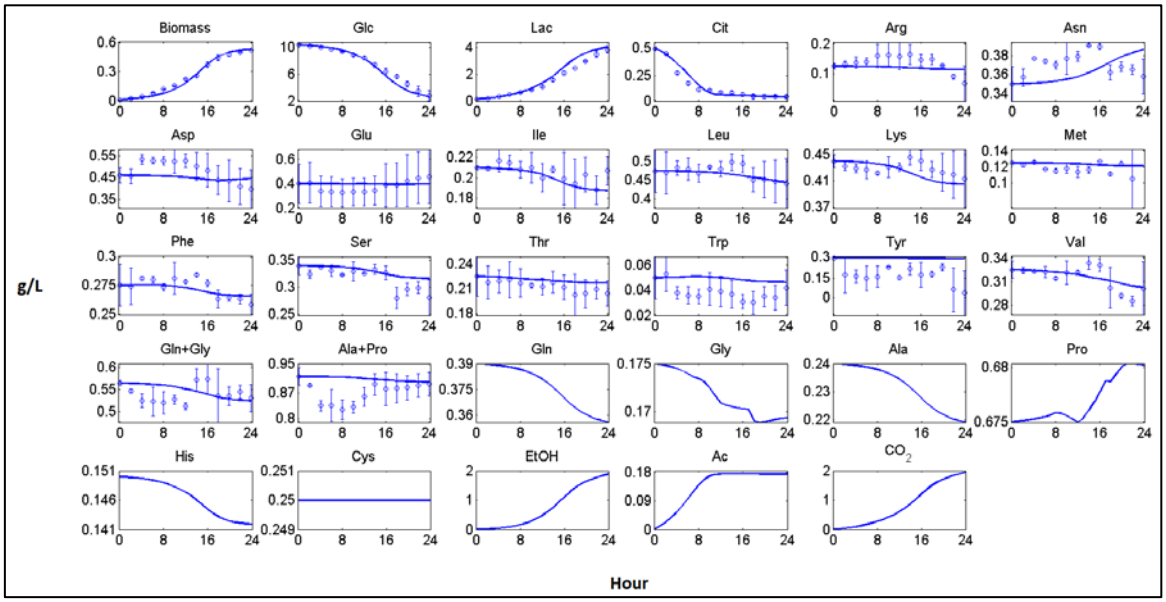

Figure 3.25. Batch culture profiles of *Leu. mesenteroides*. Solid lines denote model results simulated by dFBA, while points denote average values of two independent biological repetitions. Corresponding error bars are also given.

When we zoomed in the early phase of biomass profiles, we observed that *L. lactis* models slightly overestimated the experimental values (Fig. 3.26). The reason behind this is the structure of substrate uptake kinetics (Eq. 2.5), where *in-silico* substrate uptake rate starts the uptake with its maximum value because of the minimal undissociated lactic acid concentration at the beginning of the batch. Because the growth rate is proportional with substrate uptake rates in the models, lag phase of growth observed in *L. lactis* pure culture experiments could not be simulated by the models. On the other hand, a significant lag phase was not observed in the *S. thermophilus* pure culture experiment, which was also confirmed by *S. thermophilus* model via an accurate biomass prediction in the early phase of the batch (Fig. 3.26).

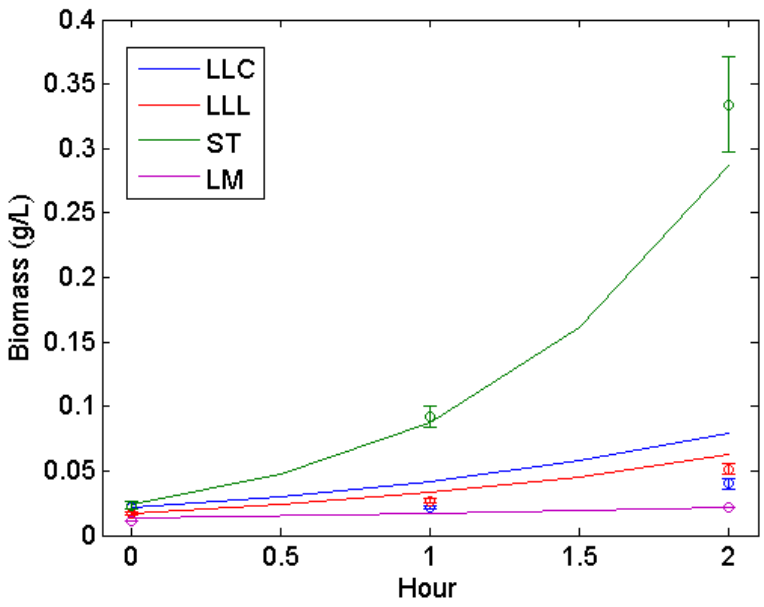

Figure 3.26. *In-silico* and *in-vitro* biomass profiles of pure cultures in the early phase. Solid lines denote model results simulated by dFBA, while points denote average values of two independent biological repetitions. Corresponding error bars are also given.

3.3.3. Dynamic co-culture metabolic modelling

The dynamic co-culture metabolic models were reconstructed for two and three-species mesophilic and thermophilic co-cultures as illustrated in Fig. 3.27. The strain specific parameters estimated using the pure culture experiments (Table 3.6) and co-culture specific parameters C_1 and C_2 (Table 3.7), which consider the co-culture specific pH profiles, were used in the co-culture models.

Table 3.7. Co-culture specific parameters, C_1 and C_2

	Two species mesophilic co-culture	**Three-species mesophilic co-culture**	**Two-species thermophilic co-culture**	**Three species thermophilic co-culture**
C_1	-0.111	-0.117	-0.126	-0.125
C_2	5.397	5.540	5.999	5.916

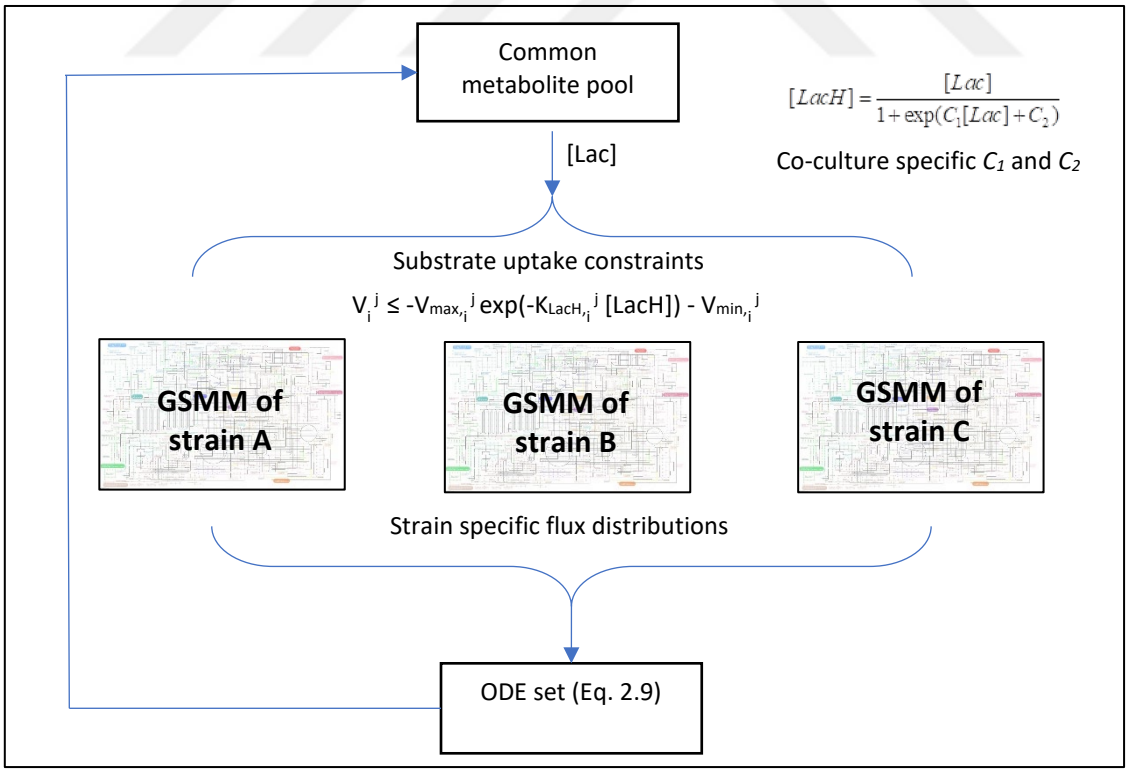

Figure 3.27. Dynamic co-culture metabolic modelling structure. *i* and *j* denote the indices for substrates (glucose and amino acids) and strains respectively.

Mesophilic co-culture model results showed that the models fitted closely to the experimental data. The mesophilic co-culture models and experiments showed the domination of *L. lactis* species over *Leu. mesenteroides*, and the contribution of *Leu. mesenteroides* to the final biomass in two and three species co-cultures were around 6% and 3.5% respectively (Fig. 3.28). This result is consistent with the previous reports (Erkus et al., 2013; van Mastrigt et al., 2019) stating that the final biomass ratio of *Leu. mesenteroides* in long term (days) is around 1% in the mesophilic cheese starter cultures comprised of *L. lactis* and *Leu. mesenteroides* strains.

The suppression of *Leu. mesenteroides* in the co-cultures could be explained by the rapid acidification of the medium by *L. lactis* strains. In other word, lactic acid pool mostly produced by *L. lactis* strains decreased the uptake rates of *Leu. mesenteroides* according to the substrate uptake kinetics, which made *Leu. mesenteroides* disadvantageous in the competition for sugar and amino acid source in co-cultures. Another reason for the suppression of *Leu. mesenteroides* could be the ATP yield of *Leu. mesenteroides* per molar glucose consumed. *Leu. mesenteroides* is obligate heterolactic lactic acid bacterium, and ATP yield of the obligate heterolactic fermentation is lower than homolactic fermentation as observed in *L. lactis* (Ganzle, 2015). On the other hand, unlike the pH-controlled co-culture of *L. lactis* and *Leu. mesenteroides* reported in literature (van Mastrigt et al., 2019), the disadvantageous nature of ATP yield was minor reason to explain the growth suppression of *Leu. mesenteroides* in our pH-uncontrolled study. Final biomass concentrations of *Leu. mesenteroides* in mesophilic co-cultures were 10-fold less than the ones produced in pure culture, which was the same result with a study investigating *L. lactis* and *Leu. mesenteroides* strains in pure and co-cultures in reconstituted skim milk (Bellengier et al., 1997). Furthermore, final biomass concentration of *L. lactis* subsp. *lactis* was lower than *L. lactis* subsp. *cremoris* in the three-species mesophilic co-culture, as observed in pure cultures.

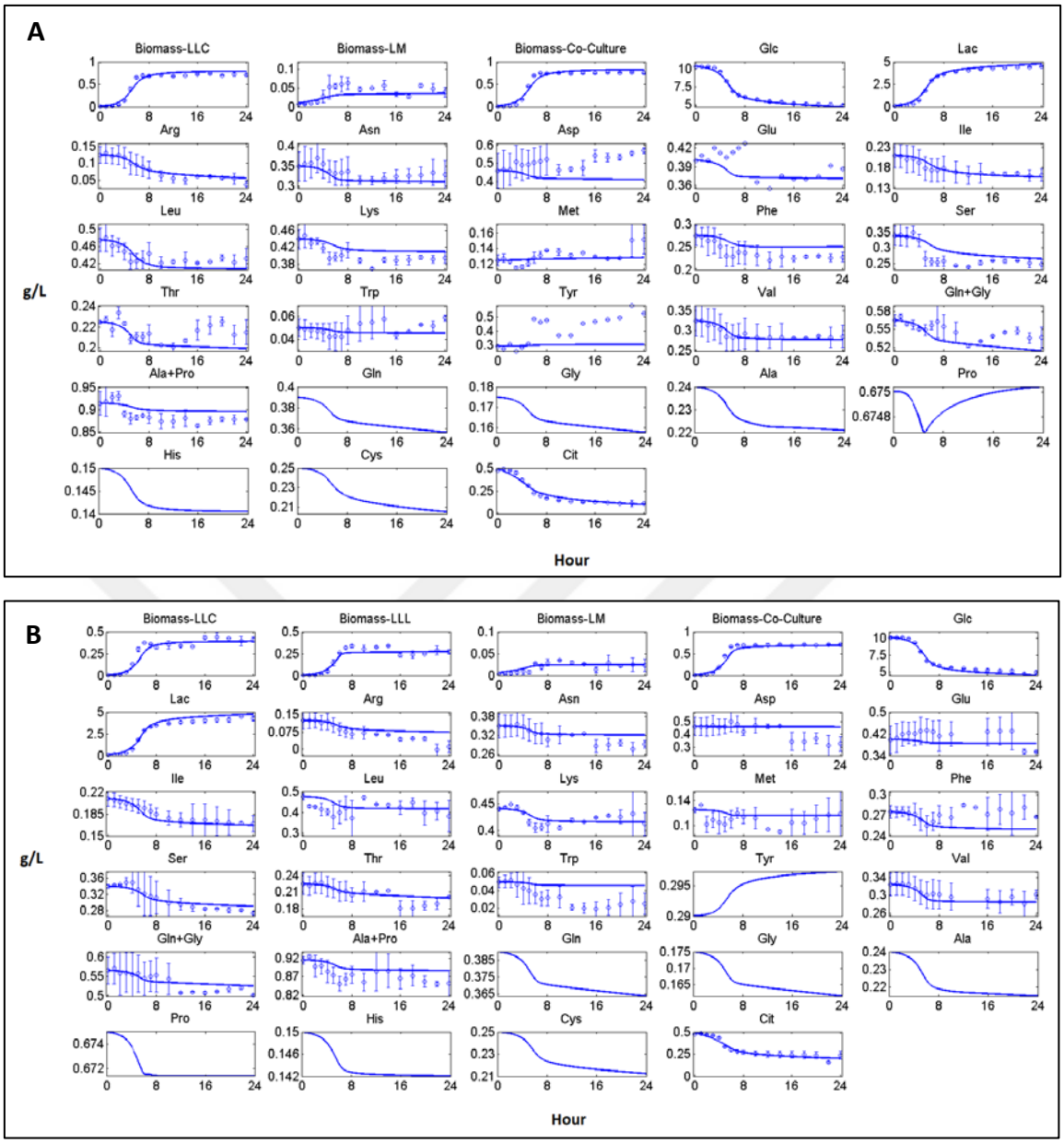

Figure 3.28. Computational and experimental mesophilic co-culture profiles. A) Two-species mesophilic co-culture comprised of *L. lactis* subsp. *cremoris* (LLC) and *Leu. mesenteroides* (LM). B) Three-species mesophilic co-culture comprised of *L. lactis* subsp. *cremoris* (LLC), *L. lactis* subsp. *lactis* (LLL) and *Leu. mesenteroides* (LM). Solid lines denote the co-culture model results, while points denote average values of two independent biological repetitions. Corresponding error bars are also given.

GSMMs of *L. lactis* and *S. thermophilus* were used for the reconstruction of the thermophilic co-culture models. Similar to the mesophilic co-cultures, *L. lactis* subsp. *cremoris* dominated the thermophilic co-cultures experimentally, but the preliminary analyses of thermophilic co-culture models showed the opposite, with *S. thermophilus* dominating the co-cultures *in-silico*. In addition to a possible interaction between *S. thermophilus* and *L. lactis*, which the co-culture models might miss, this unexpected result could be explained with the different fermentation temperature of *L. lactis* and *S. thermophilic* in pure and thermophilic co-cultures, which were 30°C, 37°C and 33°C respectively (see methods). When we focus on the growth performance of the *L. lactis* and *S. thermophilus* species based on the experimental growth rates with respect to pH values (Fig. 3.29), the growth performances of *L. lactis* and *S. thermophilus* strains were higher in the co-cultures and pure culture respectively at above the pH values causing the inhibitory effect (i.e. ~pH ≤ 5). This result is consistent with a study (Adamberg et al., 2003), where the authors investigated the effect of different temperatures on growth rate for several LAB including *L. lactis* and *S. thermophilus* at optimal pH values of related species.

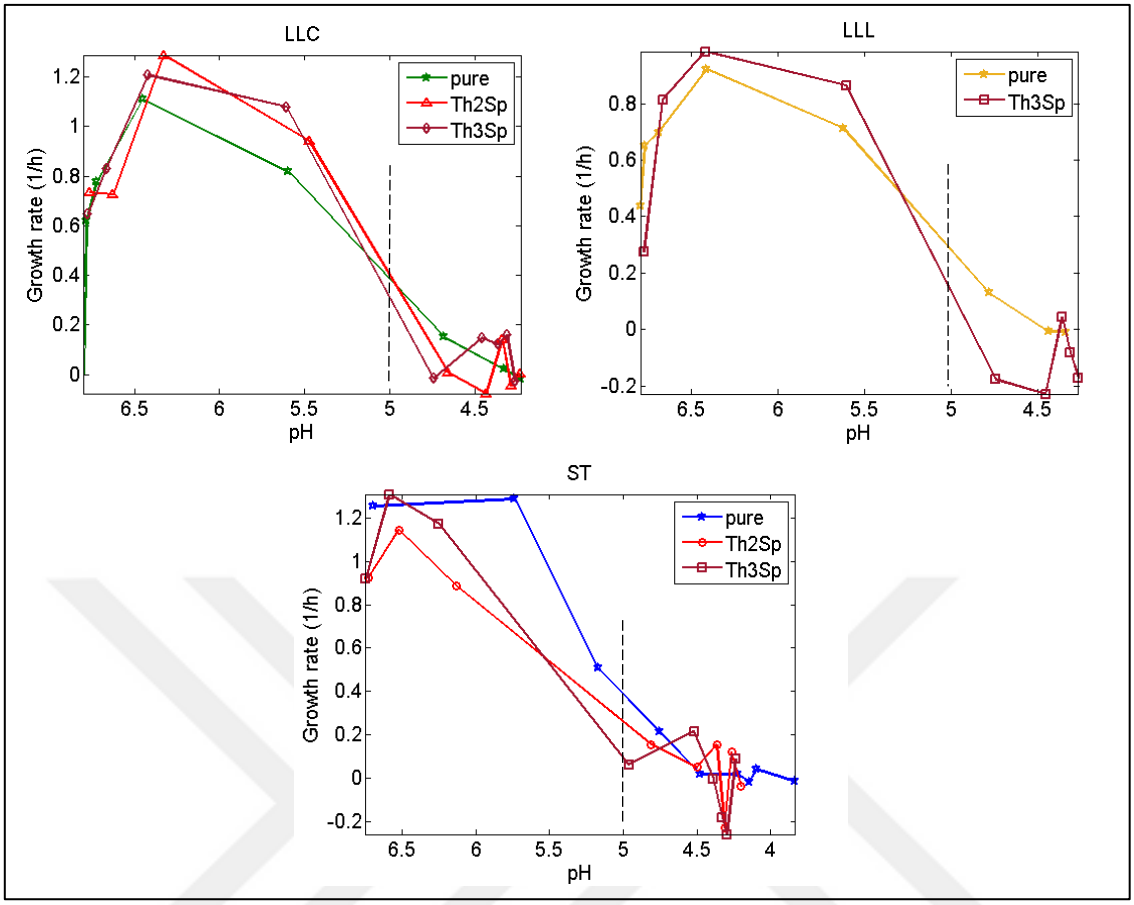

Figure 3.29. The growth performance of the *L. lactis* and *S. thermophilus* strains based on the experimental growth rate with respect to pH in pure and thermophilic co-cultures. Th2Sp and Th3Sp denote the two and three-species thermophilic co-cultures. *L. lactis* subsp. *cremoris* (LLC), *L. lactis* subsp. *lactis* (LLL) and *S. thermophilus* (ST).

Because of the temperature difference, the growth rate profile of *L. lactis* in the co-culture increased around 20%, while the growth rate profile of *S. thermophilus* in the co-culture decreased around 20%, compared to their pure cultures. Assuming the substrate uptake rates are coupled with growth rate, all substrate uptake rates of *L. lactis* and *S. thermophilus* were then multiplied by 1.2 and 0.8 respectively to consider the effect of different temperatures in pure and co-cultures on *L. lactis* and *S. thermophilus*, being around 20%.

After multiplying all the substrate uptake rates by the correction coefficients, the domination of *L. lactis* subsp. *cremoris* in thermophilus co-cultures could be simulated

(Fig. 3.30). Two-species thermophilic co-culture model fitted closely to the experimental concentration profiles of individual biomass and co-culture level extracellular compounds (Fig. 3.30-A).

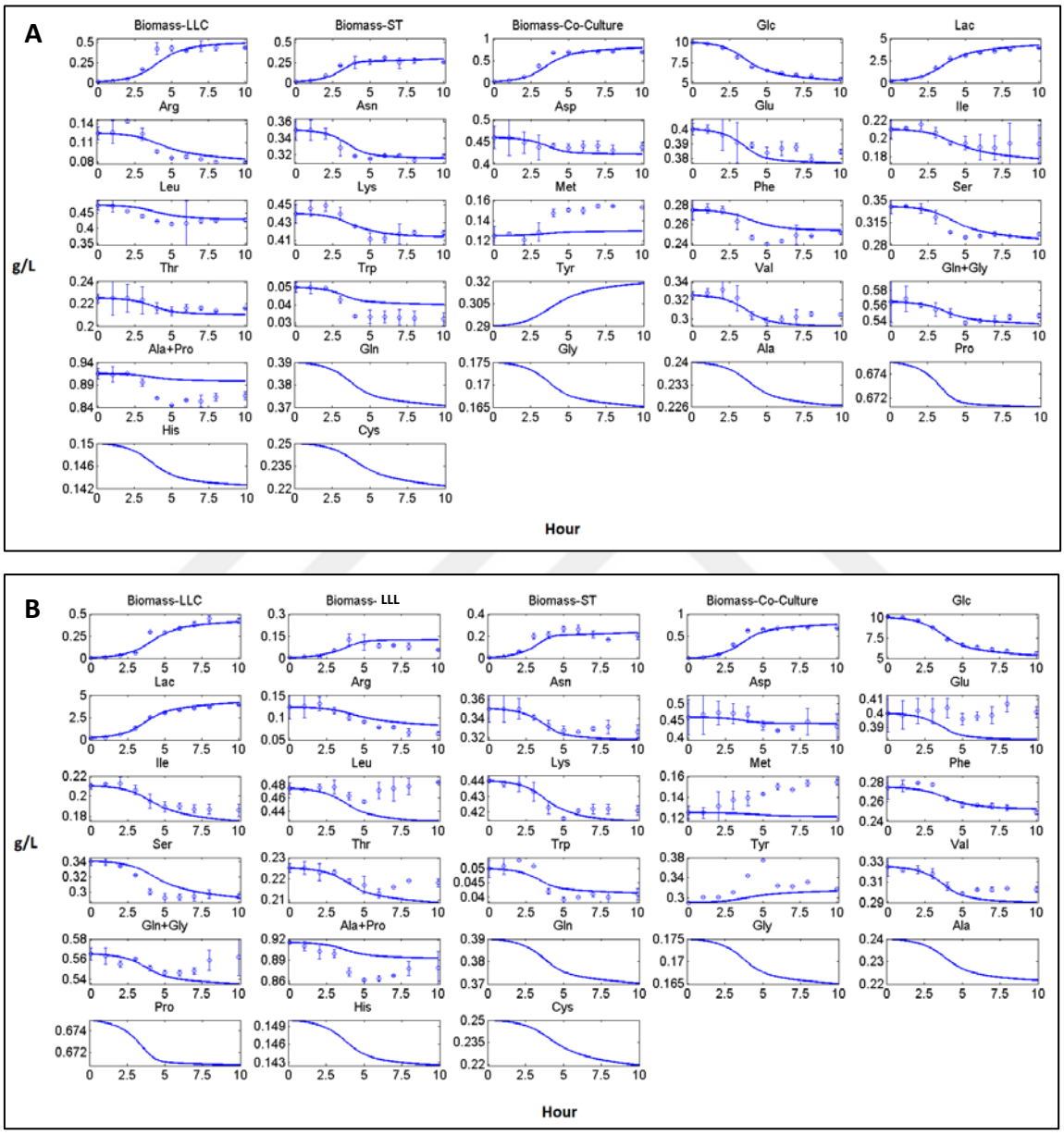

Figure 3.30. Computational and experimental thermophilic co-culture profiles. A) Two-species thermophilic co-culture comprised of *L. lactis* subsp. *cremoris* (LLC) and *S. thermophilus* (ST). B) Three-species thermophilic co-culture comprised of *L. lactis* subsp. *cremoris* (LLC), *L. lactis* subsp. *lactis* (LLL) and *S. thermophilus* (ST). Solid

lines denote the co-culture model results, while points denote average values of two independent biological repetitions. Corresponding error bars are also given.

Although individual biomass abundance ratio of *L. lactis* subsp. *cremoris* decreased in the early phase of the batch, its abundance increased afterwards, and this experimental result was also predicted by the model (Fig. 3.31).

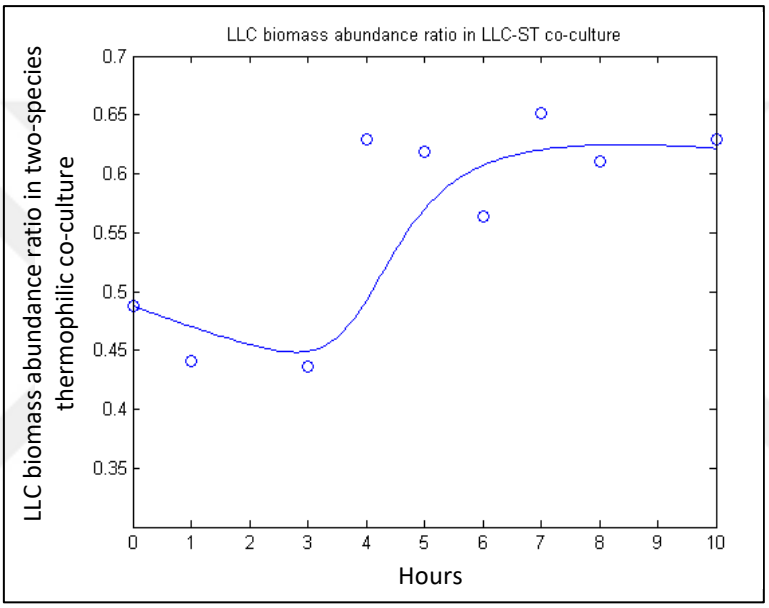

Figure 3.31. Individual biomass abundance ratio of *L. lactis* subsp. *cremoris* (LLC) in two-species thermophilic co-culture. Solid lines and points denote the model and average experimental results respectively.

Although the three-species thermophilic co-culture model predicted the final individual biomass compositions of the organisms as *L. lactis* subsp. *cremoris* being the most and *L. lactis* subsp. *lactis* being the least abundant species, the model could not predict the individual biomass profiles of *L. lactis* strains precisely (Fig. 3.30-B).

Experimentally obtained individual biomass profiles in the co-cultures were not as smooth as those observed in pure cultures. We observed some fluctuations on the individual biomass profiles of co-culture especially at stationary phase, which could be

due to the estimation method of the relative microbial abundance (see Section 2.3.3). These small and instantaneous increase/decrease at the individual biomass profiles of all co-cultures at stationary phases were assumed acceptable as they showed the general biomass dynamics of the co-culture. On the other hand, individual biomass profiles of *L. lactis* subsp. *cremoris* and subsp. *lactis* increased and decreased respectively at the late phase of the three-species thermophilic co-culture, which was not expected because of the growth inhibition by acidic conditions discussed above.

Experiments showed that glutamate, leucine and threonine were produced at the late phase of the three-species thermophilic co-culture, but the model could not simulate these productions, as the amino acids were consumed to assure the maximum growth rate, which is the objective function in the models.

3.3.4. Individual flux rate profiles of co-culture members

Although we monitored the co-culture level profiles of extracellular compounds (i.e. sugar source, organic acids and amino acids), the organism-level extracellular compound profiles of co-culture members could not be obtained experimentally. However, the co-culture metabolic models estimated the individual extracellular flux rate profiles of glucose, organic acids, ethanol, CO_2, amino acids, nucleic acids, vitamins and flavour compounds of co-culture members (Fig. 3.32-3.35), which also showed the potential metabolic interactions between the LAB in the co-cultures.

Nucleic acids in the Fig. 3.32-3.35 are adenine, guanine and uracil; vitamins are folic acid, inosine, nicotinic acid, pantothenate, orotic acid, riboflavin, thiamine and thymidine; flavour compounds are 2 hydroxy 3 methyl butanoate, 2 hydroxy 3 methyl pentanoate, 2 methylbutanal, 2 methylpropanoic acid, 3 methylbutanoic acid, acetaldehyde, methanethiol, hydrogen sulphide, phenylethyl alcohol, 4MOP, 3MOP, 3MOB.

Individual flux rate profiles showed that utilization rates of the extracellular compounds were maximum in the early stage of the batches, where undissociated lactic acid concentrations were under the rate limiting levels.

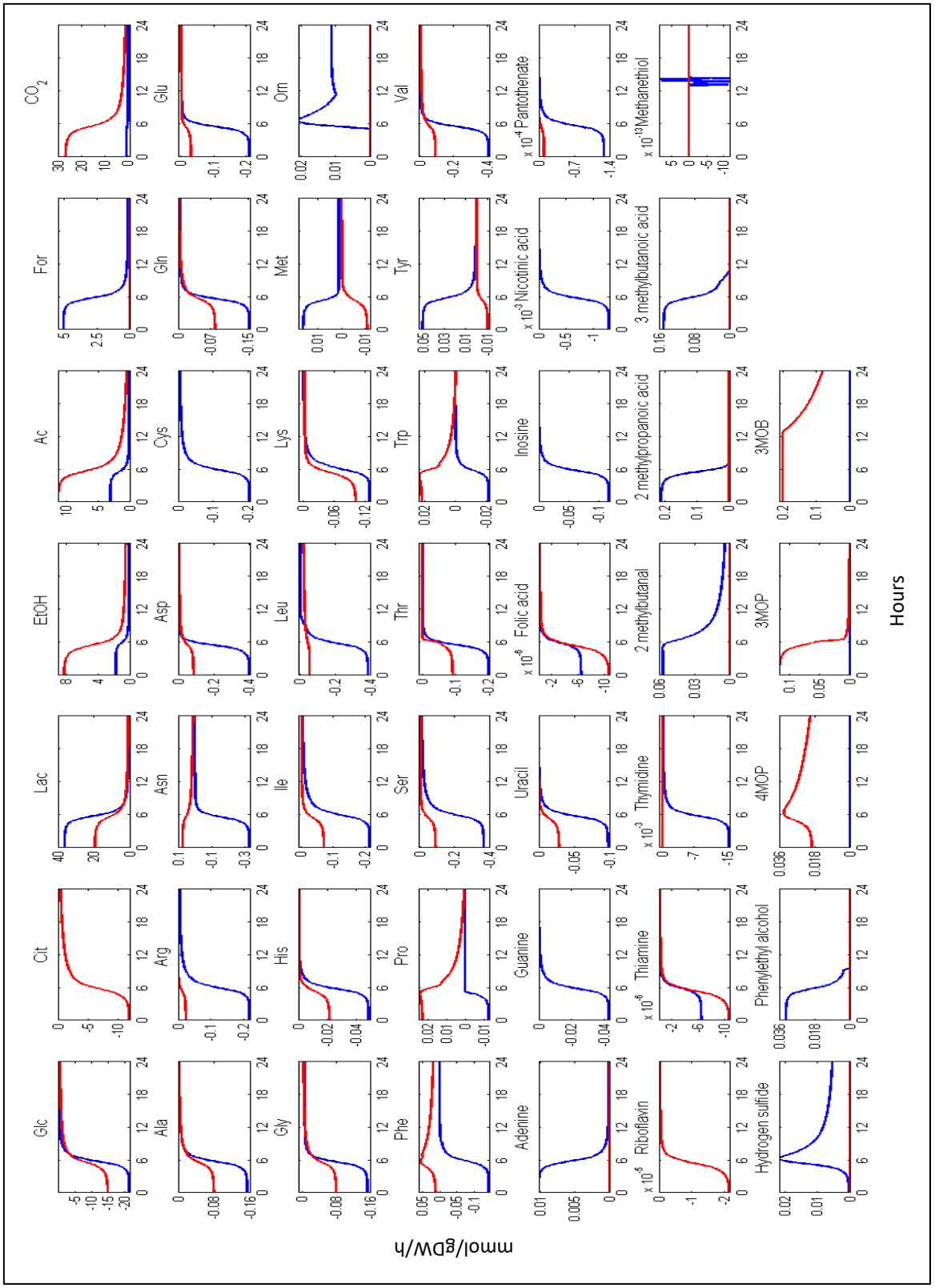

Figure 3.32. Individual flux rate profiles of *L. lactis* subsp. *cremoris* (blue line) and *Leu. mesenteroides* (red line) in two-species mesophilic co-culture. Negative and positive flux values show consumption and production respectively.

In the two-species mesophilic co-culture, asparagine, methionine, proline and tryptophan were produced by one organism, while other consumed (Fig. 3.32). In the three-species mesophilic co-culture, asparagine, aspartate, methionine, phenylalanine, proline and tryptophan were the amino acids that one organism produced while the others consumed or vice versa (Fig. 3.33). The compounds produced by an organism and consumed by other(s) have cross-feeding potential between the organisms.

In the two-species thermophilic co-culture, no compound, except adenine, was estimated by the model as being cross-fed between *L. lactis* and *S. thermophilus* (Fig. 3.34). But, in the three-species thermophilic co-culture, the model estimated that aspartate was produced, and methionine was consumed by *L. lactis* subsp. *lactis*, which was a different metabolic behaviour than other co-culture members (Fig. 3.35).

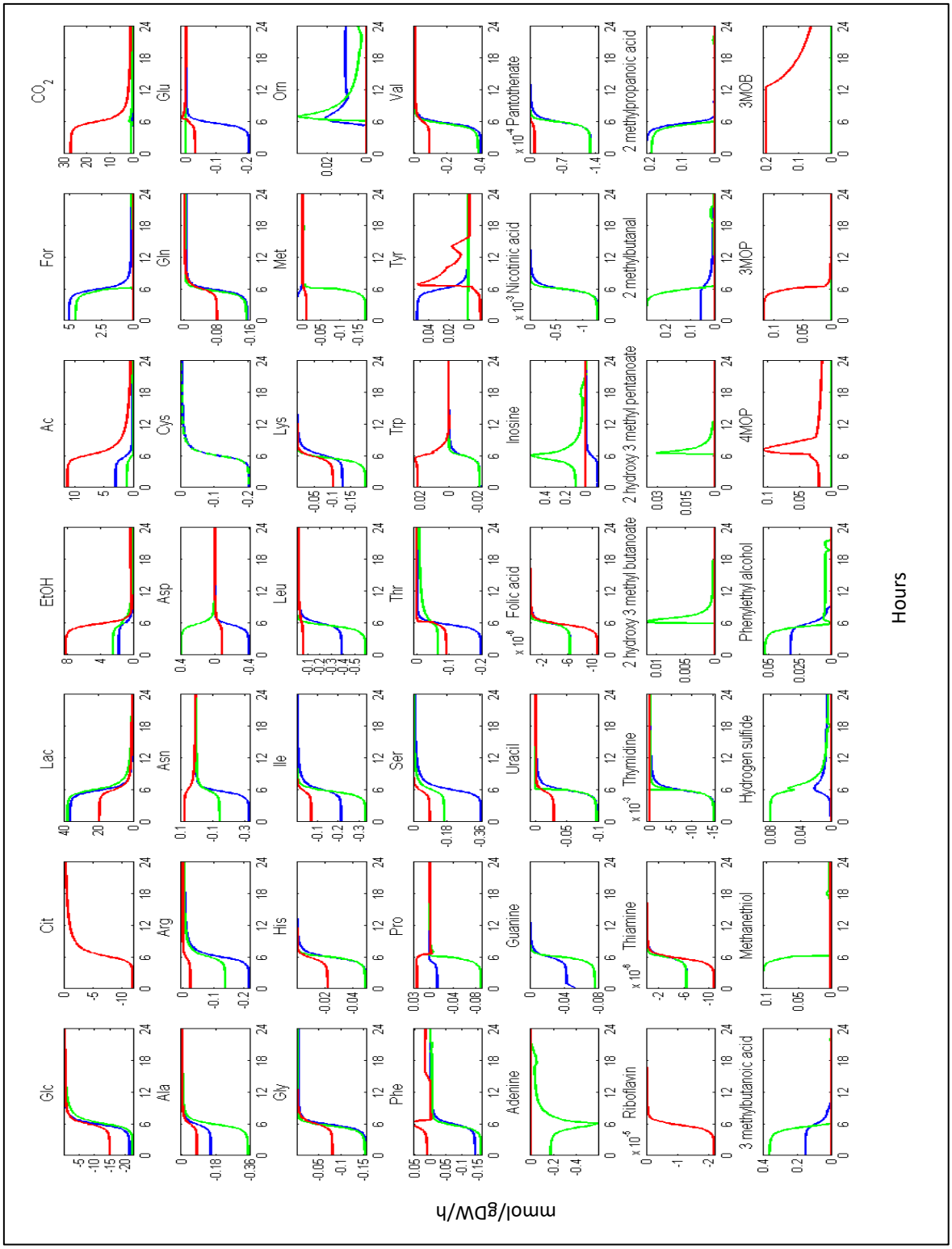

Figure 3.33. Individual flux rate profiles of *L. lactis* subsp. *cremoris* (blue line), *L. lactis* subsp. *lactis* (green line) and *Leu. mesenteroides* (red line) in three-species mesophilic co-culture. Negative and positive flux values show consumption and production respectively.

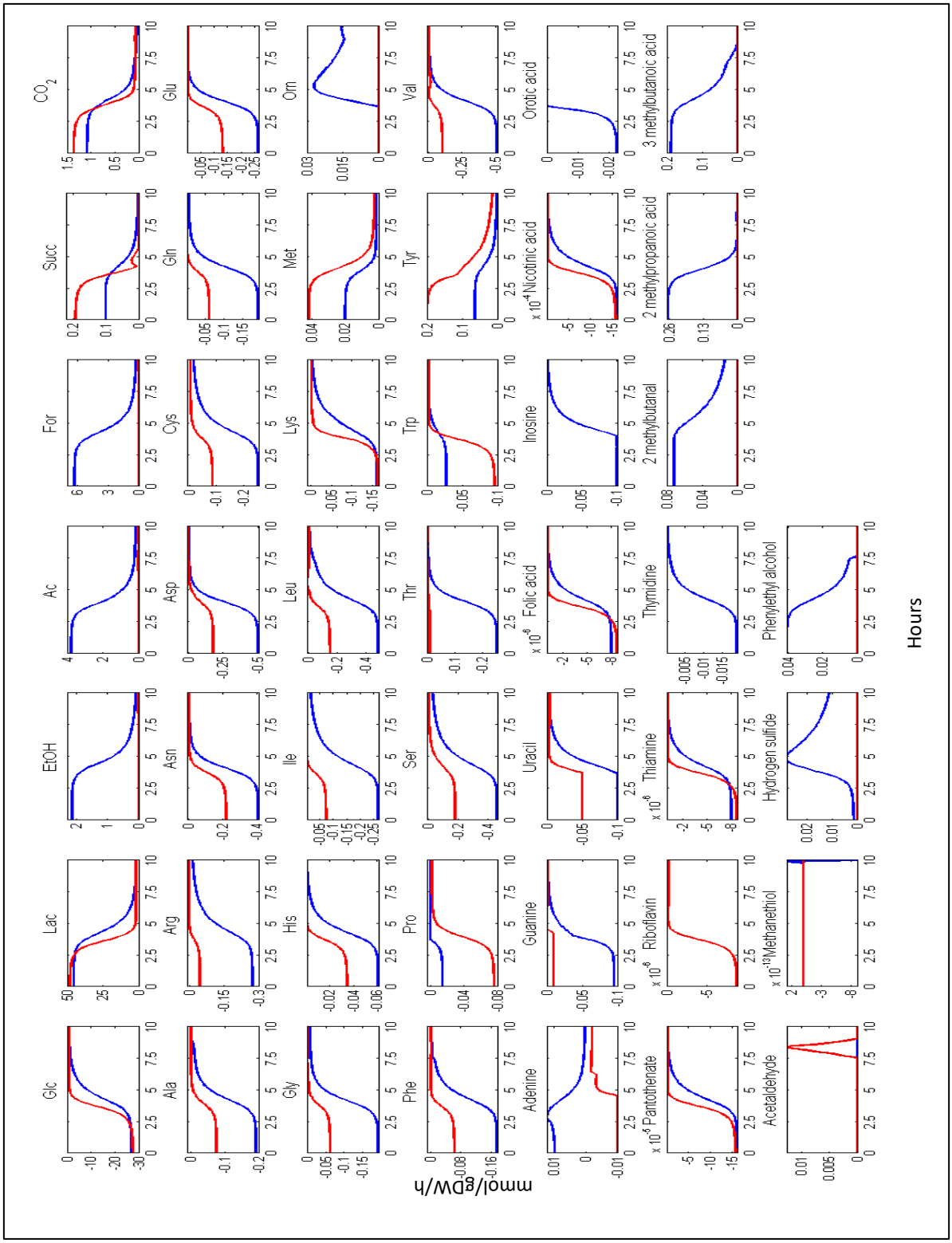

Figure 3.34. Individual flux rate profiles of *L. lactis* subsp. *cremoris* (blue line) and *S. thermophilus* (red line) in two-species thermophilic co-culture. Negative and positive flux values show consumption and production respectively.

There are several hypotheses about why microorganisms used in food fermentation processes produce flavour compounds (Carroll et al., 2016; Christiaens et al., 2014), and some mechanisms for flavour metabolite production could be inferred by our metabolic models. In the hypothetical analysis of the *Leu. mesenteroides* model in the section 3.12, we found that flavour formation occurred only after increased carbon uptake did not enhance growth rate anymore. In that analysis, although carbon uptake rate increased, growth was limited at some point because of the amino acid limitation, which suggested that flavour formation occurs under excess carbon and ATP. We expected the similar pattern in co-culture models because growth was limited by low pH and carbon source was kept being consumed. However, flux profiles of co-culture models showed that only hydrogen sulphide produced by *L. lactis* subsp. *cremoris* and acetaldehyde produced by *S. thermophilus* were produced after growth limitation, and the rest of the flavour metabolites production was coupled with growth (Fig. 3.32-3.35).

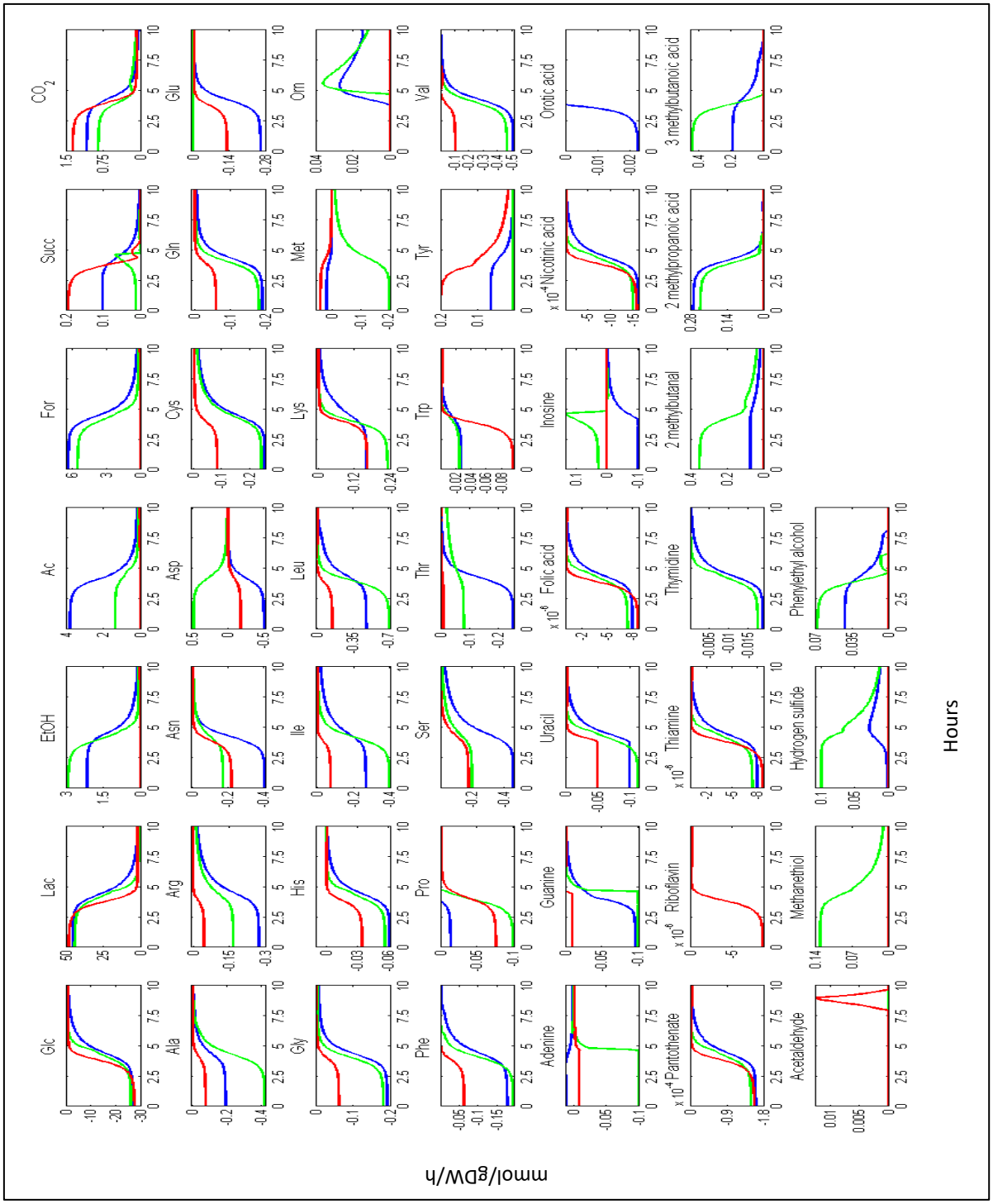

Figure 3.35. Individual flux rate profiles of *L. lactis* subsp. *cremoris* (blue line), *L. lactis* subsp. *lactis* (green line) and S. thermophilus (red line) in three-species thermophilic co-culture. Negative and positive flux values show consumption and production respectively.

4. CONCLUSION AND RECOMMENDATIONS

Thinking that different type of microorganisms living in the same habitat as a microbial community do not affect each other would be irrational. therefore, different types of lactic acid bacteria (LAB) coexisting in food fermentation affect each other and subsequently the product quality. In this thesis, lactic acid bacteria of cheese starter culture were investigated by comprehensive experimental and computational analyses in order to better understand their metabolic capacities both when they live alone and together. In this way, this study also intended to be an important contribution to the related areas. To this end, *L. lactis* subsp. *cremoris*, *L. lactis* subsp. *lactis*, *S. thermophilus* and *Leu. mesenteroides*, which are the LAB commonly used in cheese starter cultures, were grown in pure and co-cultures.

In the experimental part, the LAB were fermented in a batch bioreactor as pure and co-cultures. Biomass, glucose, organic acids and amino acids concentration profiles of pure and co-cultures were obtained experimentally. In the computational part, the pure and co-cultures were simulated via dynamic metabolic models, and their fermentation dynamics and the metabolic capacities were comprehensively investigated. In addition to the experimentally obtained compound profiles, the metabolic models predicted the profiles of other extracellular compounds such as flavour metabolites. The co-culture metabolic models also predicted the individual compound profiles of LAB in the co-cultures, which enabled the estimation of potential metabolic interactions among LAB in the co-cultures.

The results of the study were given in three subsections. In the first subsection (Section 3.1), the reconstruction and validation of GSMM of *Leu. mesenteroides* was discussed. Although GSMMs of *L. lactis* and *S. thermophilus* existed in literature (Flahaut et al., 2013; Pastink et al., 2009), GSMM of the dairy-origin *Leu. mesenteroides* was reconstructed for this thesis study for the first time. The phosphoketolase pathway (PKP) is a unique feature of the obligate heterolactic fermentation, which leads to the production of lactate, ethanol and/or acetate, and the final product profile of PKP highly depends on the energetics and redox state of the organism. GSMM of *Leu. mesenteroides* explained the energetics and redox state mechanisms of the organism in full detail. Model simulations further showed that, in co-metabolism of citrate and glucose, no flavour compounds were produced when citrate could stimulate the formation of biomass.

Significant amounts of flavour metabolites (e.g., diacetyl and acetoin) were only produced when citrate could not enhance growth, which suggests that flavour formation only occurs under carbon and ATP excess.

In the second subsection (Section 3.2), the experimental results were briefly discussed. Pure cultures of *L. lactis* and *S. thermophilus* species showed homolactic fermentation, and the pure culture of *Leu. mesenteroides* showed heterolactic fermentation. Biomass and product yields of the co-cultures were neither higher nor lower than the pure cultures of the co-culture members, which showed that the co-cultures did not create an advantage or a disadvantage compared to the pure cultures in terms of the yields. The effects of the fermentation dynamics on the pure and co-cultures were then discussed in the last subsection (Section 3.3.) through the dynamic metabolic models in a quantitative manner.

In the third subsection (Section 3.3), batch fermentation profiles of the pure and co-cultures were simulated by dFBA and dynamic co-culture metabolic models, respectively. All batch fermentations were carried out without pH control to mimic cheese fermentation, and none of the substrates were consumed completely for all batches due to pH inhibition. Hence, kinetic expressions based on the concentration of a rate-limiting substrate such as Michaelis-Menten Kinetics was not valid for this study. Rather, the lactic acid produced, which was the main reason of the low pH, was the growth-limiting compound for the experiments. Thus, the substrate uptake kinetics in the dynamic models was defined with an empirical equation as a function of lactic acid and pH. The strain-specific parameters of the substrate uptake kinetics were estimated using pure culture experiments, and they were used both in single-strain and co-culture models.

In Section 3.3.2, dFBA results showed that the *in-silico* concentration profiles of the biomass, glucose, lactic acid and most of the amino acids fitted closely to the experimental data. This showed that the calculated values of the parameters used in the models were acceptable for the study. In Section 3.3.3, LAB co-cultures were modelled with the dynamic co-culture metabolic modelling approach at genome-scale for the first time. Although the dynamic co-culture metabolic modelling can be applied to any type of microbial community, the studies that applied this approach before have used the consortia having pre-defined metabolic interactions such as cross-feeding (Hanemaaijer et al., 2017; Zhuang et al., 2011; Zhuang et al., 2012). This study is the first study that applied the dynamic co-culture metabolic modelling to a consortia having no known

metabolic interactions, but instead the co-culture models estimated the potential metabolic interactions among the microorganisms in the co-cultures. Although the co-culture models estimated some potential cross-feedings at amino acid and nucleic acid level, they were not crucial for the co-cultures. Yet, the co-culture models explained the biomass, substrate and product dynamics of the co-culture fermentations in detail.

The experiments were carried out in a chemically defined medium so that the amino acid utilization profiles of the pure and co-cultures could be obtained. Experimentally obtained amino acid utilization profiles were then used as a constraint for the metabolic models, and this increased the prediction capacity of the metabolic models.

The chemically defined medium enables one to monitor medium components during fermentation, and this is important for the understanding of the metabolic capacity of the fermentation. However, some metabolic relationship patterns among microorganisms in a community might not be observed in the same way as they are observed in complex medium.

Protease dependency is an example of the microbial community of LAB, which can be observed in a complex medium. Instead of free amino acids, the organic nitrogen source generally exists as big molecules in a complex medium, for example casein in milk. LAB having protease enzymes (Prt+) break down the casein into smaller polypeptides and amino acids, and LAB having no protease enzymes (Prt-) benefit from Prt+ LAB, consuming amino acids in the medium (Smid and Lacroix, 2013). In a study, the growth of a Prt- *L. lactis* strain was stimulated by a Prt+ *L. lactis* strain through supplying amino acids and peptides in cheese starter cultures in a complex medium. This relationship pattern had no negative effect on the Prt+ variant at the beginning of the co-culture. However, this commensal relationship turned into a parasitism by rapid growth of the Prt- variant, because the Prt- variant had a higher growth rate and the Prt- variant dominated the co-culture (Fig. 4.1) (Smid and Lacroix, 2013).

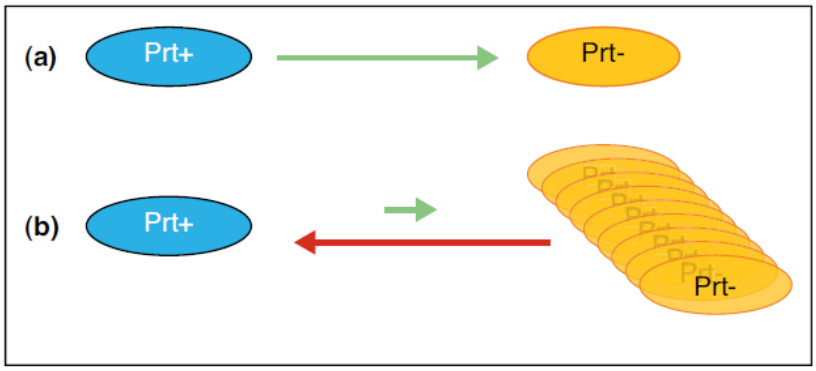

Figure 4.1. Relationship pattern of Prt+ and Prt- variants of *L. lactis* strains in a cheese starter culture in a complex medium. (a) The Prt+ variant supplies the surplus peptides and amino acids for Prt- variants, this has no negative effect on the Prt+ variant, (b) If the growth rate of the Prt- variant is higher than that of the Prt+, microbial abundance of the Prt- variant increases, and this commensal relationship eventually turns into parasitism. This figure was taken from (Smid and Lacroix, 2013).

Another example of a relationship pattern in the complex medium is associated with a flavour metabolite production. *L. lactis* SK110 strain does have protease enzyme but it lacks a decarboxylating enzyme for the production of 3-methylbutanal, while *L. lactis* B1157 strain has decarboxylating enzyme for the production of 3-methylbutanal but no protease enzyme. Hence, in order to produce the 3-methylbutanal in a complex medium, the co-culture of *L. lactis* SK110 and *L. lactis* B1157 is required. In a complex medium, *L. lactis* SK110 supplies leucine to *L. lactis* B1157 by breaking down casein into amino acids, and *L. lactis* SK110 uses leucine to produce the 3-methylbutanal by a decarboxylating enzyme (Fig. 4.2) (Ayad et al., 2001).

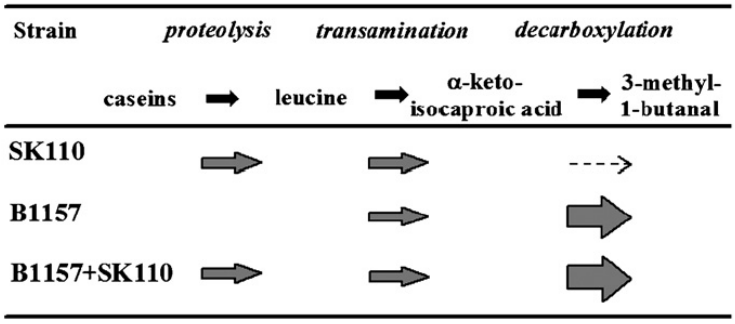

Figure 4.2. The co-culture of *L. lactis* SK110 and *L. lactis* B1157 in a complex medium. The metabolisms of these two strains complete each other to produce the flavour metabolite, 3-methylbutanal. Arrows denote the enzymatic activity. This figure was taken from (Pastink et al., 2008).

As discussed above, the co-culture studies in a chemically defined medium give important insights about the metabolic capacity of a co-culture. However, the co-culture of interest should also be grown in a complex medium to learn more about the metabolic interactions among the microorganisms in the co-culture.

Computational systems biology approaches have accelerated the studies on biotechnology for last two decades. The scientific developments have been rapid; thus, those approaches can swiftly become outdated. For instance, DNA microarray technology revolutionized transcriptome analysis by making it widely accessible (Heller, 2002). However, with the advent of the next generation sequencing technology, the RNA-seq technology has mostly replaced the DNA microarrays because of its advantages such as ability to detect novel transcripts and to quantify a larger range of expression level (Wang et al., 2009). Unlike DNA microarray, genome-scale metabolic modelling has still maintained its popularity and wide usage. However, some of the new generation metabolic modelling approaches can be alternative to the standard genome-scale metabolic modelling, as the simulations of the metabolic phenotype considering only metabolic network may not always predict the *in-vivo* behaviour. One of those new generation metabolic modelling approaches is the models of metabolism and macromolecular expression (ME-models), which calculates the metabolic flux distribution considering not only mass balances around the metabolites of a metabolic network but also the protein cost of the metabolism (King et al., 2015a; Lerman et al.,

2012; O'Brien et al., 2013). The cell might prefer less ATP-efficient pathways at higher growth rates, which can be explained by the protein cost. The ATP-efficient pathways having high protein cost become a burden for a cell at high growth rate, and the cell switches to cheaper and less ATP-efficient pathways (Basan et al., 2015). The ME-model of *E. coli* simulated the metabolic shift and the protein limitation at high growth rates (O'Brien et al., 2013). The best-known metabolic shift observed in LAB is the switch from heterolactic to homolactic fermentation. Although mixed acid fermentation is more ATP-efficient than homolactic fermentation, most of LAB prefers homolactic fermentation at high growth rates (Teusink and Molenaar, 2017). The proteomic studies investigating the metabolic shift in *L. lactis* showed that the internal proteome level hardly changed, while the expression of membrane-associated processes was significantly affected at different growth rates (Goel et al., 2015; Teusink and Molenaar, 2017). As it was discussed in the Section 3.3.2, the GSMMs of *L. lactis* and *S. thermophilus* tend to exhibit the mixed acid fermentation because of the ATP efficiency. The experimental lactic acid yield was used as a constraint for GSMMs of *L. lactis* and *S. thermophilus* to assure the homolactic fermentation which was experimentally observed in *L. lactis* and *S. thermophilus* strains. Extra constraints make a metabolic model more descriptive and less predictive. Yet, the lactic acid yield constraint was a mandatory solution for the GSMMs of *L. lactis* and S. *thermophilus*. Hence, to make less descriptive and more predictive co-culture metabolic models, the protein efficiency and allocation (Chen and Nielsen, 2019) and even the biochemical thermodynamics including a Gibbs energy balance (Niebel et al., 2019) should be considered for the model reconstruction. This thesis study is expected not only to contribute the related areas, but also to inspire the future studies as pointed out above.

5. REFERENCES

Adamberg K, Kask S, Laht TM, Paalme T (2003) The effect of temperature and pH on the growth of lactic acid bacteria: a pH-auxostat study. Int J Food Microbiol 85(1-2):171-83

Aite M, Chevallier M, Frioux C, Trottier C, Got J, Cortes MP, Mendoza SN, Carrier G, Dameron O, Guillaudeux N, Latorre M, Loira N, Markov GV, Maass A, Siegel A (2018) Traceability, reproducibility and wiki-exploration for "a-la-carte" reconstructions of genome-scale metabolic models. PLoS Comput Biol 14(5):e1006146

Aller K, Adamberg K, Timarova V, Seiman A, Festsenko D, Vilu R (2014) Nutritional requirements and media development for Lactococcus lactis IL1403. Appl Microbiol Biotechnol 98(13):5871-81

Ayad EHE, Verheul A, Engels WJM, Wouters JTM, Smit G (2001) Enhanced flavour formation by combination of selected lactococci from industrial and artisanal origin with focus on completion of a metabolic pathway. Journal of Applied Microbiology 90(1):59-67

Bachmann H, Kruijswijk Z, Molenaar D, Kleerebezem M, van Hylckama Vlieg JE (2009) A high-throughput cheese manufacturing model for effective cheese starter culture screening. Journal of Dairy Science 92(12):5868-82

Bachmann H, Starrenburg MJ, Molenaar D, Kleerebezem M, van Hylckama Vlieg JE (2012) Microbial domestication signatures of Lactococcus lactis can be reproduced by experimental evolution. Genome Res 22(1):115-24

Bang J, Li L, Seong H, Kwon YW, Lee DY, Han NS (2017) Macromolecular and Elemental Composition Analyses of Leuconostoc mesenteroides ATCC 8293 Cultured in a Chemostat. J Microbiol Biotechnol 27(5):939-942

Basan M, Hui S, Okano H, Zhang Z, Shen Y, Williamson JR, Hwa T (2015) Overflow metabolism in Escherichia coli results from efficient proteome allocation. Nature 528:99

Bellengier P, Richard J, Foucaud C (1997) Associative Growth of Lactococcus lactis and Leuconostoc mesenteroides Strains in Milk. Journal of Dairy Science 80(8):1520-1527

Biggs MB, Medlock GL, Kolling GL, Papin JA (2015) Metabolic network modeling of microbial communities. Wiley Interdiscip Rev Syst Biol Med 7(5):317-34

Blaya J, Barzideh Z, LaPointe G (2018) Symposium review: Interaction of starter cultures and nonstarter lactic acid bacteria in the cheese environment. Journal of Dairy Science 101(4):3611-3629

Bolotin A, Quinquis B, Renault P, Sorokin A, Ehrlich SD, Kulakauskas S, Lapidus A, Goltsman E, Mazur M, Pusch GD, Fonstein M, Overbeek R, Kyprides N, Purnelle B, Prozzi D, Ngui K, Masuy D, Hancy F, Burteau S, Boutry M, Delcour J, Goffeau A, Hols P (2004) Complete sequence and comparative genome analysis of the dairy bacterium Streptococcus thermophilus. Nat Biotechnol 22(12):1554-8

Bordbar A, Monk JM, King ZA, Palsson BO (2014) Constraint-based models predict metabolic and associated cellular functions. Nature Reviews Genetics 15:107

Borenstein E (2012) Computational systems biology and in silico modeling of the human microbiome. Briefings in Bioinformatics 13(6):769-780

Bouguettoucha A, Balannec B, Amrane A (2011) Unstructured Models for Lactic Acid Fermentation - A Review. Food Technology and Biotechnology 49(1):3-12

Bourel G, Henini S, Divies C, Garmyn D (2003) The response of Leuconostoc mesenteroides to low external oxidoreduction potential generated by hydrogen gas. J Appl Microbiol 94(2):280-8

Carroll AL, Desai SH, Atsumi S (2016) Microbial production of scent and flavor compounds. Current Opinion in Biotechnology 37:8-15

Carvalheiro F, Moniz P, Duarte LC, Esteves MP, Girio FM (2011) Mannitol production by lactic acid bacteria grown in supplemented carob syrup. Journal of Industrial Microbiology & Biotechnology 38(1):221-227

Caspi R, Billington R, Ferrer L, Foerster H, Fulcher CA, Keseler IM, Kothari A, Krummenacker M, Latendresse M, Mueller LA, Ong Q, Paley S, Subhraveti P, Weaver DS, Karp PD (2015) The MetaCyc database of metabolic pathways and enzymes and the BioCyc collection of pathway/genome databases. Nucleic Acids Research 44(D1):D471-D480

Chen Y, Nielsen J (2019) Energy metabolism controls phenotypes by protein efficiency and allocation. Proceedings of the National Academy of Sciences 116(35):17592-17597

Christiaens JF, Franco LM, Cools TL, De Meester L, Michiels J, Wenseleers T, Hassan BA, Yaksi E, Verstrepen KJ (2014) The Fungal Aroma Gene ATF1 Promotes Dispersal of Yeast Cells through Insect Vectors. Cell Reports 9(2):425-432

Chun BH, Kim KH, Jeon HH, Lee SH, Jeon CO (2017) Pan-genomic and transcriptomic analyses of Leuconostoc mesenteroides provide insights into its genomic and metabolic features and roles in kimchi fermentation. Sci Rep 7(1):11504

Cocaign-Bousquet M, Garrigues C, Novak L, Lindley ND, Loublere P (1995) Rational development of a simple synthetic medium for the sustained growth of Lactococcus lactis. Journal of Applied Bacteriology 79(1):108-116

Cogan TM, Beresford TP, Steele J, Broadbent J, Shah NP, Ustunol Z (2007) Invited review: Advances in starter cultures and cultured foods. Journal of Dairy Science 90(9):4005-21

Cogan TM, Hill C (1993) Cheese Starter Cultures. In: Fox PF (ed) Cheese: Chemistry, Physics and Microbiology: Volume 1 General Aspects. Springer US, Boston, MA, pp 193-255

Cosgrove MS, Naylor C, Paludan S, Adams MJ, Levy HR (1998) On the mechanism of the reaction catalyzed by glucose 6-phosphate dehydrogenase. Biochemistry 37(9):2759-67

De Man JC, Rogosa M, Sharpe ME (1960) A MEDIUM FOR THE CULTIVATION OF LACTOBACILLI. Journal of Applied Bacteriology 23(1):130-135

de Vos WM (1996) Metabolic engineering of sugar catabolism in lactic acid bacteria. Antonie Van Leeuwenhoek 70(2-4):223-42

de Vos WM (2011) Systems solutions by lactic acid bacteria: from paradigms to practice. Microbial Cell Factories 10(1):S2

Dias O, Rocha M, Ferreira EC, Rocha I (2010) Merlin: Metabolic Models Reconstruction using Genome-Scale Information*. IFAC Proceedings Volumes 43(6):120-125

Dols M, Chraibi W, Remaud-Simeon M, Lindley ND, Monsan PF (1997) Growth and energetics of Leuconostoc mesenteroides NRRL B-1299 during metabolism of various sugars and their consequences for dextransucrase production. Appl Environ Microbiol 63(6):2159-65

Douillard FP, de Vos WM (2014) Functional genomics of lactic acid bacteria: from food to health. Microbial Cell Factories 13(1):S8

Egea JA, Henriques D, Cokelaer T, Villaverde AF, MacNamara A, Danciu DP, Banga JR, Saez-Rodriguez J (2014) MEIGO: an open-source software suite based on metaheuristics for global optimization in systems biology and bioinformatics. BMC Bioinformatics 15:136

Erkus O, de Jager VC, Spus M, van Alen-Boerrigter IJ, van Rijswijck IM, Hazelwood L, Janssen PW, van Hijum SA, Kleerebezem M, Smid EJ (2013) Multifactorial diversity sustains microbial community stability. ISME J 7(11):2126-36

Flahaut NAL, Wiersma A, van de Bunt B, Martens DE, Schaap PJ, Sijtsma L, dos Santos VAM, de Vos WM (2013) Genome-scale metabolic model for Lactococcus lactis MG1363 and its application to the analysis of flavor formation. Applied Microbiology and Biotechnology 97(19):8729-8739

Gamboa-Rueda JA, Lizcano-Gonzalez VA, Ordonez-Supelano MA, Perez-Mendoza JA, Guzman-Luna C, Lopez-Giraldo LJ (2015) Unstructured Kinetic Model of Batch Fermentation of Usp Glycerol for Lactic Acid Production. Ct&F-Ciencia Tecnologia Y Futuro 6(1):81-94

Ganzle MG (2015) Lactic metabolism revisited: metabolism of lactic acid bacteria in food fermentations and food spoilage. Current Opinion in Food Science 2:106-117

Garrigues C, Loubiere P, Lindley ND, Cocaign-Bousquet M (1997) Control of the shift from homolactic acid to mixed-acid fermentation in Lactococcus lactis: predominant role of the NADH/NAD+ ratio. J Bacteriol 179(17):5282-7

Garvie EI (1986) Genus Leuconostoc. In: Sneath PHA, Mair, N.S., Sharpe, M.E. and Holt, J.G. (ed) Bergey's Manual of Systematic Bacteriology. 2nd ed. edn. Springer-Verlag, New York

Gaspar P, Carvalho AL, Vinga S, Santos H, Neves AR (2013) From physiology to systems metabolic engineering for the production of biochemicals by lactic acid bacteria. Biotechnol Adv 31(6):764-88

Gatje G, Gottschalk G (1991) Limitation of Growth and Lactic-Acid Production in Batch and Continuous Cultures of Lactobacillus-Helveticus. Applied Microbiology and Biotechnology 34(4):446-449

Giaretta S, Treu L, Vendramin V, da Silva Duarte V, Tarrah A, Campanaro S, Corich V, Giacomini A (2018) Comparative Transcriptomic Analysis of Streptococcus

thermophilus TH1436 and TH1477 Showing Different Capability in the Use of Galactose. Frontiers in Microbiology 9(1765)

Goel A, Eckhardt TH, Puri P, de Jong A, Branco dos Santos F, Giera M, Fusetti F, de Vos WM, Kok J, Poolman B, Molenaar D, Kuipers OP, Teusink B (2015) Protein costs do not explain evolution of metabolic strategies and regulation of ribosomal content: does protein investment explain an anaerobic bacterial Crabtree effect? Molecular Microbiology 97(1):77-92

Gomez JA, Höffner K, Barton PI (2014) DFBAlab: a fast and reliable MATLAB code for dynamic flux balance analysis. BMC Bioinformatics 15(1):409

Goto S, Bono H, Ogata H, Fujibuchi W, Nishioka T, Sato K, Kanehisa M (1997) Organizing and computing metabolic pathway data in terms of binary relations. Pac Symp Biocomput:175-86

Greenblum S, Turnbaugh PJ, Borenstein E (2012) Metagenomic systems biology of the human gut microbiome reveals topological shifts associated with obesity and inflammatory bowel disease. Proceedings of the National Academy of Sciences 109(2):594-599

Hanemaaijer M, Olivier BG, Roling WF, Bruggeman FJ, Teusink B (2017) Model-based quantification of metabolic interactions from dynamic microbial-community data. PLoS One 12(3):e0173183

Hanemaaijer M, Röling WFM, Olivier BG, Khandelwal RA, Teusink B, Bruggeman FJ (2015) Systems modeling approaches for microbial community studies: from metagenomics to inference of the community structure. Frontiers in Microbiology 6(213)

Hanly TJ, Henson MA (2011) Dynamic flux balance modeling of microbial co-cultures for efficient batch fermentation of glucose and xylose mixtures. Biotechnology and Bioengineering 108(2):376-85

Harney SJ, Simopoulos ND, Ikawa M (1967) Cell wall constituents of Leuconostoc citrovorum and Leuconostoc mesenteroides. J Bacteriol 93(1):273-7

Hatti-Kaul R, Chen L, Dishisha T, Enshasy HE (2018) Lactic acid bacteria: from starter cultures to producers of chemicals. FEMS Microbiology Letters 365(20)

Heller MJ (2002) DNA Microarray Technology: Devices, Systems, and Applications. Annual Review of Biomedical Engineering 4(1):129-153

Henry CS, DeJongh M, Best AA, Frybarger PM, Linsay B, Stevens RL (2010) High-throughput generation, optimization and analysis of genome-scale metabolic models. Nat Biotechnol 28(9):977-82

Henson MA, Hanly TJ (2014) Dynamic flux balance analysis for synthetic microbial communities. IET Syst Biol 8(5):214-29

Hoffner K, Harwood SM, Barton PI (2013) A reliable simulator for dynamic flux balance analysis. Biotechnology and Bioengineering 110(3):792-802

Human Microbiome Project C (2012a) A framework for human microbiome research. Nature 486(7402):215-21

Human Microbiome Project C (2012b) Structure, function and diversity of the healthy human microbiome. Nature 486(7402):207-14

Jensen NBS, Melchiorsen CR, Jokumsen KV, Villadsen J (2001) Metabolic behavior of Lactococcus lactis MG1363 in microaerobic continuous cultivation at a low dilution rate. Applied and Environmental Microbiology 67(6):2677-2682

Kashket ER (1987) Bioenergetics of Lactic-Acid Bacteria - Cytoplasmic Ph and Osmotolerance. FEMS Microbiology Letters 46(3):233-244

Kauffman KJ, Prakash P, Edwards JS (2003) Advances in flux balance analysis. Curr Opin Biotechnol 14(5):491-6

Khandelwal RA, Olivier BG, Röling WFM, Teusink B, Bruggeman FJ (2013) Community Flux Balance Analysis for Microbial Consortia at Balanced Growth. PLoS One 8(5):e64567

Kim YJ, Eom HJ, Seo EY, Lee DY, Kim JH, Han NS (2012) Development of a chemically defined minimal medium for the exponential growth of Leuconostoc mesenteroides ATCC8293. J Microbiol Biotechnol 22(11):1518-22

King ZA, Lloyd CJ, Feist AM, Palsson BO (2015a) Next-generation genome-scale models for metabolic engineering. Current Opinion in Biotechnology 35:23-29

King ZA, Lu J, Dräger A, Miller P, Federowicz S, Lerman JA, Ebrahim A, Palsson BO, Lewis NE (2015b) BiGG Models: A platform for integrating, standardizing and sharing genome-scale models. Nucleic Acids Research 44(D1):D515-D522

Kitano H (2002) Computational systems biology. Nature 420(6912):206-210

Klaenhammer TR, Altermann E, Pfeiler E, Buck BL, Goh YJ, O'Flaherty S, Barrangou R, Duong T (2008) Functional genomics of probiotic Lactobacilli. J Clin Gastroenterol 42 Suppl 3 Pt 2:S160-2

Kleerebezem M, Hugenholtz J (2003) Metabolic pathway engineering in lactic acid bacteria. Curr Opin Biotechnol 14(2):232-7

Kleessen S, Nikoloski Z (2012) Dynamic regulatory on/off minimization for biological systems under internal temporal perturbations. BMC Systems Biology 6(1):16

Koduru L, Kim Y, Bang J, Lakshmanan M, Han NS, Lee DY (2017) Genome-scale modeling and transcriptome analysis of Leuconostoc mesenteroides unravel the redox governed metabolic states in obligate heterofermentative lactic acid bacteria. Sci Rep 7(1):15721

Konings WN (2002) The cell membrane and the struggle for life of lactic acid bacteria. Antonie Van Leeuwenhoek 82(1-4):3-27

Koressaar T, Remm M (2007) Enhancements and modifications of primer design program Primer3. Bioinformatics 23(10):1289-91

Lerman JA, Hyduke DR, Latif H, Portnoy VA, Lewis NE, Orth JD, Schrimpe-Rutledge AC, Smith RD, Adkins JN, Zengler K, Palsson BO (2012) In silico method for modelling metabolism and gene product expression at genome scale. Nature Communications 3:929

Leroy F, De Vuyst L (2004) Lactic acid bacteria as functional starter cultures for the food fermentation industry. Trends in Food Science & Technology 15(2):67-78

Letort C, Juillard V (2001) Development of a minimal chemically-defined medium for the exponential growth of Streptococcus thermophilus. J Appl Microbiol 91(6):1023-9

LevataJovanovic M, Sandine WE (1996) Citrate utilization and diacetyl production by various strains of Leuconostoc mesenteroides ssp cremoris. Journal of Dairy Science 79(11):1928-1935

Levy HR (1989) Glucose-6-phosphate dehydrogenase from Leuconostoc mesenteroides. Biochem Soc Trans 17(2):313-5

Levy HR, Christoff M, Ingulli J, Ho EM (1983) Glucose-6-phosphate dehydrogenase from Leuconostoc mesenteroides: revised kinetic mechanism and kinetics of ATP inhibition. Arch Biochem Biophys 222(2):473-88

Luedeking R, Piret EL (1959) A kinetic study of the lactic acid fermentation. Batch process at controlled pH. Journal of Biochemical and Microbiological Technology and Engineering 1(4):393-412

Maarleveld TR, Khandelwal RA, Olivier BG, Teusink B, Bruggeman FJ (2013) Basic concepts and principles of stoichiometric modeling of metabolic networks. Biotechnol J 8(9):997-1008

Machado D, Andrejev S, Tramontano M, Patil KR (2018) Fast automated reconstruction of genome-scale metabolic models for microbial species and communities. Nucleic Acids Research 46(15):7542-7553

Mahadevan R, Edwards JS, Doyle FJ, 3rd (2002) Dynamic flux balance analysis of diauxic growth in Escherichia coli. Biophys J 83(3):1331-40

Mahadevan R, Schilling CH (2003) The effects of alternate optimal solutions in constraint-based genome-scale metabolic models. Metab Eng 5(4):264-76

Makarova K, Slesarev A, Wolf Y, Sorokin A, Mirkin B, Koonin E, Pavlov A, Pavlova N, Karamychev V, Polouchine N, Shakhova V, Grigoriev I, Lou Y, Rohksar D, Lucas S, Huang K, Goodstein DM, Hawkins T, Plengvidhya V, Welker D, Hughes J, Goh Y, Benson A, Baldwin K, Lee JH, Diaz-Muniz I, Dosti B, Smeianov V, Wechter W, Barabote R, Lorca G, Altermann E, Barrangou R, Ganesan B, Xie Y, Rawsthorne H, Tamir D, Parker C, Breidt F, Broadbent J, Hutkins R, O'Sullivan D, Steele J, Unlu G, Saier M, Klaenhammer T, Richardson P, Kozyavkin S, Weimer B, Mills D (2006) Comparative genomics of the lactic acid bacteria. Proc Natl Acad Sci U S A 103(42):15611-6

Mcdonald LC, Fleming HP, Hassan HM (1990) Acid Tolerance of Leuconostoc-Mesenteroides and Lactobacillus-Plantarum. Applied and Environmental Microbiology 56(7):2120-2124

Miller GL (1959) Use of Dinitrosalicylic Acid Reagent for Determination of Reducing Sugar. Anal Chem 31 (3):426-428

Monod J (1949) THE GROWTH OF BACTERIAL CULTURES. Annual Review of Microbiology 3(1):371-394

Muñoz R, Moreno-Arribas MV, Rivas Bdl (2011) Chapter 8 - Lactic Acid Bacteria. In: Carrascosa AV, Muñoz R, González R (eds) Molecular Wine Microbiology. Academic Press, San Diego, pp 191-226

Naessens M, Cerdobbel A, Soetaert W, Vandamme EJ (2005) Leuconostoc dextransucrase and dextran: production, properties and applications. Journal of Chemical Technology and Biotechnology 80(8):845-860

Naylor CE, Gover S, Basak AK, Cosgrove MS, Levy HR, Adams MJ (2001) NADP+ and NAD+ binding to the dual coenzyme specific enzyme Leuconostoc mesenteroides glucose 6-phosphate dehydrogenase: different interdomain hinge angles are seen in different binary and ternary complexes. Acta Crystallogr D Biol Crystallogr 57(Pt 5):635-48

Niebel B, Leupold S, Heinemann M (2019) An upper limit on Gibbs energy dissipation governs cellular metabolism. Nature Metabolism 1(1):125-132

Nielsen J (2017) Systems Biology of Metabolism. Annu Rev Biochem 86:245-275

O'Brien EJ, Lerman JA, Chang RL, Hyduke DR, Palsson BØ (2013) Genome-scale models of metabolism and gene expression extend and refine growth phenotype prediction. Molecular Systems Biology 9(1):693

O'Sullivan O, O'Callaghan J, Sangrador-Vegas A, McAuliffe O, Slattery L, Kaleta P, Callanan M, Fitzgerald GF, Ross RP, Beresford T (2009) Comparative genomics of lactic acid bacteria reveals a niche-specific gene set. Bmc Microbiology 9(1):50

Olive C, Geroch ME, Levy HR (1971) Glucose 6-phosphate dehydrogenase from Leuconostoc mesenteroides. Kinetic studies. Journal of Biological Chemistry 246(7):2047-57

Oliveira AP, Nielsen J, Forster J (2005) Modeling Lactococcus lactis using a genome-scale flux model. Bmc Microbiology 5

Orth JD, Thiele I, Palsson BO (2010) What is flux balance analysis? Nature Biotechnology 28(3):245-248

Otto R, Tenbrink B, Veldkamp H, Konings WN (1983) The Relation between Growth-Rate and Electrochemical Proton Gradient of Streptococcus-Cremoris. Fems Microbiology Letters 16(1):69-74

Ozcan E, Cakir T (2016) Reconstructed Metabolic Network Models Predict Flux-Level Metabolic Reprogramming in Glioblastoma. Front Neurosci 10:156

Pastink MI, Sieuwerts S, de Bok FAM, Janssen PWM, Teusink B, van Hylckama Vlieg JET, Hugenholtz J (2008) Genomics and high-throughput screening approaches

for optimal flavour production in dairy fermentation. International Dairy Journal 18(8):781-789

Pastink MI, Teusink B, Hols P, Visser S, de Vos WM, Hugenholtz J (2009) Genome-scale model of Streptococcus thermophilus LMG18311 for metabolic comparison of lactic acid bacteria. Appl Environ Microbiol 75(11):3627-33

Pedersen MB, Gaudu P, Lechardeur D, Petit MA, Gruss A (2012) Aerobic respiration metabolism in lactic acid bacteria and uses in biotechnology. Annu Rev Food Sci Technol 3:37-58

Plihon F, Taillandier P, Strehaiano P (1995) Oxygen Effect on Batch Cultures of Leuconostoc-Mesenteroides - Relationship between Oxygen-Uptake, Growth and End-Products. Applied Microbiology and Biotechnology 43(1):117-122

Poolman B, Konings WN (1988) Relation of Growth of Streptococcus-Lactis and Streptococcus-Cremoris to Amino-Acid Transport. Journal of Bacteriology 170(2):700-707

Powell IB, Broome MC, Limsowtin GKY (2011) Cheese | Starter Cultures: General Aspects. In: Fuquay JW (ed) Encyclopedia of Dairy Sciences (Second Edition). Academic Press, San Diego, pp 552-558

Pu ZY, Dobos M, Limsowtin GK, Powell IB (2002) Integrated polymerase chain reaction-based procedures for the detection and identification of species and subspecies of the Gram-positive bacterial genus Lactococcus. J Appl Microbiol 93(2):353-61

Rodríguez J, Kleerebezem R, Lema JM, van Loosdrecht MCM (2006) Modeling product formation in anaerobic mixed culture fermentations. Biotechnology and Bioengineering 93(3):592-606

Salque M, Bogucki PI, Pyzel J, Sobkowiak-Tabaka I, Grygiel R, Szmyt M, Evershed RP (2013) Earliest evidence for cheese making in the sixth millennium BC in northern Europe. Nature 493(7433):522-5

Scheer M, Grote A, Chang A, Schomburg I, Munaretto C, Rother M, Söhngen C, Stelzer M, Thiele J, Schomburg D (2010) BRENDA, the enzyme information system in 2011. Nucleic Acids Research 39(suppl_1):D670-D676

Schellenberger J, Que R, Fleming RM, Thiele I, Orth JD, Feist AM, Zielinski DC, Bordbar A, Lewis NE, Rahmanian S, Kang J, Hyduke DR, Palsson BO (2011)

Quantitative prediction of cellular metabolism with constraint-based models: the COBRA Toolbox v2.0. Nat Protoc 6(9):1290-307

Schmitt P, Divies C (1992) Effect of Varying Citrate Levels on C-4 Compound Formation and on Enzyme Levels in Leuconostoc-Mesenteroides Subsp Cremoris Grown in Continuous Culture. Applied Microbiology and Biotechnology 37(4):426-430

Schmitt P, Divies C, Cardona R (1992) Origin of End-Products from the Co-Metabolism of Glucose and Citrate by Leuconostoc-Mesenteroides Subsp Cremoris. Applied Microbiology and Biotechnology 36(5):679-683

Shi Z, Li H, Li Z, Hu J, Zhang H (2013) Pre-column Derivatization RP-HPLC Determination of Amino Acids in Asparagi Radix before and after Heating Process. IERI Procedia 5:351-356

Siezen RJ, Bachmann H (2008) Genomics of dairy fermentations. Microb Biotechnol 1(6):435-42

Smid EJ, Erkus O, Spus M, Wolkers-Rooijackers JC, Alexeeva S, Kleerebezem M (2014) Functional implications of the microbial community structure of undefined mesophilic starter cultures. Microbial Cell Factories 13 Suppl 1:S2

Smid EJ, Hugenholtz J (2010) Functional genomics for food fermentation processes. Annu Rev Food Sci Technol 1:497-519

Smid EJ, Kleerebezem M (2014) Production of aroma compounds in lactic fermentations. Annu Rev Food Sci Technol 5:313-26

Smid EJ, Lacroix C (2013) Microbe–microbe interactions in mixed culture food fermentations. Current Opinion in Biotechnology 24(2):148-154

Smit G, Smit BA, Engels WJ (2005) Flavour formation by lactic acid bacteria and biochemical flavour profiling of cheese products. FEMS Microbiol Rev 29(3):591-610

Solopova A, Bachmann H, Teusink B, Kok J, Neves AR, Kuipers OP (2012) A Specific Mutation in the Promoter Region of the Silent cel Cluster Accounts for the Appearance of Lactose-Utilizing Lactococcus lactis MG1363. Applied and Environmental Microbiology 78(16):5612-5621

Starrenburg MJC, Hugenholtz J (1991) Citrate Fermentation by Lactococcus and Leuconostoc Spp. Applied and Environmental Microbiology 57(12):3535-3540

Succurro A, Ebenhoh O (2018) Review and perspective on mathematical modeling of microbial ecosystems. Biochem Soc Trans 46(2):403-412

Tarlak F, Sadikoglu H, Cakir T (2014) The role of flexibility and optimality in the prediction of intracellular fluxes of microbial central carbon metabolism. Mol Biosyst 10(9):2459-65

Taymaz-Nikerel H, Borujeni AE, Verheijen PJT, Heijnen JJ, van Gulik WM (2010) Genome-Derived Minimal Metabolic Models for Escherichia coli MG1655 With Estimated In Vivo Respiratory ATP Stoichiometry. Biotechnology and Bioengineering 107(2):369-381

Terzaghi BE, Sandine WE (1975) Improved Medium for Lactic Streptococci and Their Bacteriophages. Applied Microbiology 29(6):807-813

Teusink B, Bachmann H, Molenaar D (2011) Systems biology of lactic acid bacteria: a critical review. Microbial Cell Factories 10(1):S11

Teusink B, Molenaar D (2017) Systems biology of lactic acid bacteria: For food and thought. Current Opinion in Systems Biology 6:7-13

Teusink B, van Enckevort FH, Francke C, Wiersma A, Wegkamp A, Smid EJ, Siezen RJ (2005) In silico reconstruction of the metabolic pathways of Lactobacillus plantarum: comparing predictions of nutrient requirements with those from growth experiments. Appl Environ Microbiol 71(11):7253-62

Teusink B, Wiersma A, Molenaar D, Francke C, de Vos WM, Siezen RJ, Smid EJ (2006) Analysis of growth of Lactobacillus plantarum WCFS1 on a complex medium using a genome-scale metabolic model. Journal of Biological Chemistry 281(52):40041-40048

Thiele I, Palsson BØ (2010) A protocol for generating a high-quality genome-scale metabolic reconstruction. Nature Protocols 5:93

Tobalina L, Bargiela R, Pey J, Herbst F-A, Lores I, Rojo D, Barbas C, Peláez AI, Sánchez J, von Bergen M, Seifert J, Ferrer M, Planes FJ (2015) Context-specific metabolic network reconstruction of a naphthalene-degrading bacterial community guided by metaproteomic data. Bioinformatics 31(11):1771-1779

Tracey RP, Britz TJ (1989) Cellular Fatty-Acid Composition of Leuconostoc-Oenos. Journal of Applied Bacteriology 66(5):445-456

Untergasser A, Cutcutache I, Koressaar T, Ye J, Faircloth BC, Remm M, Rozen SG (2012) Primer3--new capabilities and interfaces. Nucleic Acids Res 40(15):e115

van Mastrigt O, Abee T, Lillevang SK, Smid EJ (2018) Quantitative physiology and aroma formation of a dairy Lactococcus lactis at near-zero growth rates. Food Microbiology 73:216-226

van Mastrigt O, Egas RA, Abee T, Smid EJ (2019) Aroma formation in retentostat co-cultures of Lactococcus lactis and Leuconostoc mesenteroides. Food Microbiology 82:151-159

van Niel EWJ, Hahn-Hägerdal B (1999) Nutrient requirements of lactococci in defined growth media. Applied Microbiology and Biotechnology 52(5):617-627

Vinay-Lara E, Hamilton JJ, Stahl B, Broadbent JR, Reed JL, Steele JL (2014) Genome-scale reconstruction of metabolic networks of Lactobacillus casei ATCC 334 and 12A. PLoS One 9(11):e110785

Wang H, Marcisauskas S, Sanchez BJ, Domenzain I, Hermansson D, Agren R, Nielsen J, Kerkhoven EJ (2018) RAVEN 2.0: A versatile toolbox for metabolic network reconstruction and a case study on Streptomyces coelicolor. PLoS Comput Biol 14(10):e1006541

Wang Z, Gerstein M, Snyder M (2009) RNA-Seq: a revolutionary tool for transcriptomics. Nature Reviews Genetics 10(1):57-63

Watanabe LH, König M, Myers CJ (2018) Dynamic Flux Balance Analysis Models in SBML. bioRxiv:245076

Wilkins BM, Pritchard RH (1987) Escherichia-Coli and Salmonella-Typhimurium - Cellular and Molecular-Biology, Vol 1-2 - Neidhardt,Fc. Nature 330(6150):707-708

Wooley JC, Godzik A, Friedberg I (2010) A Primer on Metagenomics. PLOS Computational Biology 6(2):e1000667

Yvon M, Rijnen L (2001) Cheese flavour formation by amino acid catabolism. International Dairy Journal 11(4):185-201

Zhuang K, Izallalen M, Mouser P, Richter H, Risso C, Mahadevan R, Lovley DR (2011) Genome-scale dynamic modeling of the competition between Rhodoferax and Geobacter in anoxic subsurface environments. ISME J 5(2):305-16

Zhuang K, Ma E, Lovley DR, Mahadevan R (2012) The design of long-term effective uranium bioremediation strategy using a community metabolic model. Biotechnology and Bioengineering 109(10):2475-83

Zomorrodi AR, Maranas CD (2012) OptCom: A Multi-Level Optimization Framework for the Metabolic Modeling and Analysis of Microbial Communities. PLOS Computational Biology 8(2):e1002363

APPENDIX A

Biomass composition of *Leu. mesenteroides*

Biomass composition of *Leu. mesenteroides* used for biomass reaction in the reconstructed model was obtained based on literature data. Protein, lipid, DNA, RNA and polysaccharide contents as major biopolymers and some building blocks such as amino acids, nucleotides, fatty acids contents forming these biopolymers are based on species or strain specific data, while other compositions were based on the data of phylogenetically close bacteria.

Overall Cellular Composition of Leu. mesenteroides

Component	**Fraction % (w/w)**	**MW (g/mol)**	**mol. coeff. (mmol/gDW)**
Protein	29.7 (Bang et al., 2017)	96.42	2.7752
Lipid	7.9 (Bang et al., 2017)	1075.40 (Oliveira et al., 2005)	0.0735
DNA	2.9 (Bang et al., 2017)	326.90	0.0887
RNA	7.4 (Bang et al., 2017)	342.59	0.2160
Polysaccharides	24.4 (Bang et al., 2017)	1871.90 (Oliveira et al., 2005)	0.1303
Lipoteichoic acid (LTA)	6.05 (Oliveira et al., 2005; Teusink et al., 2006)	5384.70 (Oliveira et al., 2005)	0.0112
Peptidoglycan (PG)	13.15 (Oliveira et al., 2005; Teusink et al., 2006)	991.00 (Oliveira et al., 2005)	0.1327
Rest	8.5		

Amino Acid Composition of the Protein Fraction in Leu. mesenteroides

Amino acids	**Composi-tion (%w/w)**	**MW (g/mol)**[(f)]	**(mol a.a/mol total**	**Amino acids**	**(mol a.a/ mol total protein)**	**(mol a.a/mol free**

	(Bang et al., 2017)		protein)			protein)[e]
Alanine	9.26	89.094	0.1039	Alanine	0.1039	0.0935
Glycine	5.5	75.067	0.0733	Glycine	0.0733	0.0733
Valine	4.89	117.148	0.0417	Valine	0.0417	0.0417
Leucine	8.04	131.175	0.0613	Leucine	0.0613	0.0613
Isoleucine	5.72	131.175	0.0436	Isoleucine	0.0436	0.0436
Threonine	3.78	119.12	0.0317	Threonine	0.0317	0.0317
Serine	2.95	105.093	0.0281	Serine	0.0281	0.0281
Proline	3.21	115.132	0.0279	Proline[a]	0.0306	0.0306
Aspartate (Asx)	6.87	133.103	0.0516	Aspartate	0.0258	0.0258
Methionine	2.71	149.208	0.0182	Asparagine[b]	0.0258	0.0258
4-Hydroxyproline	0.36	131.131	0.0027	Methionine	0.0182	0.0182
Glutamate (Glx)	10.32	147.13	0.0701	Glutamate	0.0351	0.0316
Phenylalanine	7.56	165.192	0.0458	Glutamine[c]	0.0351	0.0351
Lysine	19.56	146.19	0.1338	Phenylalanine	0.0458	0.0458
Histidine	5.68	155.157	0.0366	Lysine[d]	0.1354	0.1219
Hydroxylysine	0.26	162.189	0.0016	Histidine	0.0366	0.0366
Tyrosine	3.3	181.191	0.0182	Tyrosine	0.0182	0.0182
Cysteine	Not detected	121.154		Arginine[g]		0.0401
Asparagine		132.119		Tryptophan [g]		0.0177
Glutamine		146.146				
Arginine	-	174.204				
Tryptophan	-	204.229				
Average molecular weight of protein[h]: 107.02 g/mol						

(a) Total mole amount of proline including 4-Hydroxyproline.

(b) Assuming aspartate amount obtained by (Bang et al., 2017) is sum of equimolar amount of aspartate and asparagine.

(c) Assuming glutamate amount obtained by (Bang et al., 2017) is sum of equimolar amount of glutamate and glutamine.

(d) Total mole amount of lysine including hydroxylysine.

(e) According to (Harney et al., 1967) alanine, glutamate and lysine are the major amino acids in peptidoglycan of *Leu. mesenteroides*. Molar amount of alanine, glutamate and lysine are re-calculated considering their contribution in peptidoglycan. 10% of alanine, glutamate and lysine are assumed that come from peptidoglycan.

(f) Molecular weights of amino acids are taken from PubChem (https://pubchem.ncbi.nlm.nih.gov/).

(g) Average molar fractions of arginine and tryptophan in free protein are taken from the lactic acid bacteria metabolic models published (Flahaut et al., 2013; Oliveira et al., 2005; Pastink et al., 2009; Teusink et al., 2006; Vinay-Lara et al., 2014), because there is no data for arginine and tryptophan in original study (Bang et al., 2017).

(h) Average molecular weight of protein is calculated by that sum of the molar amino acid fraction of free protein (the last column from left) multiplied by the molecular weight of the associated amino acids (the 3rd column from left).

Nucleotide Composition

DNA composition	**%(mol/mol)[(a)]**	**MW (g/mol)[(b)]**
dAMP	31.05	331.225
dTMP	31.05	322.21
dCMP	18.95	307.199
dGMP	18.95	347.224
Average molecular weight of DNA[(c)]: 326.9047 g/mol		

(a) The deoxyribonucleotide composition is based on the GC content of 37.9 % which is the exact GC content of *Leu. mesenteroides* ATCC 19254 obtained by RAST annotation tool (http://rast.nmpdr.org/).

(b) Molecular weights of components are taken from PubChem (https://pubchem.ncbi.nlm.nih.gov/).

RNA composition	**%(mol/mol)[(a)]**	**MW (g/mol)[(b)]**
AMP	26.2	347.224
TMP	21.6	324.182
CMP	20	323.198
GMP	32.2	363.223
Average molecular weight of DNA: 342.5934 g/mol		

(a) Based on E. coli (Wilkins and Pritchard, 1987). This content was also used for the studies reconstructing the lactic acid bacteria in the literature (Flahaut et al., 2013; Oliveira et al., 2005; Pastink et al., 2009; Teusink et al., 2006).

(b) Molecular weights of components are taken from PubChem (https://pubchem.ncbi.nlm.nih.gov/).

Lipid Composition

Lipid composition	**%(mol/mol) (Oliveira et al., 2005)**	**MW (g/mol) (Oliveira et al., 2005)**
Phosphatidylglycerol	18.9	754.3
Cardiolipin	42.5	1413.6
Lysophosphatidylglycerol	4.3	500.2
Diglucosyl diacylgycerol	30.3	924.3
Monoglucosyl diacylgycerol	4.0	762.3
Average molecular weight of Lipid: 1075.4 g/mol		

Lipid fatty acid composition of Leu. mesenteroides

Lipid fatty acid composition of *Leu. mesenteroides*	**%(w/w)[(a)]**	**%(w/w) (w/o others)**	**MW (g/mol) (Oliveira et al., 2005)**	**mol/mol**
Tetradecanoic (myristic) acid (C14:0)	6.3	6.7236	228.4	0.0753
Hexadecanoic (palmitic) acid (C16:0)	29.9	31.9104	256.4	0.3184
Octadecanoic (stearic) acid (C18:1)	40.9	43.6499	282.5	0.3953
cis-9.10-methyleneoctadecenoic (dihydrosterculic) acid (C19-cyc-9)	16.6	17.7161	296.5	0.1529
Others	6.3			

(a) Specific to *Leu. mesenteroides ATCC 19254* (Tracey and Britz, 1989)

Lipoteichoic Acid (LTA) Composition

LTA composition	**%(mol/mol) (Oliveira et al., 2005)**
Glycerol phosphate	16
L-alanine	6.08
D-galactose	9.76
Diglucosyl diacylglycerol	1
Average molecular weight of LTA: 5384.7 g/mol(Oliveira et al., 2005)	

Peptidoglycan (PG) Composition

PG composition	**%(mol/mol) (Oliveira et al., 2005)**
N-acetylmuramate	1
N-acetyl-D-glucosamine	1
L-alanine	1
D-glutamate	1
L-lysine	1
D-alanine	1
D-aspartate	1
Average molecular weight of PG: 991.1 g/mol(Oliveira et al., 2005)	

Polysaccharide composition

Polysaccharide composition	**%(mol/mol) (Oliveira et al., 2005)**
D-glucose	5.5
D-rhamnose	5.6
D-galactose	1
Average molecular weight of polysaccharide: 1872.9 g/mol (Oliveira et al., 2005)	

Energy requirement for polymerisation of macromolecules

Process	Energy required (Wilkins and Pritchard, 1987)
Protein synthesis and processing	4.306 mmol ATP / mmol amino acid
RNA synthesis and processing	0.4 mmol ATP / mmol RNA [(a)]
DNA synthesis and processing	1.372 mmol ATP / mmol DNA [(a)]

(a) DNA assembly reaction can be simply described as DNA_n + dNMP -> DNA_{n+1}, where dNMP represents a deoxyribonucleotide monophosphate. However, as DNA synthesis takes deoxyribonucleotide triphosphates as precursors, DNA assembly costs an additional 2 mol ATP per mol DNA (Oliveira et al., 2005).

Protein, DNA and RNA reactions and required ATP amounts are as follows:

- 0.0281 L_Serine + 0.0316 L_Glutamate + 0.0733 Glycine + 0.0258 L_Aspartate + 0.0458 L_Phenylalanine + 0.0935 L_Alanine + 0.0401 L_Arginine + 0.0613 L_Leucine + 0.0351 L_Glutamine + 0.0306 L_Proline + 0.0182 L_Tyrosine + 0.0182 L_Methionine + 0.0436 L_Isoleucine + 0.1219 L_Lysine + 0.0317 L_Threonine + 0.0177 L_Tryptophan + 0.0366 L_Histidine + 0.0417 L_Valine + 0.0258 L_Asparagine + 3.5332 ATP + 3.5332 H2O -> 3.5332 H_c + 3.5332 ADP + 3.5332 Phosphate + PROTEIN

- 2.4 ATP + 0.2 CMP + 0.262 AMP + 0.216 UMP + 0.322 GMP + 2.4 H2O -> 2.4 H_c + 2.4 ADP + 2.4 Phosphate + RNA

- 3.372 ATP + 0.1895 dCMP + 0.1895 dGMP + 0.3105 dAMP + 0.3105 dTMP GMP + 3.372 H2O -> 3.372 H_c + 3.372 ADP + 3.372 Phosphate + DNA

Biomass Assembly

In addition to the polymers mentioned above, some vitamin, co-factors and metal ions included into the biomass equation -with a low molar coefficient (10^{-5} mmol/gDW) to make sure it was not limiting in the simulations- to consider the vitamin, co-factor and metal ion requirements(Teusink et al., 2006). Vitamin, co-factors and metal ions added into the biomass reactions are selected according to the metabolites obtained by ModelSEED (http://modelseed.org/) automatic metabolic reconstruction tool.

- 30.651 H2O + 5e-05 CoA + 30.651 ATP + 5e-05 NAD + 5e-05 Riboflavin + 5e-05 Fe2 + 5e-05 Zn2 + 5e-05 Mg + 5e-05 Thiamin + 5e-05 K + 5e-05 fe3 + 5e-05 Mn2 + 5e-05 Co2 + 5e-05 Cl_ + 5e-05 FAD + 5e-05 Folate + 5e-05 Sulfate + 5e-05 Ca2 + 0.0735 LIPID + 0.0112 LTA + 0.1327 PG + 0.1303 POLYS + 2.7752 PROTEIN + 0.0887 DNA + 0.216 RNA -> 30.651 H + 30.651 ADP + 30.651 Phosphate + BIOMASS_LM

APPENDIX B

Energetic Requirement for the Growth and Non-growth Associated Maintenance of *Leu. mesenteroides*

Growth associated maintenance is the amount of ATP required for biomass assembly from biopolymers, whereas non-growth associated maintenance (ATP maintenance rate) is the amount of ATP required to maintain the biomass that is not related to growth. Growth (K_x) and non-growth associated maintenance (m_{atp}) can be calculated by Pirt equation (Flahaut et al., 2013; Taymaz-Nikerel et al., 2010)

$$\sum q_{ATP,i} - K_X \mu - m_{ATP} = 0$$

Slope and intercept of the plot of total ATP rates (q_{ATP}, mmol/gDW/h) with respect to growth rates (μ, 1/h) give K_x and m_{ATP} respectively. In this study, growth (K_x) and non-growth associated maintenance (m_{atp}) were estimated using the experimental data obtained in Dols et. al., (1997)(Dols et al., 1997) and the metabolic model reconstructed. Dols et. al., (1997)(Dols et al., 1997) obtained the rates of energy syntheses (q_{ATP}) for various sugar source for *Leu. mesenteroides*, and the rates of energy synthesis (q_{ATP}) were estimated using the theoretical stoichiometric ATP yield, which is 2 and 1 mole ATP per one mole lactate and acetate produced respectively. However, such an approach causes potential errors due to omitting the whole cell metabolism that produces or consumes ATP with different mechanisms (Teusink et al., 2006). Hence, the measured fluxes were set as constraints for the genome-scale metabolic model reconstructed and FBA was used to calculate the maximal amount of ATP that could be generated.

The quantitative values of the rates of energy synthesis (q_{ATP}) and corresponding growth rates (μ) from the original paper (Dols et al., 1997) were obtained via via GetData Graph Digitizer (http://www.getdata-graph-digitizer.com/).

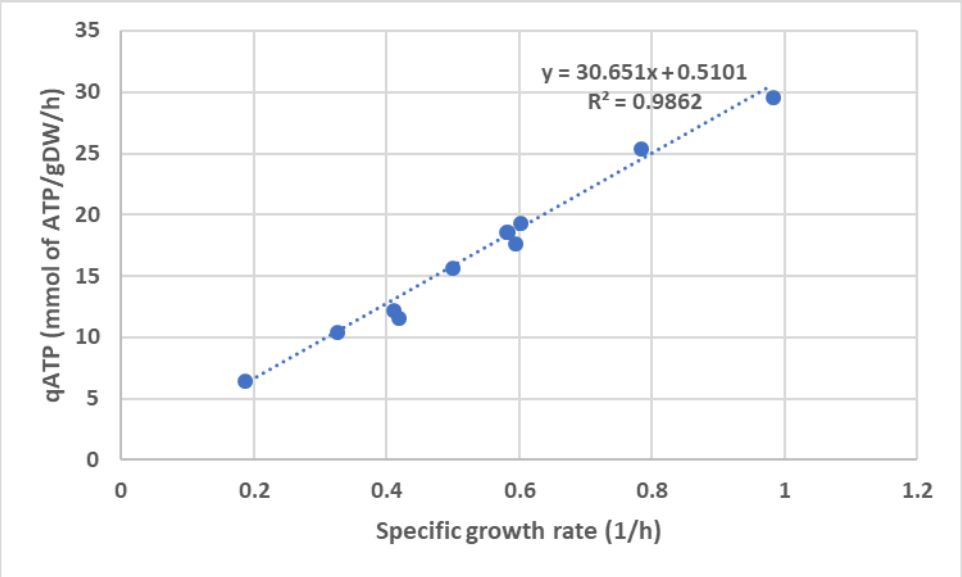

Growth associated maintenance (K_x)	30.651 mmol/gDW
Non-growth associated maintenance (m_{atp})	0.5101 mmol/gDW/h

APPENDIX C

Batch data used in the study of the metabolic model reconstruction of *Leu. mesenteroides*

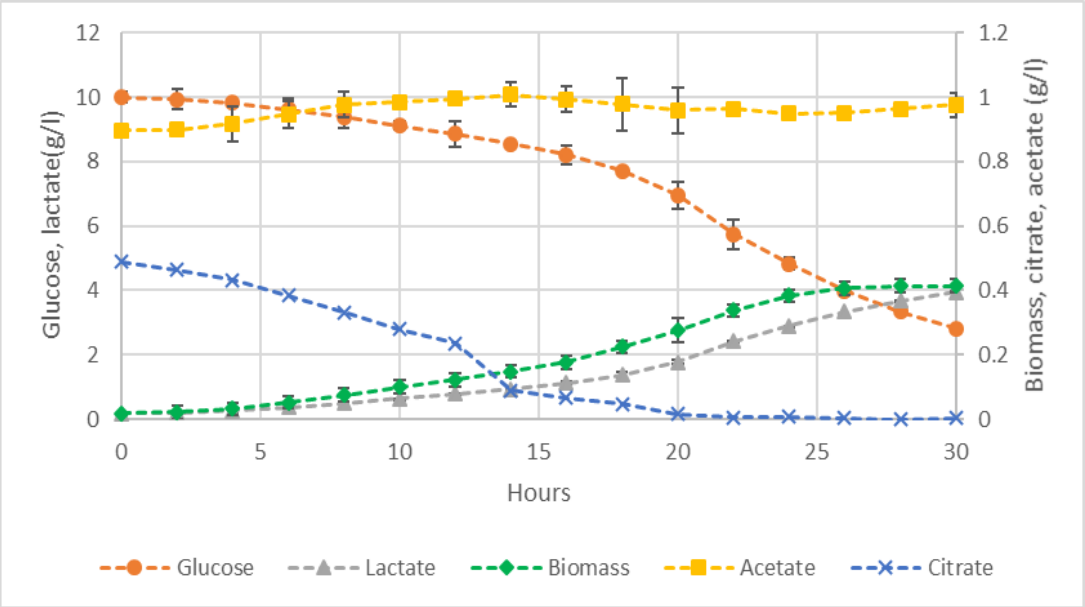

Carbon recovery (%) = 101.3 ± 2.4 %

APPENDIX D

Maximum amino acid uptake rate constraints used in the study of metabolic model reconstruction of *Leu. mesenteroides* for the analysis in the table 3.2.

Amino acid	**Maximum uptake rate (mmol/gDW/h)**	**Amino acid**	**Maximum uptake rate (mmol/gDW/h)**
Ala	-0.08	Lys	-0.193
Arg	-0.031	Met	-0.01
Asn	-0.047	Phe	-0.065
Asp	-0.083	Pro	-0.08
Gln	-0.08	Ser	-0.09
Glu	-0.03	Thr	-0.087
Gly	-0.08	Trp	-0.06
Ile	-0.071	Tyr	-0.07
Leu	-0.05	Val	-0.092
Note: Cys and His could not be measured in our analyses. Maximum uptake rates of His and Cys were constrained to -0.03 mmol/gDW/h			

APPENDIX E

Flux span of Figure 3.5 obtained by FVA

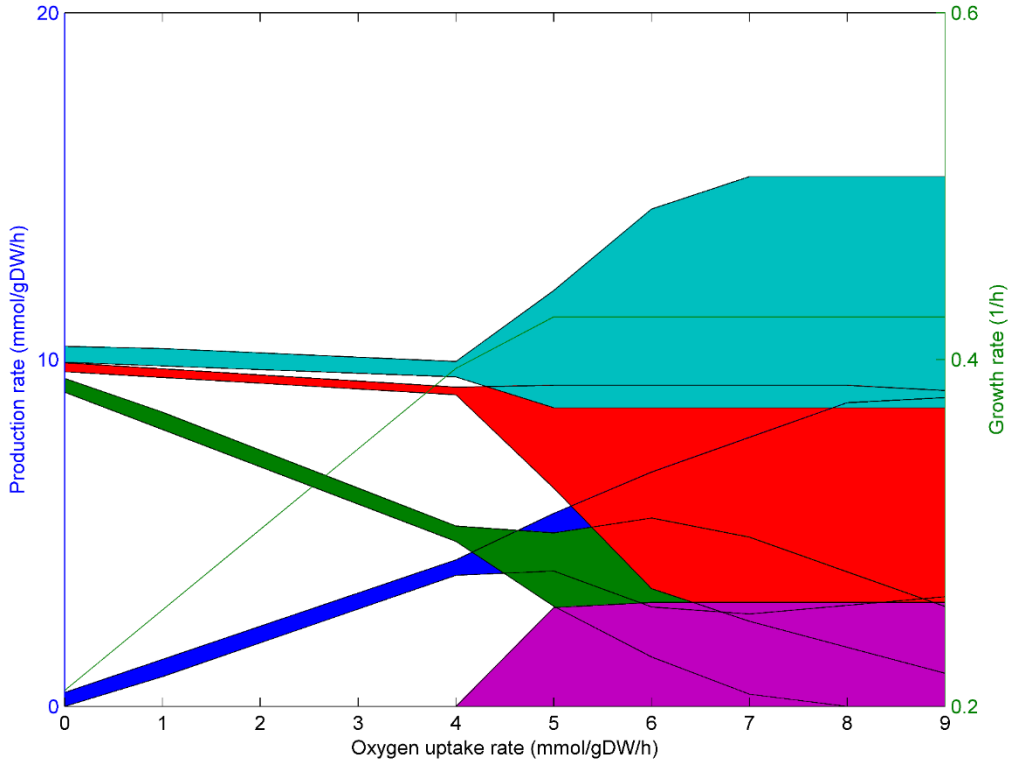

APPENDIX F

The statistics for the genome and annotation of *Leu. mesenteroides* ATCC 19254

Organism Overview for Leuconostoc mesenteroides subsp. cremoris ATCC 19254 (586220.9)

For each genome we offer a wide set of information to browse, compare and download.

Genome	Leuconostoc mesenteroides subsp. cremoris ATCC 19254 (Taxonomy ID: 586220)
Domain	Bacteria
Taxonomy	Bacteria; Terrabacteria group; Firmicutes; Bacilli; Lactobacillales; Leuconostocaceae; Leuconostoc; Leuconostoc mesenteroides; Leuconostoc mesenteroides subsp. cremoris; Leuconostoc mesenteroides subsp. cremoris ATCC 19254
Neighbors	View closest neighbors
Size	1,638,511
GC Content	37.9
N50	27923
L50	19
Number of Contigs (with PEGs)	126
Number of Subsystems	273
Number of Coding Sequences	1751
Number of RNAs	52

Browse | Compare | Download | Annotate

Browse through the features of Leuconostoc mesenteroides subsp. cremoris ATCC 19254 both graphically and through a table. Both allow quick navigation and filtering for features of your interest. Each feature is linked to its own detail page.

Click here to get to the Genome Browser

Subsystem Information

Subsystem Statistics | Features in Subsystems

Subsystem Coverage

Subsystem Category Distribution

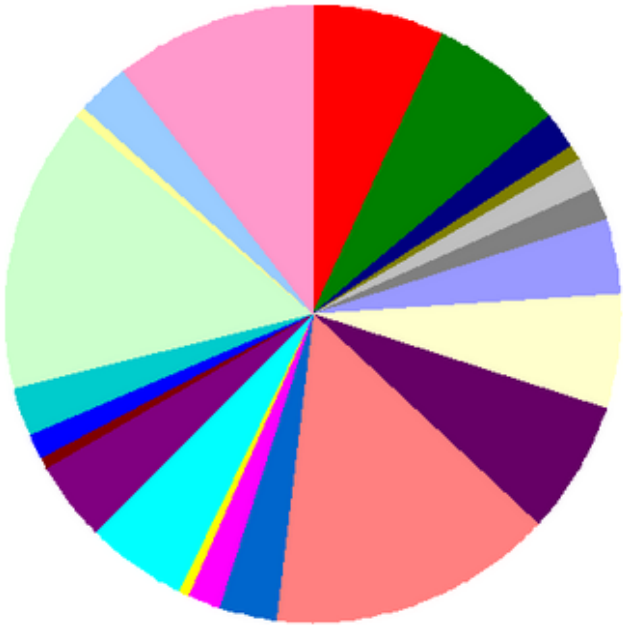

Subsystem Feature Counts

- Cofactors, Vitamins, Prosthetic Groups, Pigments (89)
- Cell Wall and Capsule (86)
- Virulence, Disease and Defense (25)
- Potassium metabolism (10)
- Photosynthesis (0)
- Miscellaneous (20)
- Phages, Prophages, Transposable elements, Plasmids (21)
- Membrane Transport (49)
- Iron acquisition and metabolism (0)
- RNA Metabolism (75)
- Nucleosides and Nucleotides (89)
- Protein Metabolism (184)
- Cell Division and Cell Cycle (39)
- Motility and Chemotaxis (0)
- Regulation and Cell signaling (23)
- Secondary Metabolism (5)
- DNA Metabolism (67)
- Fatty Acids, Lipids, and Isoprenoids (52)
- Nitrogen Metabolism (7)
- Dormancy and Sporulation (1)
- Respiration (18)
- Stress Response (30)
- Metabolism of Aromatic Compounds (3)
- Amino Acids and Derivatives (187)
  - Glutamine, glutamate, aspartate, asparagine; ammonia assimilation (11)
  - Histidine Metabolism (11)
  - Arginine; urea cycle, polyamines (41)
  - Lysine, threonine, methionine, and cysteine (58)
  - Amino Acids and Derivatives - no subcategory (0)
  - Branched-chain amino acids (15)
  - Polyamines (0)
  - Aromatic amino acids and derivatives (32)
  - Proline and 4-hydroxyproline (3)
  - Alanine, serine, and glycine (16)
- Sulfur Metabolism (8)
- Phosphorus Metabolism (34)
- Carbohydrates (125)

APPENDIX G

The comparison of sucrose metabolisms of dairy-origin *Leu. mesenteroides* ATCC 19254 and plant-origin *Leu. mesenteroides* ATCC 8293

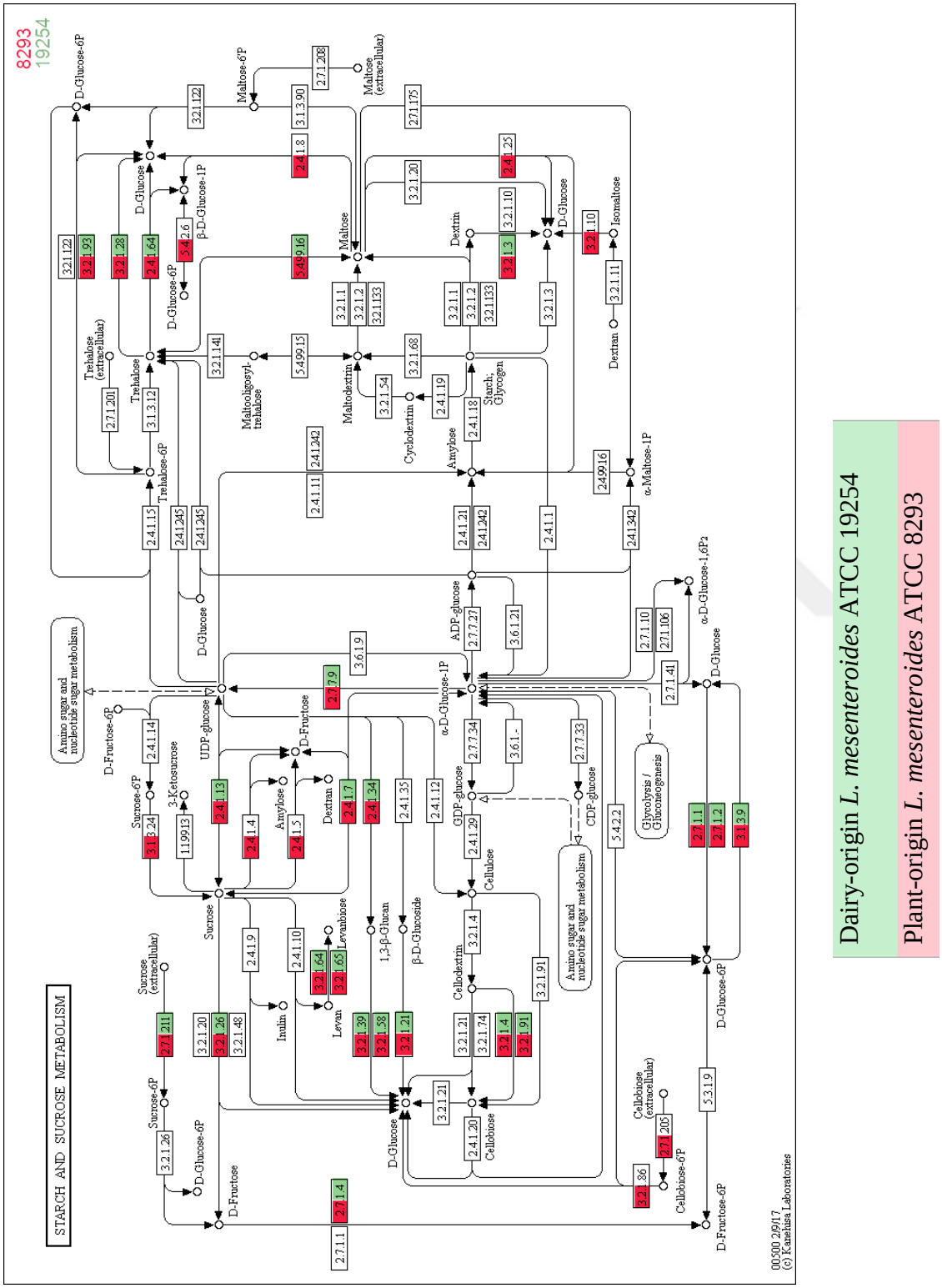

APPENDIX H

Carbon balance calculation of pure and co-cultures

Total compounds produced and consumed (g/L)						
Batch	ΔBiomass	ΔGlc	ΔLac	ΔFor	ΔAc	ΔCit
LLC I	0.680	-4.150	3.519	-0.105	-0.220	-0.082
LLC II	0.680	-4.228	3.525	-0.112	-0.233	-0.089
LLL I	0.573	-3.929	3.274	-0.090	-0.150	-0.082
LLL II	0.573	-3.867	3.223	-0.128	-0.147	-0.089
ST I	0.694	-4.756	4.151	0.299	-0.102	-0.074
ST II	0.669	-4.674	4.009	0.240	-0.114	-0.099
LM I	0.514	-8.264	3.906	-0.052	-0.086	-0.422
LM II	0.511	-6.887	3.478	-0.064	-0.087	-0.437
LLC-LM I	0.734	-5.260	4.375	0.043	-0.092	-0.366
LLC-LM II	0.747	-5.618	4.380	0.025	-0.116	-0.365
LLC-LLL-LM I	0.705	-5.154	4.295	-0.004	-0.080	-0.278
LLC-LLL-LM II	0.682	-5.080	3.914	-0.014	-0.128	-0.195
LLC-ST I	0.681	-4.465	3.767	-0.016	-0.139	-0.117
LLC-ST II	0.663	-4.419	3.829	0.041	0.062	-0.120
LLC-LLL-ST I	0.657	-4.696	3.737	-0.044	-0.094	-0.062
LLC-LLL-ST II	0.667	-4.398	3.773	-0.066	-0.130	-0.103

Compound	**Formula**	**MW**	**Carbon ratio**
Biomass(A)	$CH_{1.95}O_{0.63}N_{0.22}P_{0.02}S_{0.01}$	28.030	0.428
Biomass(B)	C(39.34%), O(23.88%), N(9,04%), H(6,72%), Others(6,72%)	1	0.393
Glc	$C_6H_{12}O_6$	180.000	0.400
Lac	$C_3H_6O_3$	90.000	0.400
For	CH_2O_2	46.000	0.261

Ac	$C_2H_4O_2$	60.000	0.400
Cit	$C_6H_8O_7$	192.000	0.375
EtOH	C_2H_6O	46.00	0.522
CO_2	CO_2	44.00	0.273

(A) Biomass formula used for the pure cultures of LLC, LLL and ST, and the co-cultures of LLC-LLL-ST and LLC-ST (Oliveira et al., 2005).

(B) Biomass formula used for the pure cultures of LM (Koduru et al., 2017).

Biomass formula used for the co-culture of LLC-LM and LLC-LLL-LM is the the average values of (A) and (B).

	LLC I	**LLC II**	**LLC I**	**LLL II**	**ST I**	**ST II**	**LM I**	**LM II**
C in biomass	0.291	0.291	0.245	0.245	0.297	0.286	0.202	0.201
C in Glc	-1.660	-1.691	-1.572	-1.547	-1.902	-1.870	-3.306	-2.755
C in Lac	1.407	1.410	1.310	1.289	1.660	1.603	1.562	1.391
C in For	-0.028	-0.029	-0.023	-0.033	0.078	0.063	-0.014	-0.017
C in Ac	-0.088	-0.093	-0.060	-0.059	-0.041	-0.046	-0.034	-0.035
C in Cit	-0.031	-0.034	-0.031	-0.033	-0.028	-0.037	-0.158	-0.164
C in EtOH							1.042	0.927
C in CO_2							0.273	0.464
C recovery (%)	94.013	92.109	92.236	91.756	103.290	99.996	87.664	100.445
	LLC-LM I	**LLC-LM II**	**LLC-LLL-LM I**	**LLC-LLL-LM II**	**LLC-ST I**	**LLC-ST II**	**LLC-LLL-ST I**	**LLC-LLL-ST II**
C in biomass	0.302	0.307	0.290	0.280	0.292	0.284	0.281	0.286
C in Glc	-2.104	-2.247	-2.062	-2.032	-1.786	-1.768	-1.879	-1.759
C in Lac	1.750	1.752	1.718	1.566	1.507	1.531	1.495	1.509
C in For	0.011	0.007	-0.001	-0.004	-0.004	0.011	-0.012	-0.017

C in Ac	-0.037	-0.046	-0.032	-0.051	-0.056	0.025	-0.038	-0.052
C in Cit	-0.137	-0.137	-0.104	-0.073	-0.044	-0.045	-0.023	-0.039
C recovery (%)	90.564	84.978	91.300	85.419	95.186	102.169	91.021	96.139

All carbon values in corresponding compounds are given as g/L

AUTOBIOGRAPHY

Name surname : Emrah Özcan

Place and date of birth : Mersin, Turkey / 06.07.1986

E-mail : emrahozcan.bioeng@gmail.com

EXPERIENCE

2017 - 2019	Guest PhD researcher at Vrije Universiteit Amsterdam, The Netherlands
2013 - 2018	Research assistant at Department of Bioengineering, Gebze Technical University, Gebze, Turkey
2011 - 2013	Researcher at Ege University Scientific Research Project, Ege University, Izmir, Turkey

EDUCATION

2014-2019	**Ph.D.**, Department of Bioengineering, Marmara University, Istanbul (Thesis title: Metabolic Network-Based Analysis of Cheese Starter Cultures as a Microbial Community)
2011-2014	**M.Sc.**, Department of Bioengineering, Ege University, Izmir (Thesis title: Production of pullulan with *Aureobasidium Pullulans* in airlift and bubble column bioreactors and optimization of process parameters)

2009 Fall **Student Exchange Program**, Department of Biotechnology, Lund University, Lund, Sweden

2006-2011 **B.Sc.,** Department of Bioengineering, Ege University, Izmir

AWARDS OR GRANTS

- **2214-A International Research Fellowship Program** by The Scientific and Technological Research Council of Turkey (Oct 2017- Oct 2018)
- **FEMS Young Scientist Meeting Grant (YSMG)** to support attendance at the FEMS Meeting: 12th Symposium on Lactic Acid Bacteria, Egmond aan Zee (Aug 2017)
- **2211-C Priority Areas PhD Bursary Program** by The Scientific and Technological Research Council of Turkey (Mar 2016-Aug 2018)

RESEARCH AREA & EXPERTISE

- Data analysis, statistical inference and visualization of high throughput biological data using systems biology tools
- Genome-scale metabolic network reconstruction and modelling
- Mechanistic and kinetic modelling of bioprocesses
- Bioprocess engineering
- Determining the fermentation dynamics

PUBLICATIONS

- **E. Özcan, S. S. Selvi, E. Nikerel, B. Teusink, E. Toksoy Öner, T. Çakir (2019)** A genome-scale metabolic network of the aroma bacterium *Leuconostoc mesenteroides* subsp. *cremoris*. **Appl Microbiol Biotechnol doi:10.1007/s00253-019-09630-4**
- **S. S. Selvi, E. Eminagic, M. Y. Kandur, E. Özcan, C. Kasavi, E. Toksoy Öner (2019)** Research and Production of Microbial Polymers for Food Industry. *In Bioprocessing for Food Ingredients Production, Editors: Gustavo Molina, Vijai K. Gupta and Brahma N. Singh.* Wiley-Blackwell.
- **E. Özcan, T. Çakir (2018)** Genome-scale brain metabolic networks scaffolds for the systems biology of neurodegenerative diseases: mapping metabolic alterations. Adv Neurobiol, 21, 195-217. doi:10.1007/978-3-319-94593-4_7
- **E. Özcan and T. Çakir (2016)** Reconstructed Metabolic Network Models Predict Flux-Level Metabolic Reprogramming in Glioblastoma. *Front. Neurosci.* 10:156. doi: 10.3389/fnins.2016.00156
- **E. Özcan, E. Toksoy Öner, T. Çakir (2016)** Metabolic network-based analysis of probiotic cheese starter cultures. **FEBS J**, 283: P-03.01.1-001. doi:10.1111/febs.13808
- **E. Özcan and E. Toksoy Öner (2015)** Microbial Production of Extracellular Polysaccharides from Biomass Sources. *In K. G. Ramawat & J.-M. Mérillon (Eds.), Polysaccharides: Bioactivity and Biotechnology* (pp. 161-184). Cham: Springer International Publishing
- **E. Özcan, S. Sargin, Y. Goksungur (2014)**. Comparison of pullulan production performances of air-lift and bubble column bioreactors and optimization of process parameters in air-lift bioreactor, **Biochem Eng J.** 92, 9-15. doi:10.1016/j.bej.2014.05.017

CONFERENCE PROCEEDINGS

- **E. Özcan, E. Nikerel, T. Çakir, E. Toksoy Öner.** Microbial Community Metabolic Modeling of Lactic Acid Bacteria. *12th International Symposium of Lactic Acid Bacteria,* Egmond aan Zee, The Netherlands, 27-31/08/2017 (Poster Presentation)
- **E. Kırdök, İ. Yüksel, E. Özcan, T. Çakır.** Reconstruction of Cold Stress Specific Genome-scale Metabolic Models for *Arabidopsis thaliana*. *Green Biotechnology Workshop*, Kocaeli-TURKEY, 21-23 /09/ 2015 (Poster presentation)
- **E. Özcan, T. Çakır.** Investigation of the Effects of Glioblastoma Tumors on Brain Metabolism Using Computational Systems Medicine Approaches. *International Symposium on Advances in Predictive and Personalized Medicine (APPM-2015)*, İstanbul-TURKEY, 2-3 /04/ 2015 (Poster presentation)
- **E. Özcan, E. Toksoy Öner, T. Çakır.** Metabolic Network-Based Analysis of Microbial Communities. 3rd National Bioengineering Student Congress, Istanbul-TURKEY, 12-13 /03/ 2015 (Poster presentation)
- **E. Özcan, T. Çakır.** Understanding Brain Metabolic Network Changes in case of Glioblastoma Using Computational Systems Biology Approaches. *International Conference on Applied Informatics for Health and Life Sciences (AIHLS-2014)*, Kuşadası-TURKEY, 19-22 /09/ 2014 (Poster presentation)
- **Z. O Çalışkaner, A. A. Waheed, E. Özcan, T. Çakır.** Bioinformatic Analysis of Parkinson's Disease, Huntington's Disease and Multiple Sclerosis to Reveal Disease-Specific Metabolic Patterns. *3rd International Congress of the Molecular Biology Association of Turkey (MolBioKon2014)*. Izmir / TURKEY. 10-12/09/2014 (Poster presentation)

- **E. Özcan, T. Çakır.** Bioinformatic Analysis of the Effect of Glioblastoma Tumors on Brain Metabolism. 11th National Conference of Chemical Engineering. Osmangazi University, Eskişehir/TURKEY. 02-05/09/2014 (Oral presentation)
- **Ü. Alkaya, E. Özcan, T. Çakır.** The Flux Balance Analysis of Human Brain Metabolic Network Affected by Alzheimer's Disease. *International ITU Molecular Biology and Genetics Student Congress*. Istanbul / TURKEY 15-17/08/2014 (Poster presentation)
- **E. Özcan, T. Çakır**. Investigation of the Effects of Glioblastoma Tumors on Cell Metabolism Using Computational Systems Medicine Approaches. *12nd National Neuroscience Congress*, Bahçeşehir University, Istanbul/TURKEY 28-31/05/2014 (Poster presentation)